

REFLECTION HIGH ENERGY ELECTRON DIFFRACTION STUDIES
OF INTERFACE FORMATION

A THESIS

SUBMITTED TO THE FACULTY OF THE GRADUATE SCHOOL
OF THE UNIVERSITY OF MINNESOTA

BY

PAUL PUKITE

IN PARTIAL FUFILLMENT OF THE REQUIREMENTS
FOR THE DEGREE OF
DOCTOR OF PHILOSOPHY

1988

ABSTRACT

The epitaxial growth of semiconductors, such as GaAs, by the technique of molecular beam epitaxy (MBE) has led to many improvements in device performance and capabilities. One important system is the epitaxial growth of GaAs on Si. This holds great promise for integrating optical and electronic devices on the same chip. The key to achieving this is to grow high quality GaAs layers on Si substrates.

In this investigation, single-crystal GaAs was grown on Si and Ge substrates by MBE. The growth of the epitaxial layers was investigated in situ with reflection high-energy electron diffraction (RHEED). Important in this heteroepitaxial system is that two possible GaAs crystal orientations can be obtained. By using a theory of kinematic electron diffraction developed in the course of this work, the mechanisms and growth conditions which choose between the two GaAs orientations have been determined for the first time. A further result is that the epitaxial growth processes are anisotropic on the two orientations. This leads to different crystalline qualities dependent on the orientation. To understand this in more detail, the crystal growth process was formulated mathematically. By incorporating the concepts of anisotropic diffusion and adsorption into a nonlinear differential equation, the time-dependent growth and RHEED behavior has been calculated and

compared to experiment. The experimental observations of RHEED intensity oscillations and two-dimensional clustering are in excellent agreement with the diffraction and growth theories. It is concluded that surface steps play a vital role in the crystal growth and interface formation processes reported in this study.

Acknowledgements

I wish to thank Dr.P.I.Cohen, Dr.J.M.Van Hove,
Dr.C.S.Lent, Dr.S.Batra, Dr.K.D.Jamison, G.J.Whaley,
G.S.Petrich, A.M.Wowchak, D.N.Zhou, and J.N.Kuznia for
encouragement and assistance through all phases of this
project. I also wish to thank my father for providing
insight and encouragement on countless problems.

Table of Contents

| Chapter | Page |
|---|------|
| 1. Introduction..... | 1 |
| 2. Diffraction Analysis..... | 8 |
| 2.1. Kinematic Diffraction..... | 8 |
| 2.1.A. Constructive and Destructive Interference... | 8 |
| 2.1.B. Surface Scattering & Column Approximation.. | 15 |
| 2.1.C. Ewald's Construction..... | 17 |
| 2.2. Diffraction from Surface Steps..... | 22 |
| 2.2.A. Diffraction from a Two-Level Surface..... | 22 |
| 2.2.B. Diffraction from Two-Dimensional Clusters.. | 33 |
| 2.2.C. Diffraction from Vicinal Surfaces..... | 41 |
| 2.2.D. Diffraction from Facets..... | 50 |
| 3. Crystal Growth Mechanisms and Theoretical Results...55 | |
| 3.1. Molecular Beam Epitaxy..... | 56 |
| 3.2. Classification of Growth Modes..... | 63 |
| 3.3. Layer-by-Layer Growth on Vicinal Surfaces..... | 68 |
| 3.3.A. The Time Dependent BCF Model..... | 68 |
| 3.3.B. Monolayer Cluster Formation..... | 81 |
| 3.4. RHEED Intensity Oscillations..... | 84 |
| 4. Experimental..... | 88 |
| 4.1. Diffraction and Growth Apparatus..... | 88 |
| 4.2. Preparation and Growth of GaAs..... | 92 |
| 4.3. Preparation and Growth of Ge and GaAs/Ge..... | 93 |

| | |
|--|-----|
| 4.4. Preparation of Si Substrates for GaAs growth... | 94 |
| 5. Results..... | 97 |
| 5.1. GaAs Surface and Growth Characterization..... | 97 |
| 5.2. Ge Surface and Growth Characterization..... | 115 |
| 5.3. GaAs on Ge(100) Growth..... | 132 |
| 5.4. GaAs on Si(100) Growth..... | 149 |
| 6. Summary and Conclusions..... | 163 |
| Appendix A Surface Lattice Diffraction..... | 167 |
| Appendix B Diffraction from Rectangular Clusters.... | 171 |
| Appendix C Disordered Staircase Diffraction..... | 173 |
| Appendix D Solution to Linear Diffusion Equation.... | 175 |
| Appendix E Stability of Propagating Steps..... | 177 |
| Appendix F Staircase Diffusion Computer Program.... | 179 |
| Appendix G Diffraction from Adatom Profile..... | 181 |
| References..... | 184 |

Chapter 1

Introduction

Reflection high-energy electron diffraction (RHEED) is an in situ surface sensitive tool that allows instant feedback on the molecular beam epitaxy (MBE) growth process. The most fundamental information that the RHEED pattern gives is the lattice constant and surface reconstruction. Additionally, information on the morphology of the surface is obtained from the shape of the diffracted beams. For example, we take two limits of surface morphology. A very rough surface containing three-dimensional asperities gives a transmission-like diffraction pattern. At the other extreme, smooth, atomically stepped surfaces exhibit RHEED patterns with short streaks that have structure along their length. By analyzing the shape of these streaks, the nature of the steps on the surface can be understood.

The surface processes that are being studied in this thesis include crystal growth and diffusion. Surface steps are important elements in these processes since they affect adatom incorporation [Burton, 1951] and impurity adsorption [Somorjai, 1981]. It is convenient to distinguish two types of step distributions. Cut and polished surfaces invariably have a staircase of steps due to misorientation from a low-

index plane. On well-oriented and flat crystals the substrate steps approach the instrument limit. During growth on such a surface, clusters consisting of up and down steps become important. In this investigation, diffraction from both staircases and clusters will be calculated and described. With this basis one can begin to understand the particular growth mechanisms of epitaxy.

As can be deduced already, a connecting theme in this thesis is the role of steps in the epitaxial growth process. In particular, we will show that steps are important during the formation of the heteroepitaxial interface and that they play an important role in the subsequent growth. The main goal is to understand the interface formation in two important systems, namely that of GaAs on Ge(100) and GaAs on Si(100).

These systems have promising technological applications, but the growth is only poorly understood. For example, the recent successful efforts to grow high quality GaAs on both Ge and Si by MBE [Fischer, 1985] has led to questions concerning the microscopic processes of the heteroepitaxy. For either Si or Ge substrates one needs to determine the growth mode in which antiphase domains are avoided. These antiphase domains have long been an issue [Kroemer, 1986] and are an expected consequence of the growth

of zincblende on diamond. It had been suggested that surface steps have an important role in eliminating antiphase domains. As we will show, the previous explanations for the lack of antiphase domains have been too simplistic, but the effect of steps is still crucial to the single domain formation.

Further goals in this investigation are (1) to characterize step distribution and morphology using RHEED on GaAs, Ge, and Si, and (2) develop models of epitaxial growth consistent with the temporal behavior of the RHEED patterns. Both are fundamental to the understanding of heteroepitaxial and homoepitaxial growth processes.

For the first of these two goals, we find that the complexity in the step structure is comparable to the complexity in the crystal structure. For example, the polar nature of the GaAs lattice allows two types of steps to form. Using RHEED, we show that the different steps have different growth and structural properties. Furthermore, the diamond lattices of Si and Ge allow a similar distinction in step types to be made. Here we find that the interaction of As with one of the two types of steps controls the GaAs domain formation on both Ge(100) and Si(100).

For the second goal of obtaining growth models

consistent with the RHEED measurements, we have developed a non-linear partial differential equation to describe the time dependent behavior of homoepitaxial growth. The steps of the substrate are important in determining the boundary conditions for these equations. We find that the solutions of these equations show damped oscillations in quantities such as adatom concentration and step velocity. These oscillations are sensitive functions of step separations and surface diffusion coefficients. The calculation of RHEED intensities from such a time dependent surface also show damped oscillations. What is most remarkable is the close correspondence of these oscillations to the RHEED oscillations observed experimentally on intentionally stepped surfaces. As GaAs heteroepitaxy on Si and Ge is typically performed on intentionally stepped substrates, direct comparisons between the surface evolution during growth via homoepitaxy and heteroepitaxy can be made.

As these findings will demonstrate, RHEED is a powerful tool for the study of surface processes. Because of the glancing geometry of RHEED, the high energy electrons only interact strongly with the first few layers of material. The glancing angle also makes it exceedingly sensitive to surface morphology. This can be seen clearly in the striking variation between a surface experiencing layer-by-layer growth and one that exhibits rough, three-dimensional

growth. However, the strong scattering of the electrons by the atomic potentials causes strong dynamical (multiple) scattering events to occur. This makes the diffracted intensities difficult to interpret.

To try to understand the observed diffraction patterns, one must separate the more simply understood features, like positions of diffracted beams, from the more difficult problems such as absolute intensities of diffracted beams. Likewise this investigation will separate the issues regarding the shape of diffracted beams into more manageable terms. The view presented here is that kinematic diffraction can be used to understand the shape of a diffracted beam.

In the next section, diffraction from stepped surfaces will be explained in more detail. The kinematic diffraction theory will be outlined. The characteristic dependence on scattering angle will be emphasized here. Previous measurements (including RHEED intensity oscillations) will be reviewed and compared to the theory. New calculations of stepped surfaces which include spatial disorder and two-dimensional shape effects will be given. Diffraction from three-dimensional asperities will also be described.

In the third section, the mechanisms of crystal growth will be discussed as a basis for interpreting the RHEED

measurements. The roles of adatom adsorption, surface diffusion, and cluster formation will be introduced here. The problems associated with heteroepitaxial growth will also be outlined. In particular, the problems unique to growth of GaAs on Si(100) and Ge(100) will be reviewed. The model of homoepitaxial growth on a stepped surface will also be developed here. The connection of this model to RHEED oscillations will be made.

In the fourth section the experimental apparatus and sample and growth preparation will be described.

In the final section, RHEED measurements from growing surfaces of GaAs and Ge on stepped substrates of GaAs(100), Ge(100), and Si(100) will be presented. We first examine the homoepitaxial growth processes of GaAs and Ge. Particular attention will be paid to the differences in step character and surface anisotropy for each surface. We find that As as an intentional impurity has a strong interaction with Ge. The heteroepitaxial growth of GaAs on Ge(100) and Si(100) is then presented. The RHEED results obtained indicate that the substrate step distribution is crucial to the subsequent growth mode and that the step distribution is changed by reaction with an As ambient. Finally we compare the surface morphology of heteroepitaxially grown layers of GaAs to the bulk layers previously measured. The ultimate goal is to

understand the interactions between adatoms and steps that lead to the growth of a smooth epitaxial layer.

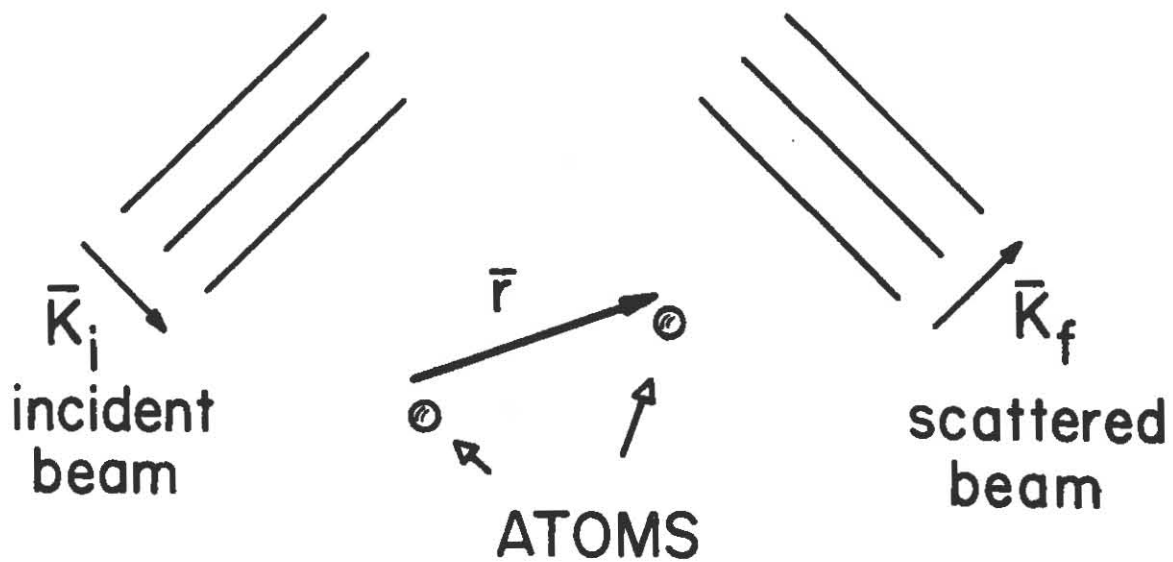
Chapter 2

Diffraction Analysis

2.1. Kinematic Diffraction

2.1.A. Constructive and Destructive Interference

Path length differences are the key to understanding electron diffraction from solid surfaces. Electrons scattered from atoms separated by \underline{r} can interfere constructively or destructively depending on the wave function phase shift between the points. This is shown in Fig.1. The phase shift is a function of the vector separation between the atoms and of the incoming and outgoing electron wavevectors, \underline{k}_i and \underline{k}_f , where $k=2\pi/\lambda$. When the phase shift is equivalent to some multiple of 2π , then the waves are scattered constructively or "in-phase". When the phase shift is odd π , then the waves are scattered destructively or "out-of-phase". Since a 10 keV electron has a wavelength of 0.12 Å and the separation between atoms in a crystalline lattice is a few Å, there is a great opportunity for both constructive and destructive interference. A RHEED pattern shows this interference if a crystalline substrate with a surface suitably prepared is used as a reflecting target.



$$\text{phase difference } \Phi = (\bar{K}_f - \bar{K}_i) \cdot \bar{r}$$

Fig.1 Constructive and destructive interference.

Figure 2 shows a RHEED pattern from a GaAs surface and Fig.3 shows the schematic RHEED geometry. The phosphor screen clearly shows intensity maximum due to "in-phase" or diffracted beams. Generally, the more perfect the surface is, the sharper the intensity maximum will be, as in Fig.3a. If defects such as clusters, asperities, or steps are present on the surface as in Fig.3b, the diffracted beams will tend to dim and broaden. This is further shown in Fig.4. The details of the beam shape or the intensity profile of Fig.4 gives information on the arrangement of the defects on the surface.

As an example of an arrangement of steps, consider a regularly stepped surface, as in Fig.5. Electron diffraction from such an ordered array of steps causes a sharp splitting in final angle of the diffracted beams [Pukite, 1984a,b]. To understand this, realize that waves diffracted from adjacent terraces can either constructively or destructively interfere. Under the condition of destructive interference, the splitting is the sharpest and clearest. The corresponding separation between the split beams is inversely related to the average terrace length.

If the terrace lengths are disordered, the splitting will not be as sharp and the individual components will broaden [Pukite, 1985]. The broadening can be related to a

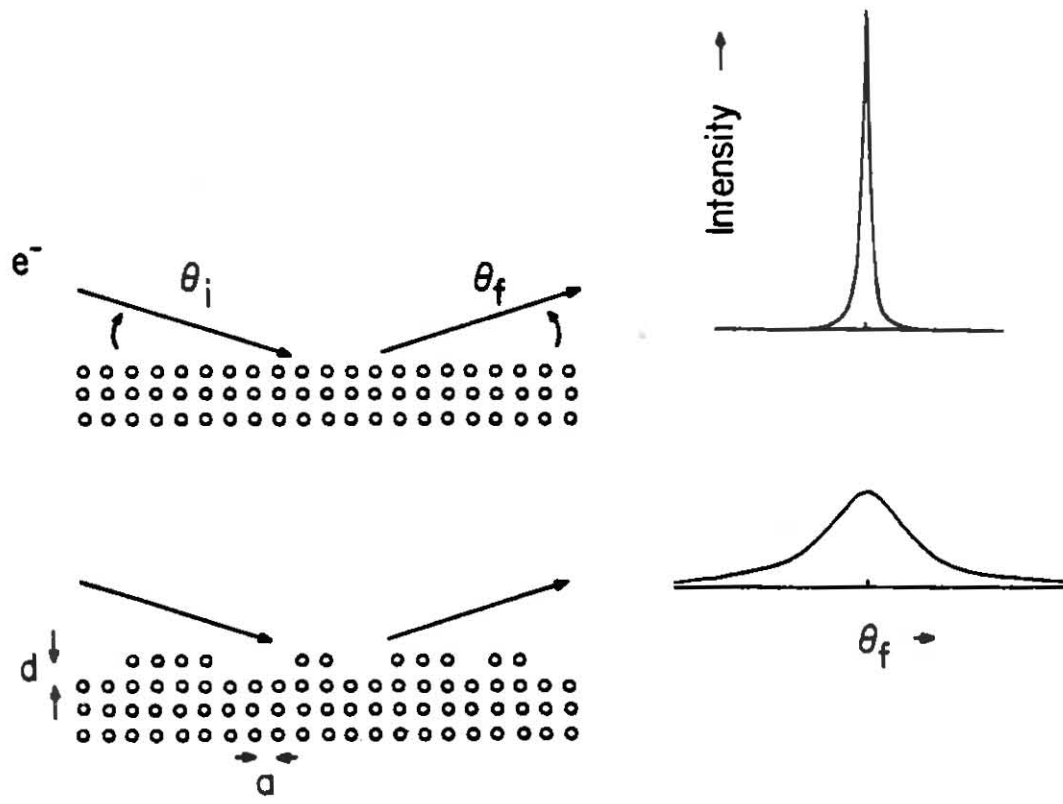


Fig.4 RHEED angular profile.

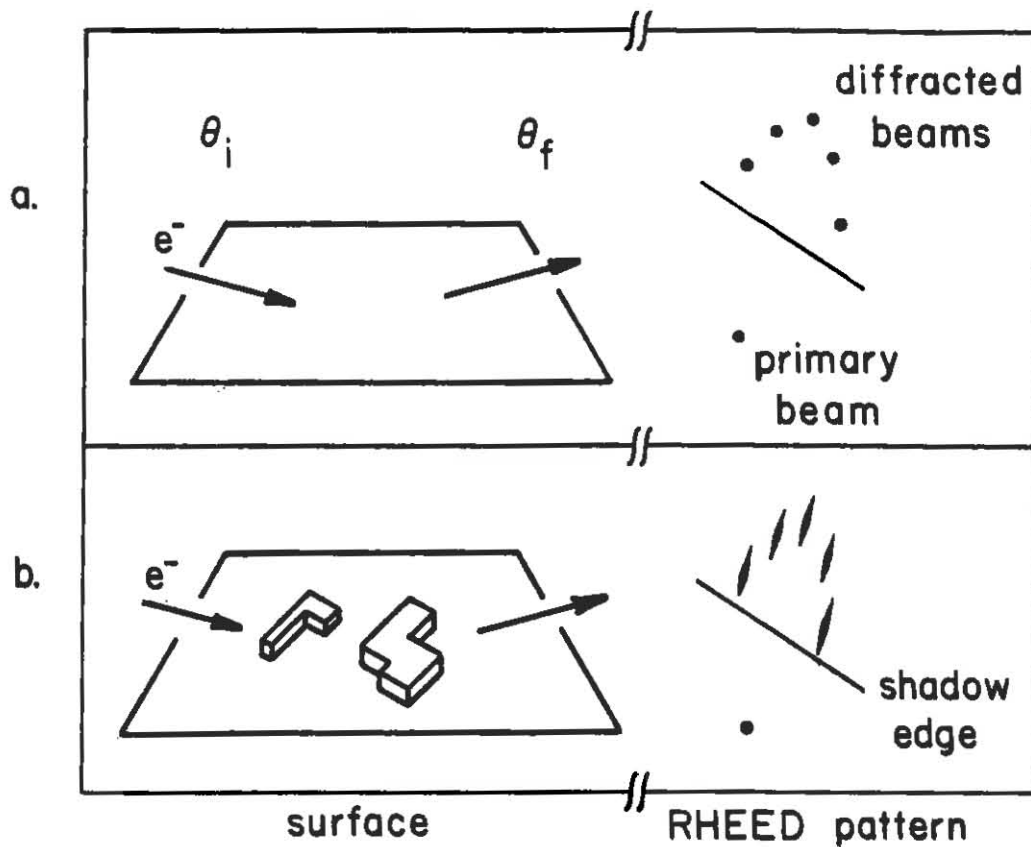


Fig.3 Perspective view of RHEED pattern formation.

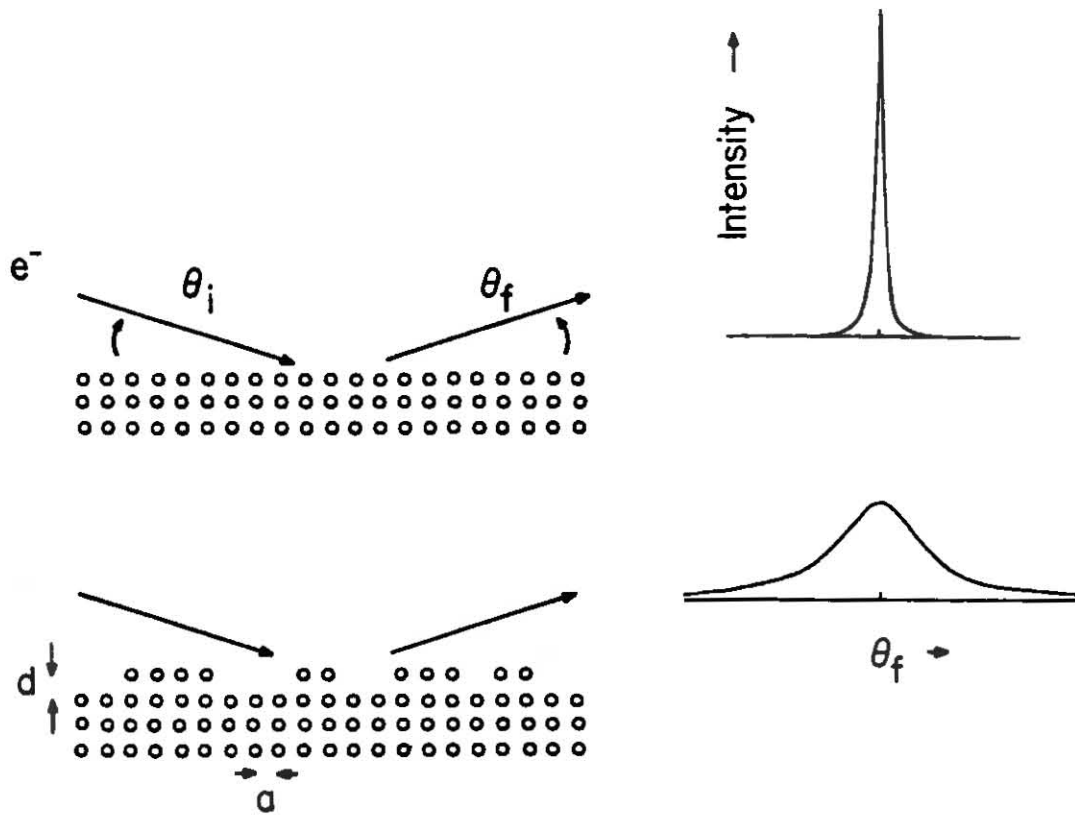


Fig.4 RHEED angular profile.

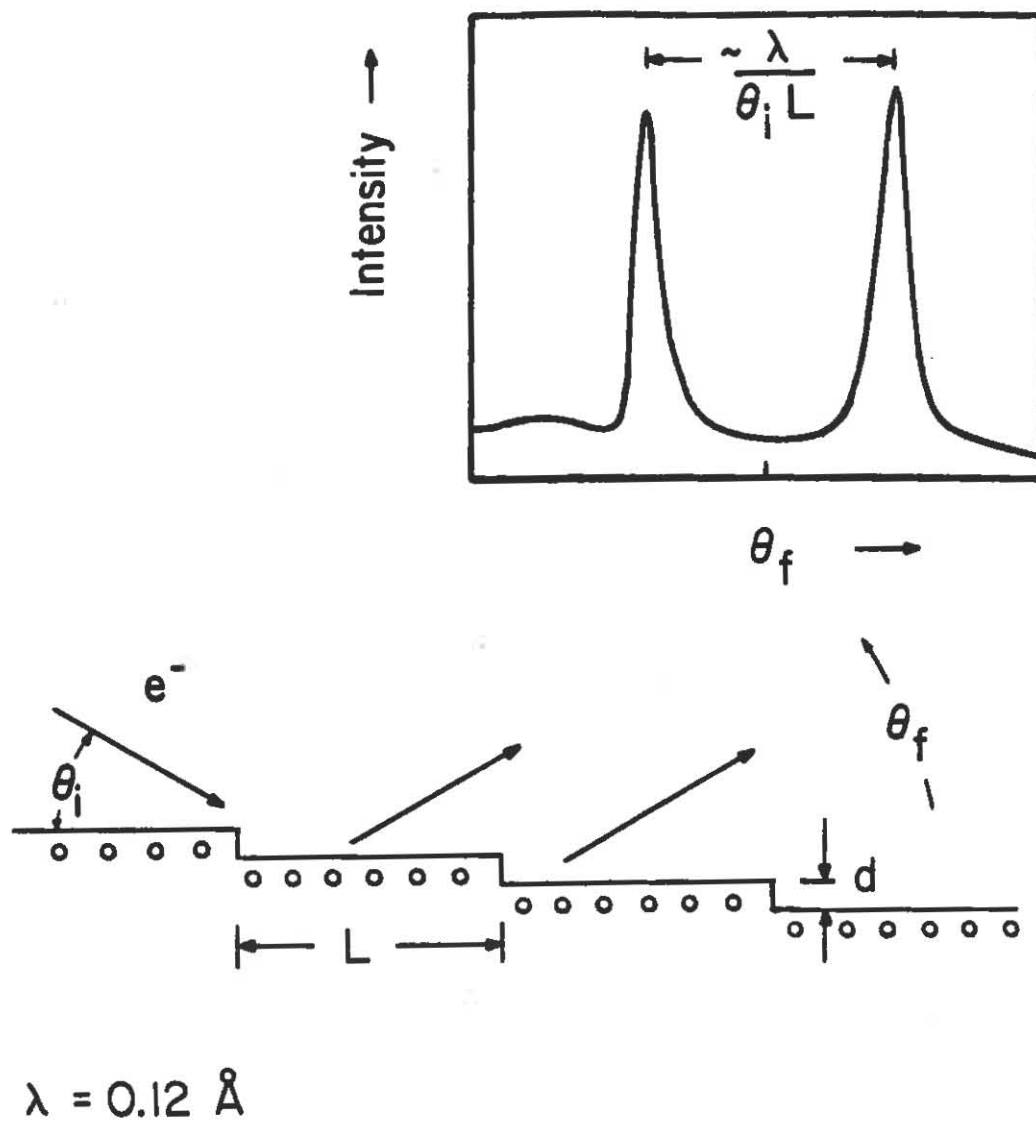


Fig. 5 RHEED splitting from vicinal surface.

root-mean-square (rms) fluctuation in the terrace lengths if the lengths are statistically independent. Similarly if random up and down steps, due to clusters, are formed on the terraces, the peak shape will broaden as in Fig.4 [Lent, 1984]. To obtain more accurate and quantitative information on the distribution of steps requires a calculation of the diffracted intensity from an assumed arrangement of steps. The simplest approach to calculating diffracted intensity is based on the kinematic approximation. In Fourier optics, this is equivalent to Fraunhofer diffraction.

2.1.B. Surface Scattering and the Column Approximation

The calculation of the diffracted beam shape within the kinematic approximation first requires a definition of the reciprocal space intensity. The reciprocal space coordinates can then be related to observable quantities via the Ewald construction. As a result, the kinematic scattering approximation gives characteristic beam shapes for various step distributions.

Diffraction from a surface assuming kinematic or single-scattering can be formulated as,

$$I(\underline{S}) = |f(\theta, \phi, E)|^2 \cdot |\sum_{\underline{r}_j} e^{i\underline{S} \cdot \underline{r}_j}|^2 , \quad (1)$$

where $I(\underline{S})$ is the diffracted intensity, $\underline{S} = \underline{k}_f - \underline{k}_i$ is the scattering wavevector and \underline{r}_j gives the positions of the atoms. The summation is the reciprocal space intensity and the prefactor takes into account angular and energy dependent atomic scattering factors. In the simplest approximation, the scatterers are assumed identical and scattering factors taken to be unity. Multiple scattering between atoms is included if we rewrite the scattered intensity as,

$$I(\underline{S}) = |\sum_{\underline{R}_j} e^{i\underline{S} \cdot \underline{R}_j} \cdot A_j(\underline{S})|^2 , \quad (2)$$

where $A_j(\underline{S})$ is the dynamically scattered amplitude from the jth column of atoms and \underline{R}_j is a vector from the origin to the center of the jth column. Here we have replaced a single atom by a column of atoms defined by a surface area times a subsurface depth. The important point is that $A_j(\underline{S})$ is still allowed to contain all multiple scattering processes within the jth column and the underlying atoms. This kinematic calculation is equivalent to a column approximation [Cowley, 1973] in which multiple scattering between large columns of atoms is neglected [Lent, 1984]. Then $\underline{S} \cdot \underline{R}_j$ contains all the necessary path length differences between

surface areas at different positions for diffraction to occur. These assumptions have been used before in low-energy electron diffraction (LEED) studies by Henzler (1984) and Lagally (1985). The limitation is that the columns must be smaller than the size of the terraces that are being considered, if reasonable agreement with intensities (but not necessarily positions of peaks) is to be achieved.

2.1.C. Ewald's Construction

The kinematic diffraction conditions are given by the intersection of a (Ewald) sphere of radius k with the reciprocal space intensity, where $k = 2\pi/\lambda$ is the electron wavenumber. Using the polar coordinates of the Ewald sphere we write the rectilinear projections of the scattering vector as,

$$S_x = k \cdot (\cos\theta_f \cos\phi_f - \cos\theta_i \cos\phi_i), \quad (3)$$

$$S_y = k \cdot (\cos\theta_f \sin\phi_f - \cos\theta_i \sin\phi_i), \quad (4)$$

$$S_z = k \cdot (\cos\theta_f + \sin\theta_i), \quad (5)$$

where S_x and S_y are in the low-index surface plane, S_z is perpendicular to the plane, θ_i and θ_f are the glancing

incident and final angles from the low-index plane, and ϕ_i and ϕ_f are the azimuthal incident and final angles. The geometry is shown in Fig.6. These are all angles external to the crystal with no refraction correction. The incoming azimuth, $\phi_i = 0$, is referenced to some known crystallographic orientation.

Note that the instrumental response in RHEED is asymmetric due to the glancing angles. In particular, the diffractometer is quite sensitive to disorder on the surface along the direction of the incident beam, but much less to disorder along the surface in a direction perpendicular to the beam. As an illustration, suppose the surface consisted of a mosaic of domains of average diameter L . The reciprocal space of one domain gives a (00) rod whose thickness is $2\pi/L$. Parallel to the surface, but normal to the beam direction, the diffraction streaks will have an angular thickness of $\Delta\phi_f \approx 2\pi/(L \cdot k \cdot \cos\theta_f)$. In contrast, in the direction normal to the surface, the specular beam will have a range of angles $\Delta\theta_f \approx 2\pi/(L \cdot k \cdot \sin\theta_f)$. Figure 7 illustrates the Ewald sphere intersection for the former and latter case. This broadening is along the streak and points out the sensitivity of $\Delta\theta_f$ for small θ_f to surface order. For our system it is possible to resolve order over distances greater than 8000 Å. Note that the broadening decreases smoothly as $1/(\sin\theta_f)$. This is not observed for many systems

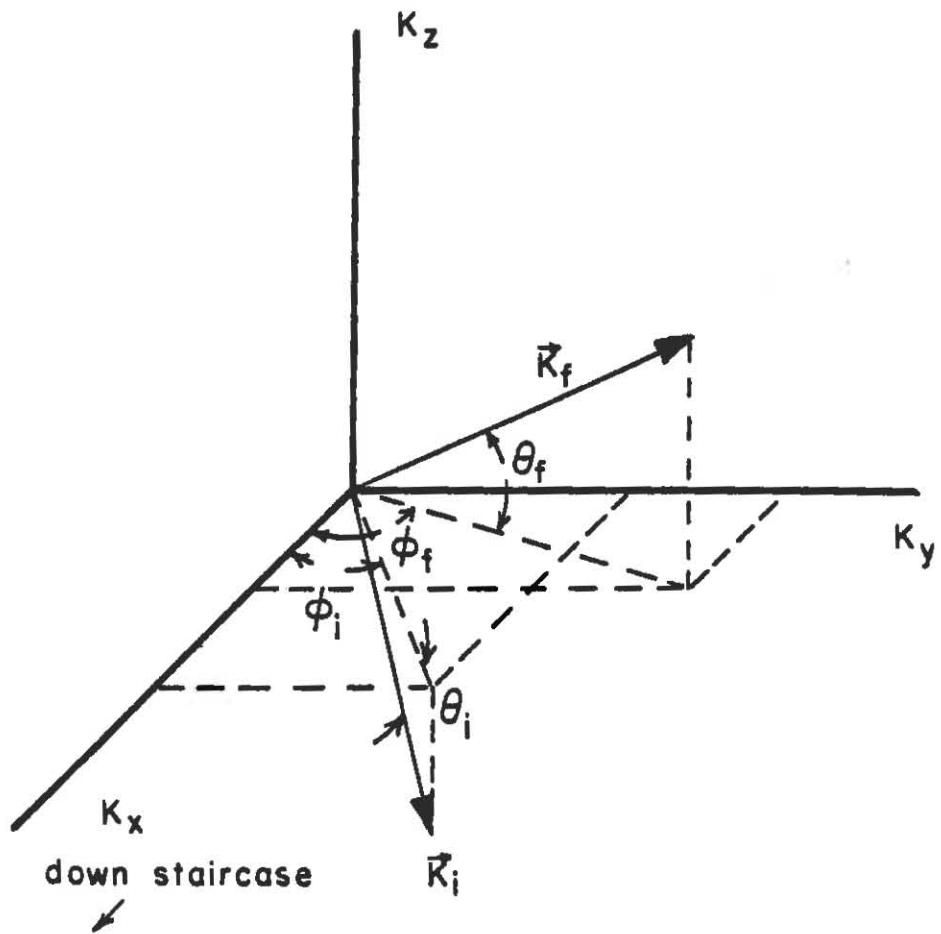


Fig.6 RHEED scattering geometry.

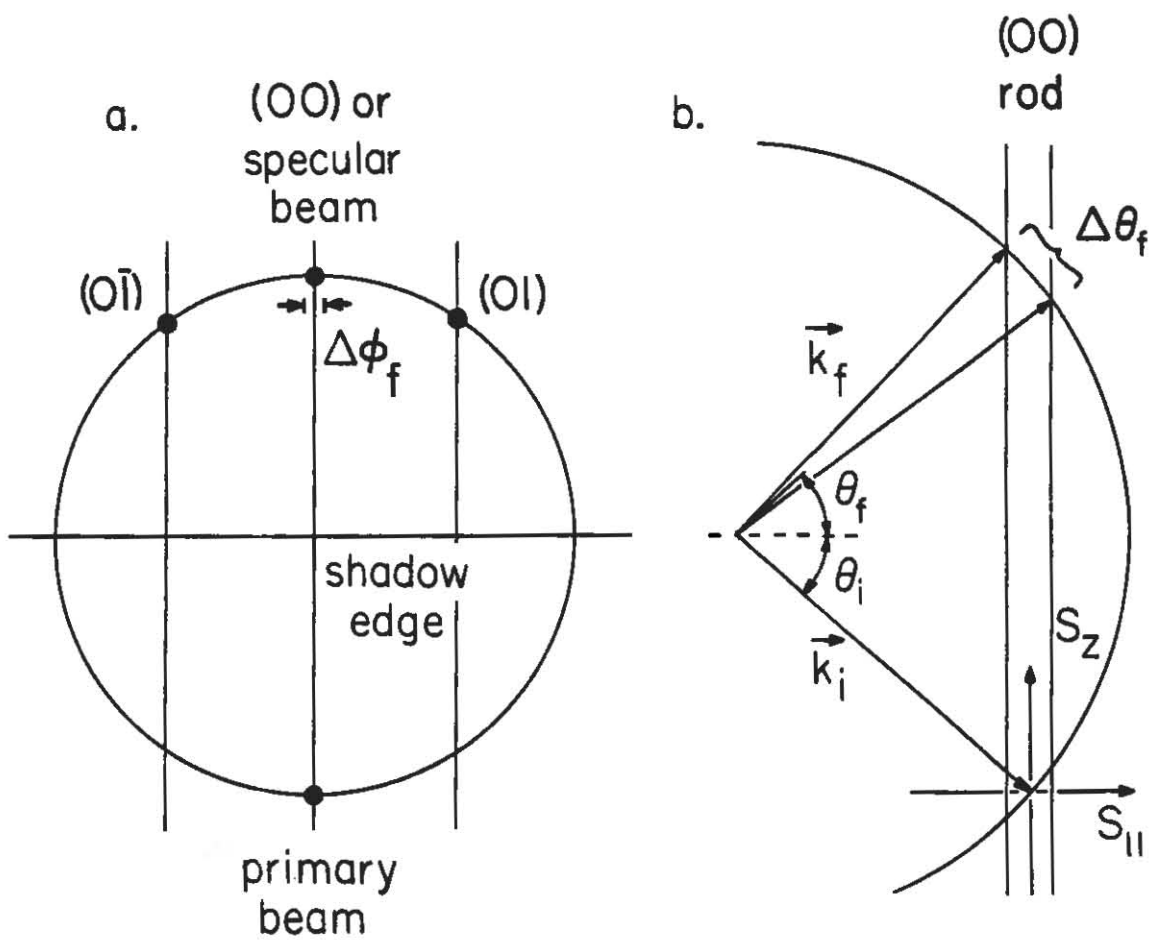


Fig. 7 a. Front view of Ewald construction.

b. Side view.

since, as will be shown, the introduction of random up and down steps modulates the broadening in a characteristic way.

It should be added that the above Ewald sphere equations are equally valid for determining lattice constants and surface reconstruction periodicities, which is the standard information normally obtained from RHEED patterns (see Appendix A). Here the columns are the same size as the lattice constant, so that good agreement with the peak positions but only poor agreement with intensities would be expected. The resolving power within a RHEED pattern therefore lies between the surface lattice constant (few Å's) to $\sim 1 \mu$.

The preceding analysis gives a framework for determining contributions to beam shape. Summarizing, one must first calculate the reciprocal space via the column approximation in terms of the scattering wave vector, \underline{S} . Then the Ewald sphere construction must be included to connect the observable quantities, θ and ϕ , to \underline{S} . Next we will calculate the diffracted intensity as a function of scattering angles for specific distributions of steps. Within the kinematic approximation, we will be able to separate disorder due to steps from other disorder by observing the dependence on scattering angles.

2.2. Diffraction from Steps

2.2.A. Diffraction from a Two-Level Surface

We first consider diffraction from a two-level surface. This is the simplest approximation to a surface that grows via a layer-by-layer mechanism. The upper level consists of the monoatomic, single-layer clusters while the lower level is the exposed substrate, as shown in Fig.8. The pair correlation $C(\underline{r})$ is defined as the probability that two surface scatterers are separated by a vector $\underline{r} = \underline{x}\hat{x} + \lambda \underline{d}\hat{z}$, where d is the interlayer separation, x is distance parallel to the surface, and z is perpendicular to the surface. For a two-level system, λ can be 0, 1, or -1. The diffracted intensity is the Fourier transform of $C(\underline{r})$:

$$I(\underline{s}) = \int C(\underline{r}) e^{i\underline{s} \cdot \underline{r}} d^3 r \quad \sum_{\mathbf{h}, \mathbf{k}} \delta(\underline{s} - \underline{G}_{\mathbf{h}, \mathbf{k}}^H) , \quad (6)$$

This formulation is equivalent to that found in Eq.1 if the clusters are much larger than the lattice constant [Lent, 1984]. Moreover, by expressing in integral form, the calculation is simplified considerably. Importantly, the correlation function approach is necessary when the arrangement of steps is not ordered.

To understand the convolution of the integral with the

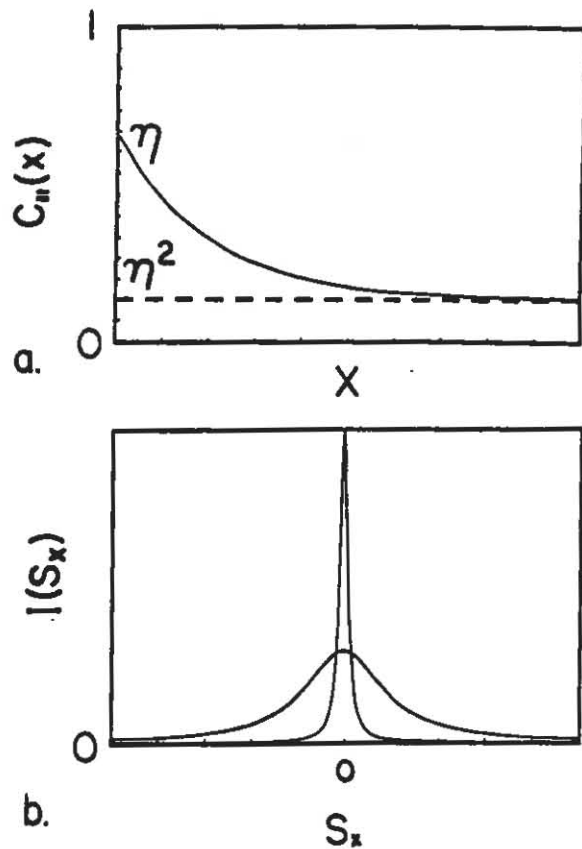
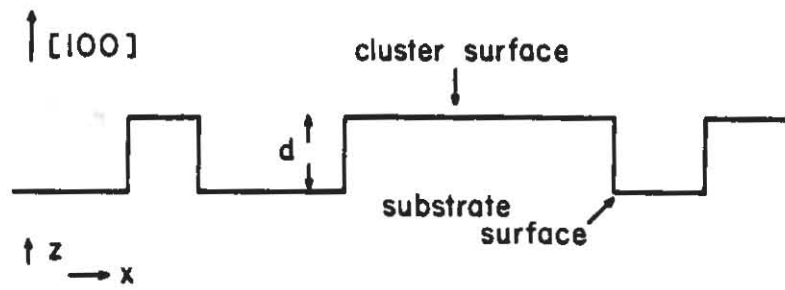


Fig.8 (top) Two-level surface.

Fig.9 a. Correlation function for two level surface.
b. Intensity profile for two-level surface.

sum in Eq.6, realize that diffraction from clusters and diffraction from surface atoms is occurring simultaneously. The integral represents scattering from the continuous clusters while the sum gives the scattering from the discrete surface atoms. The convolution in effect repeats the fundamental beam shape at each of the surface reciprocal lattice vectors, $\underline{G}_{h,k}^H = (h \cdot 2\pi/a, k \cdot 2\pi/a)$, or equivalently, each of the (hk) diffracted beams (see Figs.2 and 7a). For specular or (00) beam scattering, $\underline{G}^H = 0$. Equation 6 therefore requires only the calculation of the correlation function (in the continuum limit) for a particular disordered arrangement of steps.

The diffracted intensity within the integral of Eq.6 consists of two terms: one due to the asymptotic limiting value of $C(\underline{r})$ and the other due to the step disorder. This is the major point of the following discussion and is illustrated in Fig.9. The figure shows that the Fourier transform of the limiting value of $C(\underline{r})$ contributes a sharp spike to the measured intensity and that the decreasing portion of $C(\underline{r})$ gives broad wings. The relative size of these two components will change during growth as the interference between the two levels varies.

To see this basic form, first break $C(\underline{r})$ into a sum of partial correlation functions which explicitly show the

correlation between scatterers on different levels. For a two-level system define coverages η and $1-\eta$ for each level. The diffracted intensity is the Fourier transform of the total correlation function:

$$I(\underline{s}) = \sum_{\lambda=-1}^1 e^{-is_z \lambda d} \circ \int_{-\infty}^{\infty} C(x, \lambda) e^{-is_x x} dx , \quad (7)$$

where $C(x, \lambda)$ is the correlation function between two levels separated by λ . Explicitly, for the two-level system this can be calculated as,

$$\begin{aligned} I(\underline{s}) = & [\eta^2 + (1-\eta)^2 + 2\eta(1-\eta)\cos(s_z d)] \cdot 2\pi\delta(s_x) \\ & + 2C'_{ii}(s_x) \cdot [1 - \cos(s_z d)] . \end{aligned} \quad (8)$$

Here $C'_{ii}(s_x)$ is the Fourier transform of the reduced correlation function between atoms on the same level [Pukite, 1985].

Equation 8 is illustrated in Fig.9b. The reduced correlation function gives the broad function while the delta function gives the central spike. The central spike shown would be a delta function if the instrument and crystal had been perfect. To take into account the broadening introduced by an imperfect instrument, this function should be convoluted with the instrument's response

function. In practice, the broadening is usually limited by the macroscopic curvature of the crystal or by misorientation steps.

The correlation function transform $C'_{ii}(S_x)$ depends on the particular distribution of steps. In general it is $n(1-n)$ times a function whose integral over S_x is 2π . As an example, for a geometric distribution [Lent, 1984] in which the probability of making a step at any lattice site is a constant, independent of position, this function is a Lorentzian in S_x . The Lorentzian has full width at half-maximum (FWHM) of $2(L_1+L_2)/L_1 L_2$, where L_i is the average terrace length for the i th level. For an arbitrary distribution,

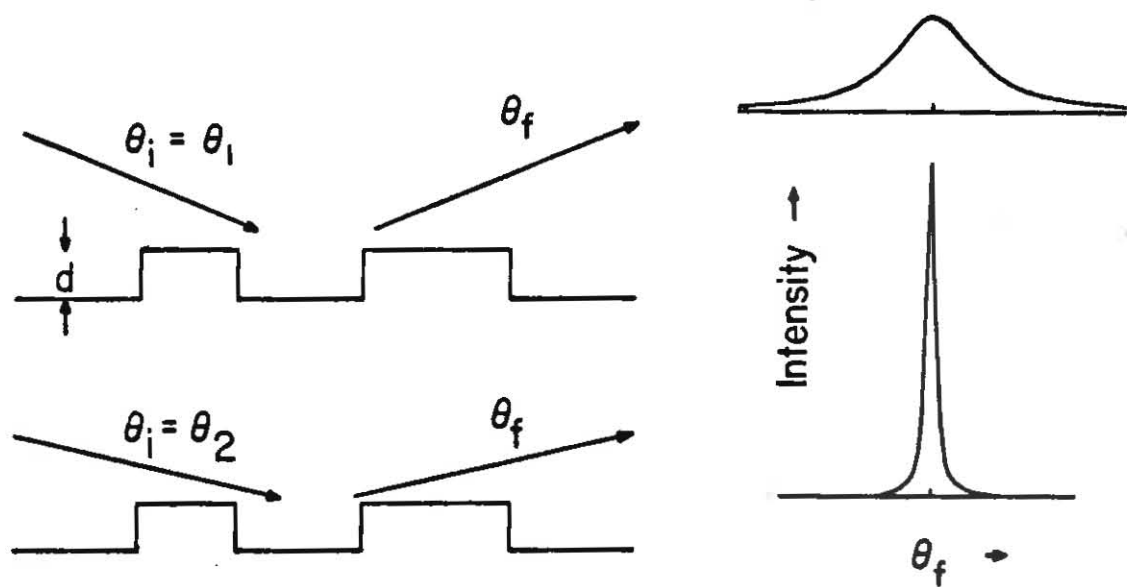
$$C'_{ii}(S_x) = \frac{2n}{S_x^2 \cdot L_2} \text{Real} \left\{ \frac{(1-P_1(S_x)) \cdot (1-P_2(S_x))}{(1-P_1(S_x)) \cdot P_2(S_x)} \right\}, \quad (9)$$

where $P_1(S_x)$ and $P_2(S_x)$ are the Fourier transforms of the one-dimensional terrace length probability density functions [Pukite, 1985].

Equation 8 also points out the main coverage and incident angle dependence (S_z from Eq.5 and S_x from Eq.3) of the two-level system. At angles where $S_z d$ is an even multiple of π (an in-phase angle), the diffraction is

insensitive to steps since scattering from the different levels is in phase, giving only a central spike. At angles where $S_z d$ is an odd multiple of π (out-of-phase angle), the diffraction is most sensitive to steps. These two conditions are shown in Fig.10. At values of $S_z d$ intermediate to the in-phase and out-of-phase angles, the diffraction profile will be a sum of the central spike and broadened components. Figure 11 shows experimentally measured profiles from a Ge(111) surface that experienced a low temperature ($T=520K$) submonolayer deposition of Ge. The separation between central spike and broad function is clearly observable, with the maximum contrast near the out-of-phase angle of 29 mrad.

Lent (1986) has previously made use of the two-level analysis to describe RHEED streak formation during low temperature (400° to 500°C) sub-monolayer deposition of GaAs. Under these conditions, the same separation of central spike and broad function is observed. At higher temperatures (near 600°C) the broad function disappears. It is concluded that sufficient thermal energy is given to the adatom clusters that migration to the step edges of the substrate occurs. The surface is then as smooth as possible and a sharp, intense profile is obtained. If the growth is monitored continuously from this point, a related phenomenon is observed. Upon reinitiating the Ga flux, the intensity of the beam oscillates in time as shown in Fig.12. The period



$$2d \sin \theta_i = n\lambda$$

Fig.10 (top) "out-of-phase" angle.

(bottom) "in-phase" angle.

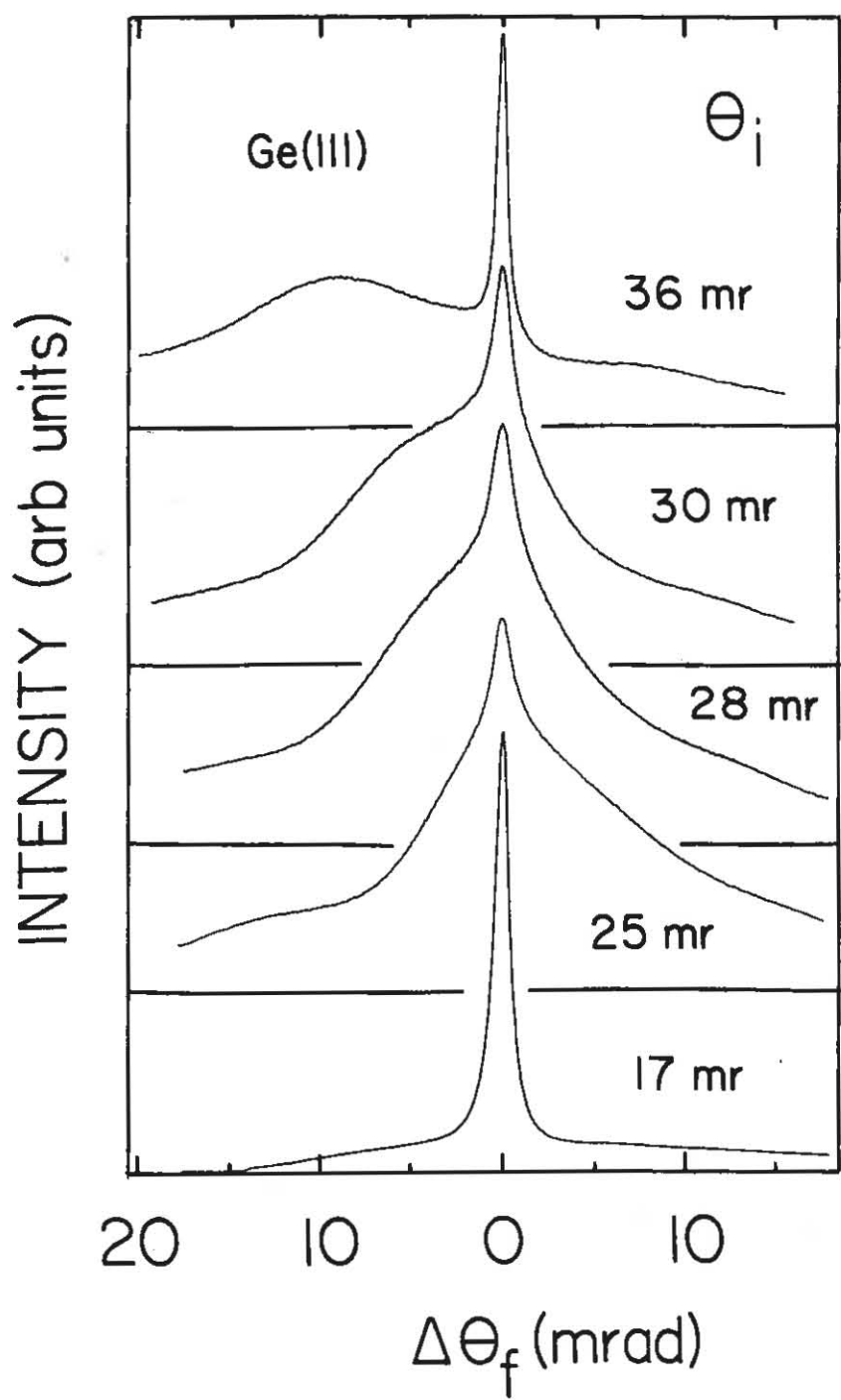


Fig. 11 Measured profiles for two-level system.

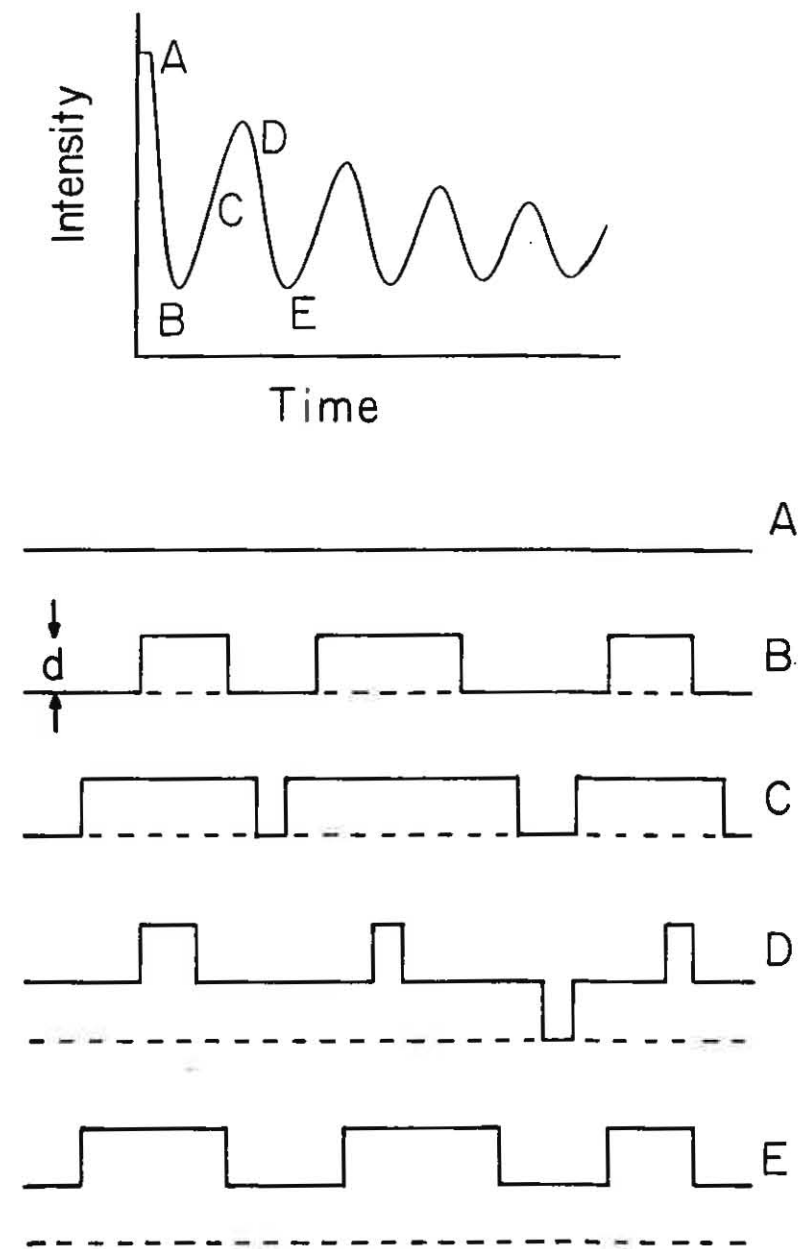


Fig.12 RHEED oscillations and cyclic surface morphology.

of these oscillations is the time required to deposit a monolayer. The intensity oscillations were first reported by Harris, 1981. The current evidence [Van Hove, 1983 and Neave, 1983] is that they are due to cyclic variations in the distribution of steps on the surface during epitaxial growth.

The mechanism that gives rise to these intensity oscillations comes from the same sensitivity to surface morphology as Fig.4. Beginning with a smooth surface the diffracted beam is sharp at all angles of incidence (point A of Fig.12). As soon as growth is started, small clusters are formed so that on an atomic scale the surface is rougher (point B Fig.12). As growth continues, adatoms preferentially diffuse to step edges until the layer is completed (points C and D of Fig.12). The cyclic variation in diffracted intensity results from this cyclic variation in morphology between smooth and rough. Like Fig.10, at incident angles corresponding to the out-of-phase condition the beam initially broadens and decreases in intensity [Van Hove, 1983]. By contrast, at angles corresponding to the in-phase angles, the width of the profile is constant. At the out-of-phase angles where the diffraction is maximally sensitive to surface steps, the amplitude of the intensity oscillations is largest. This is demonstrated in Figs.13 and 14. In Fig.13, the data for oscillations measured at several

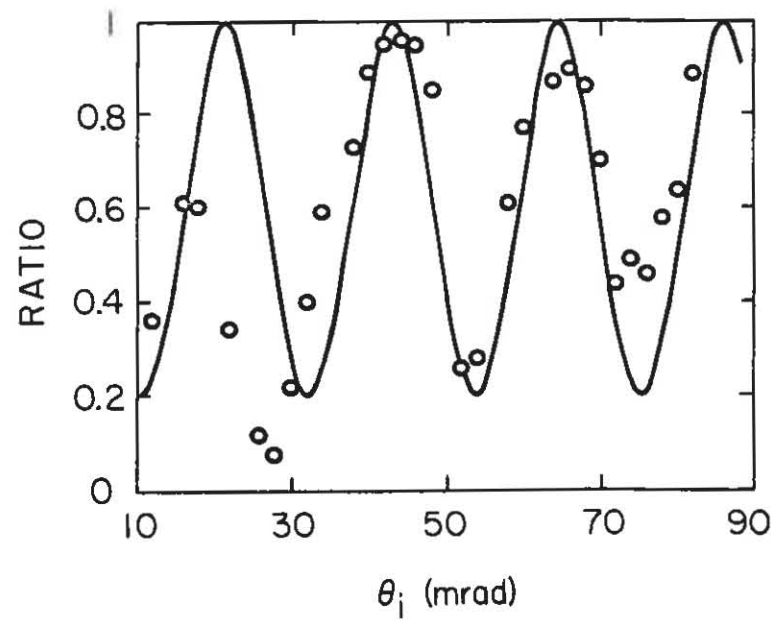
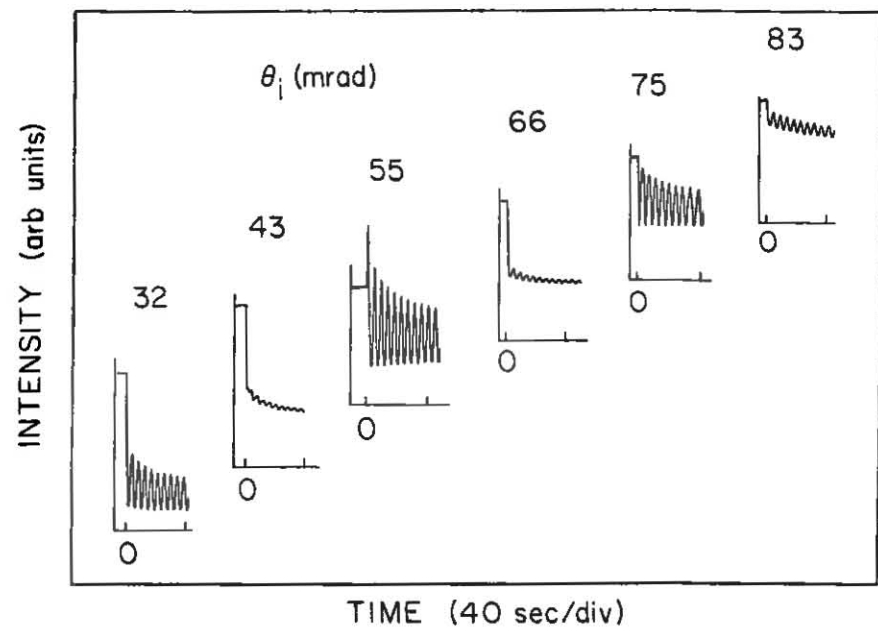


Fig.13 (top) GaAs RHEED oscillations vs incident angle.

Fig.14 (bottom) Oscillation amplitude vs incident angle.

angles of incidence are displayed; in Fig.14 the amplitude of the oscillations is plotted versus angle of incidence. The variation with angle, or equivalently scattering phase shift between different surface levels, is evident. However we should note two details. First, at low angles there is a shift in the maximum and minimum oscillation amplitude. Secondly, note that some intensities initially increase instead of decrease in Fig.13. These two effects are not well understood.

Even with these difficulties, however, much information can be obtained from temporal RHEED measurements. This will be further discussed in Sec.3, where a simple model of layer-by-layer growth is introduced and Sec.5, where RHEED measurements of growing surfaces of GaAs and Ge will be presented.

2.2.B. Diffraction from Two-Dimensional Clusters

The previous description of diffraction from a two-level surface is sufficiently general to understand the contributions of step disorder and one-dimensional distributions of steps to beam shape. In reality, monolayer-high clusters are two-dimensional objects and RHEED should be sensitive to this.

To calculate the diffraction from an arbitrary distribution of two-dimensional clusters requires a knowledge of the two-dimensional correlation function. The diffracted intensity is then the Fourier transform of this function. However, the two-dimensional correlation function is in general difficult to calculate [Pimbley, 1985]. To make the calculation more tractable, a simple system is analyzed as shown in Fig.15a. In this example, the clusters are square in shape and arranged in a checkerboard configuration. The black is one level and the white is an uncorrelated level, with a random probability of a cell being black or white of 1/2. What makes the intensity distribution particularly easy to calculate here is that this forces random or incoherent sums of phases for the various cells.

Assuming random occupancy, the correlation function for the surface is the correlation function of a single cell,

$$C(x,y) = \left[1 - \frac{|x|}{L} \right] \cdot \left[1 - \frac{|y|}{L} \right], \quad (10)$$

where $C(x,y)$ is the two-dimensional correlation function and L is the cell size. The Fourier transform of this gives the diffracted intensity,

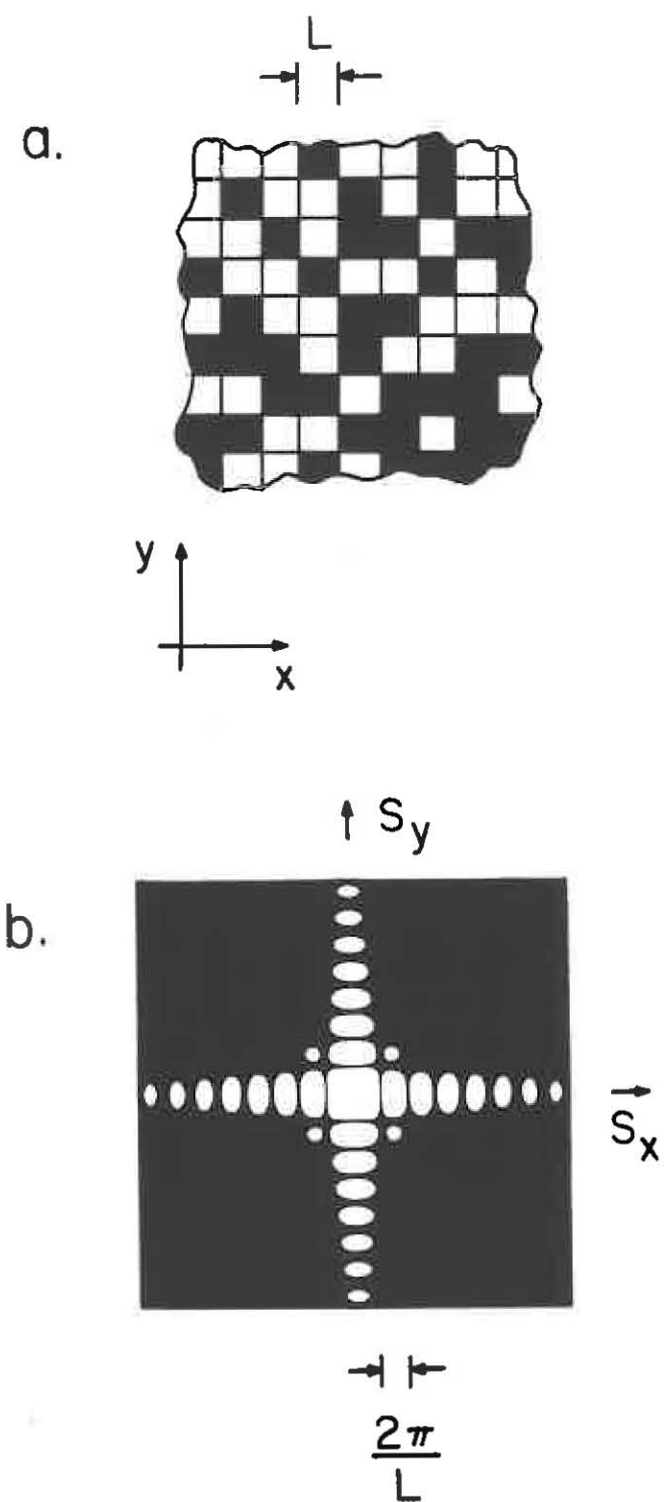


Fig.15 a. Checkerboard configuration of clusters.

b. Reciprocal space of checkerboard.

$$I(s_x, s_y) = L^2 \cdot \frac{\sin^2(Ls_x/2)}{(Ls_x/2)^2} \cdot \frac{\sin^2(Ls_y/2)}{(Ls_y/2)^2} . \quad (11)$$

Here, s_x and s_y are the reciprocal space coordinates. The most interesting feature of this intensity distribution is that most of the intensity is located along the two reciprocal space axes. This is a purely geometric diffraction effect, known from Fourier optics. A contour map of the intensity distribution is shown in Fig.15b. In a real system, disorder in the sizes of clusters would be expected to occur. This would tend to smoothen out the zeros in the shape in Fig.15b. However, the tails along the axis would remain.

The smoothed shape described can be derived if we assume independent geometric distributions for the x and y coordinates. If the cell size distributions are given as,

$$P_x(L) = \alpha \exp(-\alpha L), \quad (12)$$

$$P_y(L) = \beta \exp(-\beta L), \quad (13)$$

then a Markov-like or geometrically random two-dimensional grid of lines can be made on the surface. The correlation function can then be calculated if the cells describing the intersections are randomly occupied with probability 1/2.

This is shown in Fig.16a, with black describing clusters and white describing substrate. In this example $\alpha=\beta$. The intensity distribution from such a surface is given by (see Appendix B),

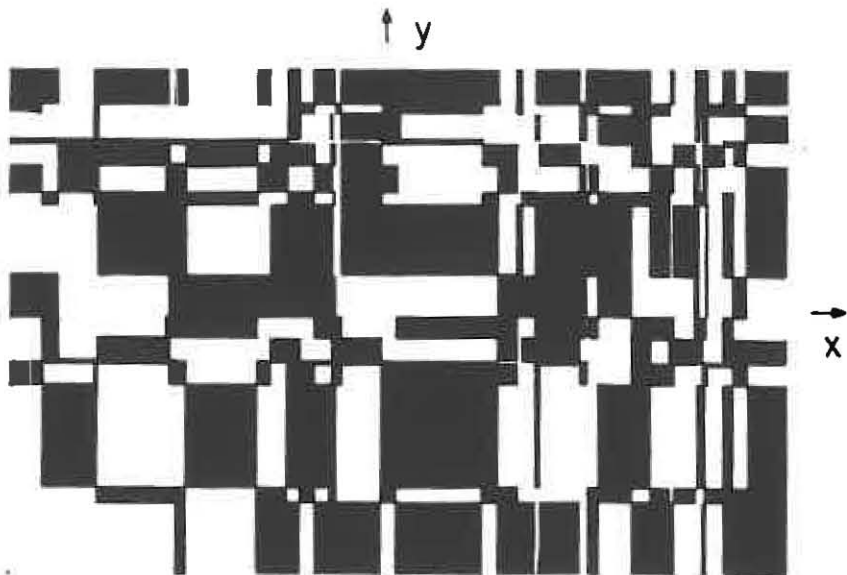
$$I(s_x, s_y) = \frac{\alpha}{s_x^2 + \alpha^2} \cdot \frac{\beta}{s_y^2 + \beta^2}, \quad (14)$$

which is the product of two Lorentzians. The 0.001 of peak maximum contour of this distribution is shown in Fig.16b. The average length of terraces in the two directions are given by $\langle L_x \rangle = 2/\alpha$ and $\langle L_y \rangle = 2/\beta$.

The transformation of the intensity map to a diffraction pattern is straightforward when applied to LEED. In this case, the diffraction pattern would be exactly Fig.16b. The spot shape can then be considered as a finite size effect and a direct comparison to experiment can be made. However in RHEED, the transformation is more complex. If one is to compare to experiment, the RHEED transformed intensity map must be calculated.

As a rule the glancing geometry of RHEED will elongate the distribution of Fig.16b along the direction of the incident beam. For example, if the electron beam was oriented along the x axis of the clusters, the projected diffraction pattern would show the profile along s_x to

a.



b.

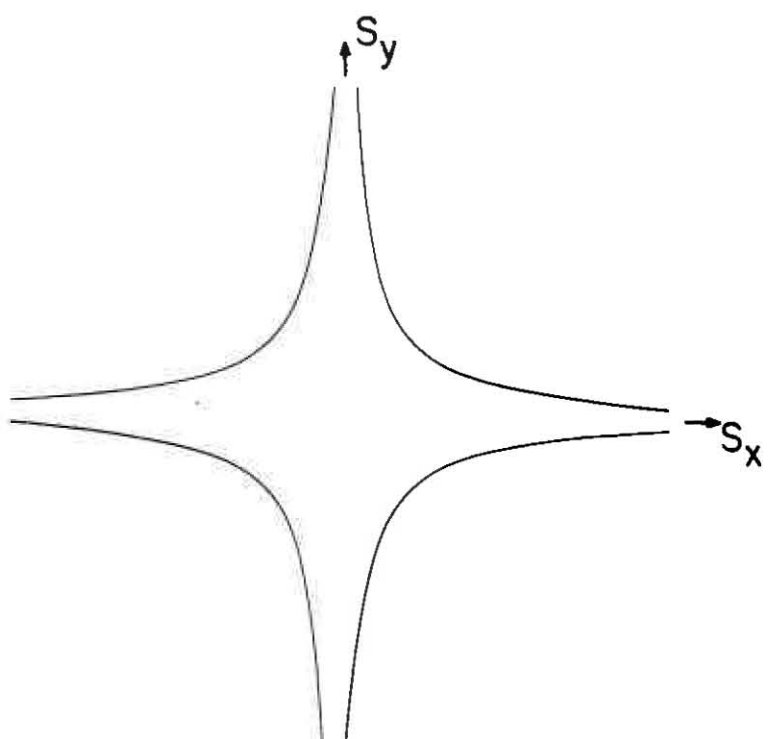


Fig.16 a. Geometric distribution clustering.

b. Reciprocal space of geometric clustering.

elongate. To determine what the expected beam shape should be requires the inclusion of Eqs. 3 and 4. When $\phi_j = 45^\circ$, the electron beam is directed along the diagonal of a cell. Figure 17 shows the RHEED projected intensity distribution at this azimuth for an angle of incidence of 28 mrad. Here the streaking is normal to the surface much like Figs. 3b and 7b, but with structure resulting from intensity lying along the two reciprocal space axes. In the results section, we will compare this plot to measurements. The shape of the clusters measured will help in determining the nature of the growth process and the nature of the static surface step configuration. In particular, strong geometric effects are observed in the case of Ge with adsorbed amounts of As.

The ideal behavior of a surface with clusters is closely realized if the initial surface is a low-index plane. Cut and polished surfaces that are slightly misoriented will possess a staircase of steps in one direction. The diffraction from such a surface exhibits its own dependence on scattering angles, which is described next.

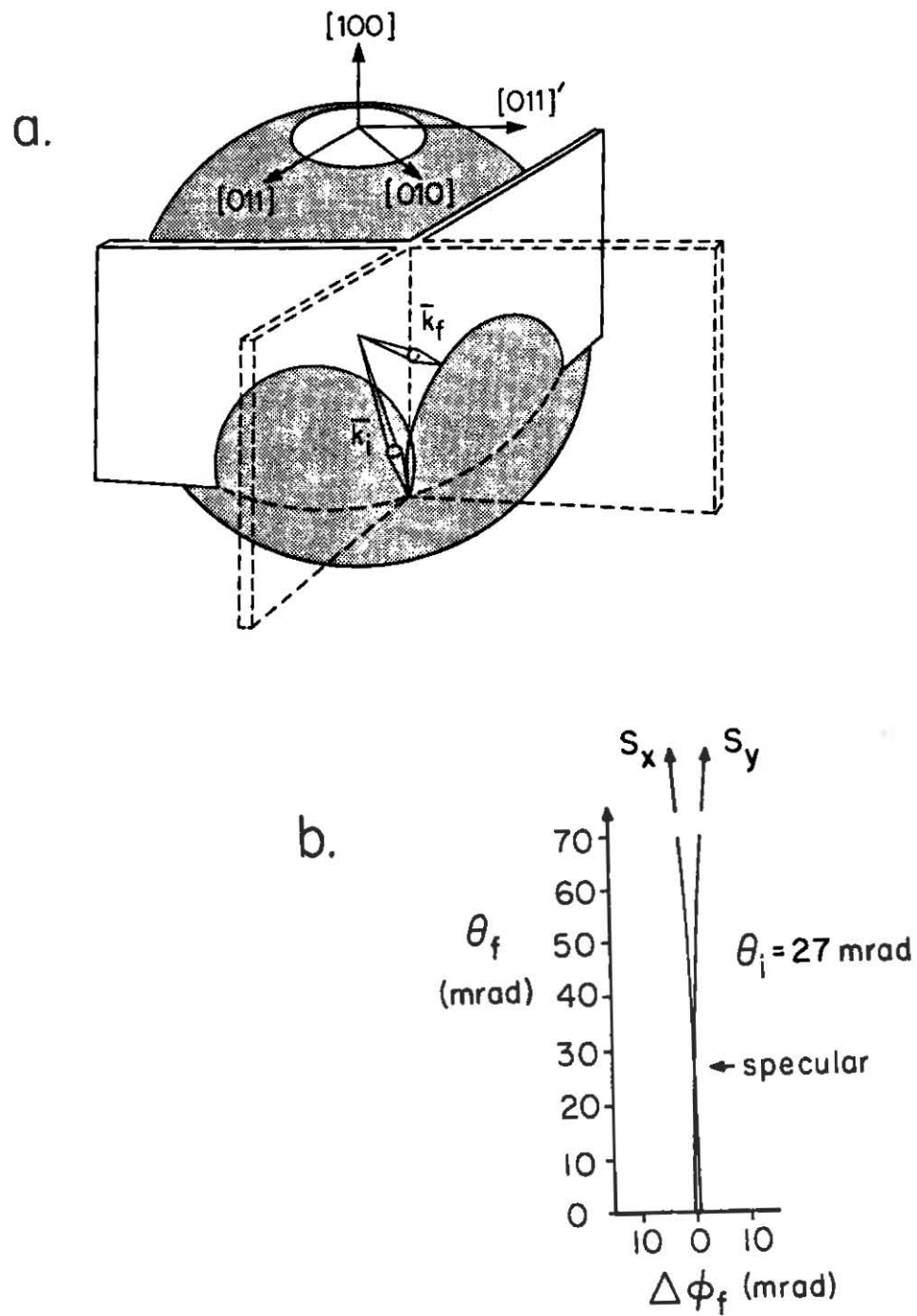


Fig.17 a. Ewald sphere intersection of Fig.16b.
b. RHEED projection on phosphor screen.

2.2.C. Diffraction from Vicinal Surfaces

A vicinal surface consists of low-index terraces separated by steps of some multiple of the interlayer spacing. We define an ordered array of steps, often called a regular staircase [Henzler,1984], to mean that all the steps are the same height and separated by the same distance (see Fig.5). To calculate the diffracted intensity from the regular staircase, one can use Eq.1 directly. Qualitatively, one should expect that diffraction from a vicinal surface at in-phase angles should give a narrow profile. This is explained by waves scattered from adjacent terraces possessing a path length difference of an integral multiple of λ and therefore not being sensitive to the step separation. Away from these angles, the specular peak splits into two or more components (see Fig.5). The periodicity or, more accurately, quasiperiodicity of the steps is responsible for this splitting.

The Ewald construction for a vicinal surface, shown in Fig.18, illustrates these ideas in more detail. Following Henzler (1984), the surface can be thought of as the convolution of a finite terrace with an infinite grating of the step edges, inclined at an angle θ_c to the low-index plane. The reciprocal lattice is the Fourier transform of this convolution and equals the product of the Fourier

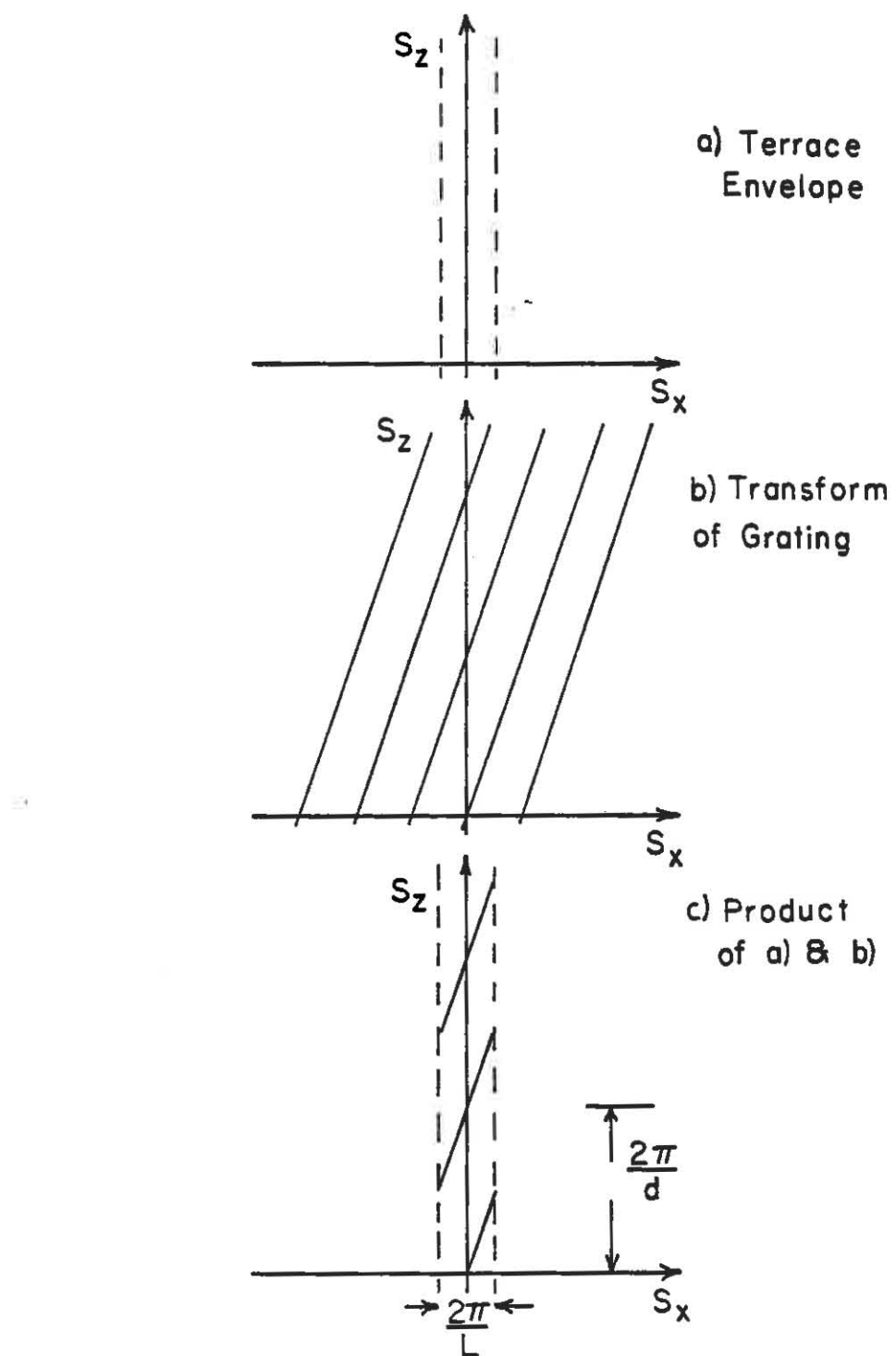


Fig.18 Reciprocal space of staircase.

transform of the finite terrace and the transform of the grating of step edges. This product reciprocal lattice is graphically shown in Fig.18 for the (00) rod, where the dashed lines indicate the broadened rod due to a finite sized terrace and the inclined slashes correspond to the reciprocal lattice of the longer grating of step edges. Since the product of the two are taken, one does not expect that slashes extending past the dashed envelope will contribute very much intensity to the diffraction. In Fig.19a, the Ewald sphere is superposed on the product reciprocal lattice, and one can see that there are two strong intersections with the staircase reciprocal lattice.

On real surfaces, there is randomness in the distribution of terrace lengths and step heights as shown in Fig.20a. Qualitatively, this will broaden the slashes beyond the instrument limit, with the greatest broadening occurring near the out-of-phase condition. This is shown in Fig.20b with the ratio indicating a 50% fluctuation in terrace lengths (c.f.[Pukite,1985]). If a quantitative measure of the step array disorder is desired, then a correlation function approach is needed. For a given probability distribution of terrace lengths, $P(L)$, the intensity profile can be calculated as,

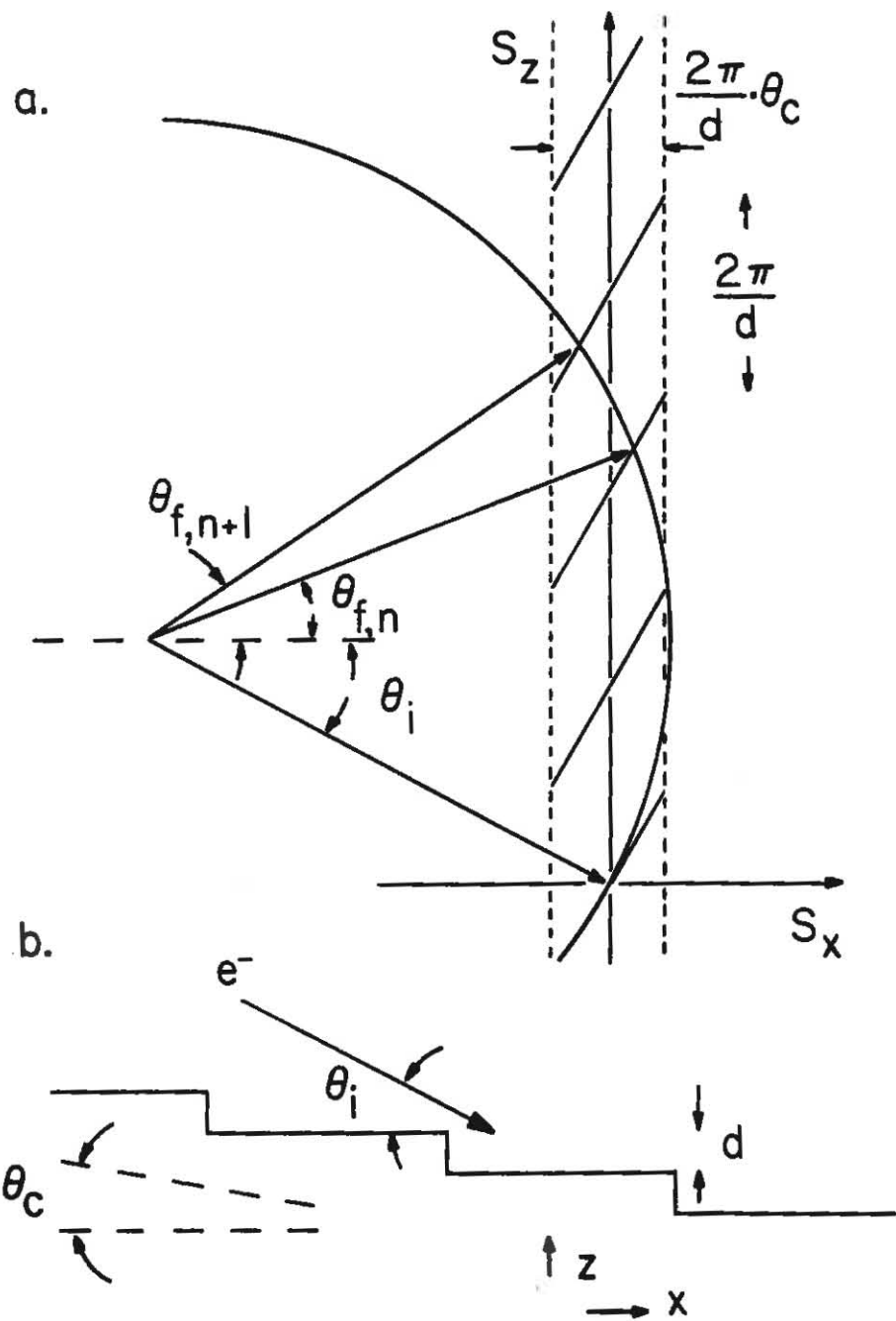


Fig.19 a. Ewald sphere intersection of Fig.18.
b. Real space scattering geometry.

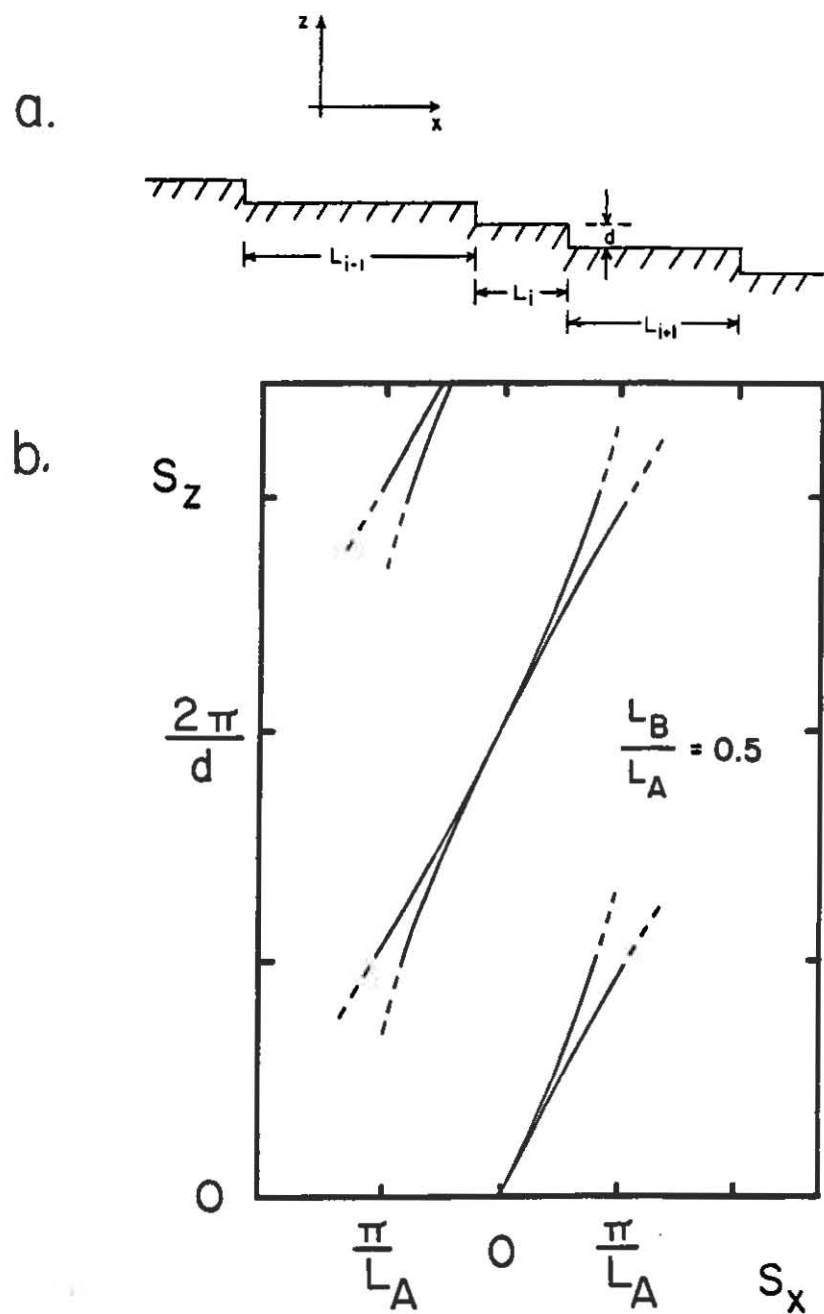


Fig. 20 a. Disordered staircase.

b. Reciprocal space of disordered staircase.

$$I(s_x, s_y, s_z) = \frac{2}{s_x^2 \langle L \rangle} \cdot \frac{(1 - |P(s_x)|^2) \cdot (1 - \cos(s_z d)) \cdot \delta(s_y)}{|1 - P(s_x) e^{-is_z d}|^2}, \quad (15)$$

where $P(s_x)$ is the Fourier transform of $P(L)$ [Pukite, 1985].

It should be noted that the staircase can be remarkably disordered and still give observable splitting. This means that there are still two strong intersections with the broadened staircase reciprocal lattice rods. The precise condition for splitting is that the probability of a terrace of length L be peaked at a value greater than zero and less than the distance resolvable by the instrument. The larger the mean square fluctuation in the distribution of terrace lengths, the weaker the splitting will be. An example is worked out in Appendix C.

To determine the kinematic scattering angles from a sufficiently ordered staircase, use the Ewald construction in the form of Eqs.(3,4,5). Choose the incident azimuth, $\phi_i = 0$, to be directed down the staircase. Then the reciprocal lattice of the staircase edges is given by,

$$s_x = \theta_c \cdot (s_z - 2\pi n/d) , \quad (16)$$

$$s_y = 0 , \quad (17)$$

where d is the step height and $n = 0, 1, 2, 3, \dots$. A characteristic dependence of the splitting in diffracted final angles is observed if the incident azimuth is rotated away from the staircase direction.

The separation in θ_f can be analytically calculated as a function of the glancing scattering angles:

$$\theta_f^2 + 2\theta_c(\cos\phi_i)\theta_f = \theta_i^2 - 2\theta_c(\cos\phi_i)\theta_i + 4\pi n\theta_c(\cos\phi_i)/kd \quad (18)$$

gives for $\Delta n=1$,

$$\Delta\theta_f = \frac{(2\pi/kd) \cdot \theta_c \cos\phi_i}{\langle\theta_f\rangle + \theta_c \cos\phi_i} , \quad (19)$$

where $\theta_c \cos\phi_i$ is the projected misorientation along the incident beam direction and $\langle\theta_f\rangle$ is the average final angle corresponding to the n and $n+1$ diffraction peaks.

To show the dependence on azimuth we take a particular example. We choose 10 keV electrons ($k = 51.5 \text{ \AA}^{-1}$), $d = 2.83 \text{ \AA}$, and $\theta_c = 2^\circ$ ($L = 81 \text{ \AA}$). For a fixed incident angle of 75°

mrad (fourth out-of-phase condition), Fig.21 shows how the two primary peaks change their separation as ϕ_i is varied. Clearly the maximum separation is observed in θ_f when the beam is directed down the staircase. This is the geometry of Fig.19. Away from this azimuth $\Delta\theta_f$ is decreased but $\Delta\phi_f$ is increased. A rotation of $\pi/2$ from the staircase direction gives the maximum $\Delta\phi_f$ but it still is 10 times less than the splitting observed in θ_f . This illustrates the great resolution inherent in RHEED. Previous studies of vicinal surfaces [Hottier,1977] have concentrated on $\Delta\phi_f$, ignoring the high resolving power along the beam direction.

Figure 22 shows the comparison of theory with the measured diffraction from several misoriented GaAs samples [Pukite,1984]. Here, the difference between the final angles is plotted, $\Delta\theta_f = \theta_{f,1} - \theta_{f,2}$, where $\theta_{f,1}$ and $\theta_{f,2}$ are the intersections of the Ewald sphere with the inclined slashes of the reciprocal lattice (of the step edges) that are separated by $n = 1$. Note from Fig.21 that when the incident azimuth ϕ_i is not zero, these two Ewald intersections are also separated azimuthally, but that difference is not plotted. In the figure, the closed symbols are data and the solid curves are calculations described next, with both measurements and calculation made at the out-of-phase angle of 51 mrad.

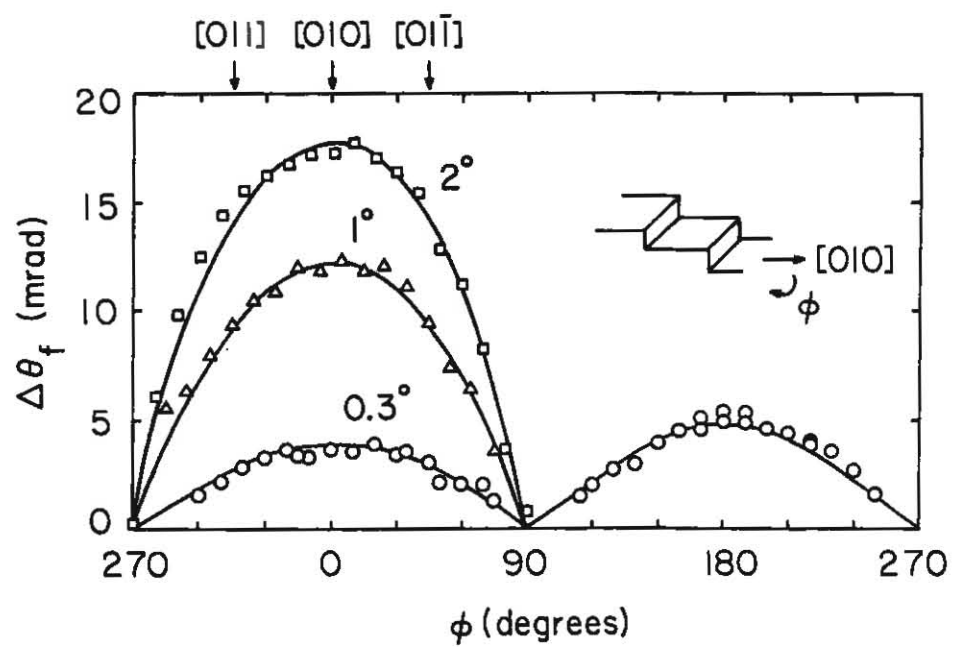
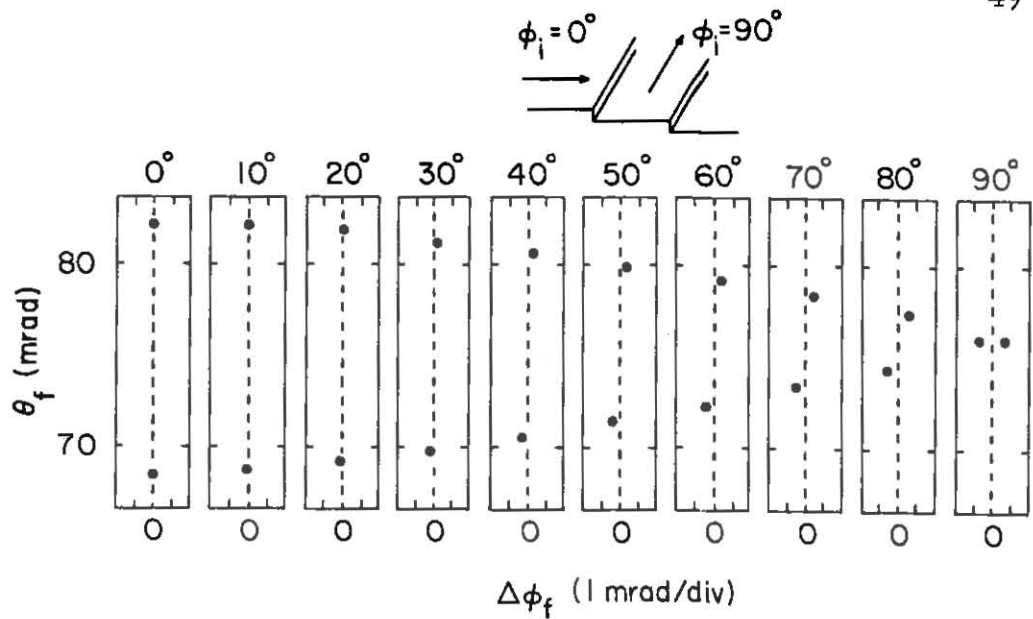


Fig.21 (top) Azimuthal dependence of staircase splitting.

Fig.22 (bottom) Measurement of splitting from GaAs.

Figure 23 shows the dependence of splitting as a function of incident angle from a GaAs surface misoriented by 6.5 mrad. The shadow edge is used to determine the scattering angles. The position of the measured points to those calculated from Eq.19 is shown in Fig.24. It should be stressed that this technique can be used to determine step heights and periodicities from any misoriented crystalline surface. In this investigation, misoriented surfaces of GaAs, Ge, and Si will be measured in Sec.5. This will further the understanding of the homoepitaxial and heteroepitaxial growth processes on stepped surfaces.

2.2.D. Diffraction from Facets

Diffraction from three-dimensional asperities can be treated in a very similar way to that of vicinal surfaces, if the asperities have a preferred shape. If the shape exposes predominately one kind of (hkl) plane then the asperities can be interpreted as pyramids or truncated pyramids as shown in Fig.25a,b. These are referred to as pyramidal facets. Since the sides of a facet are inclined to the (100) surface, these can be considered as stepped surfaces, albeit with very short terraces. Following the analysis of the last section, the angle of the reciprocal lattice rods can be calculated as shown in Fig.25c. Therefore, the RHEED pattern of this surface gives the

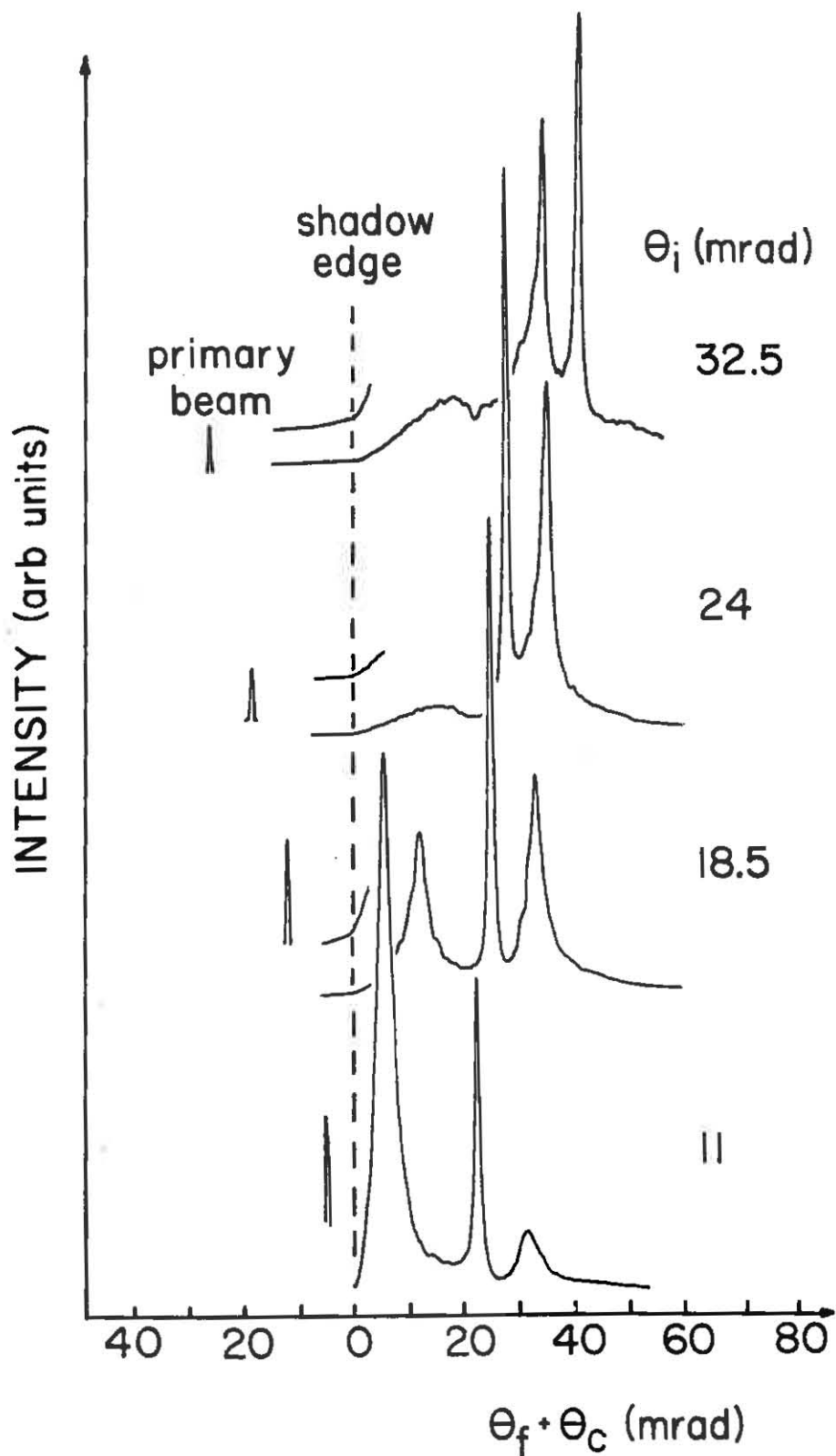


Fig. 23 Measured splitting profiles vs incident angle.

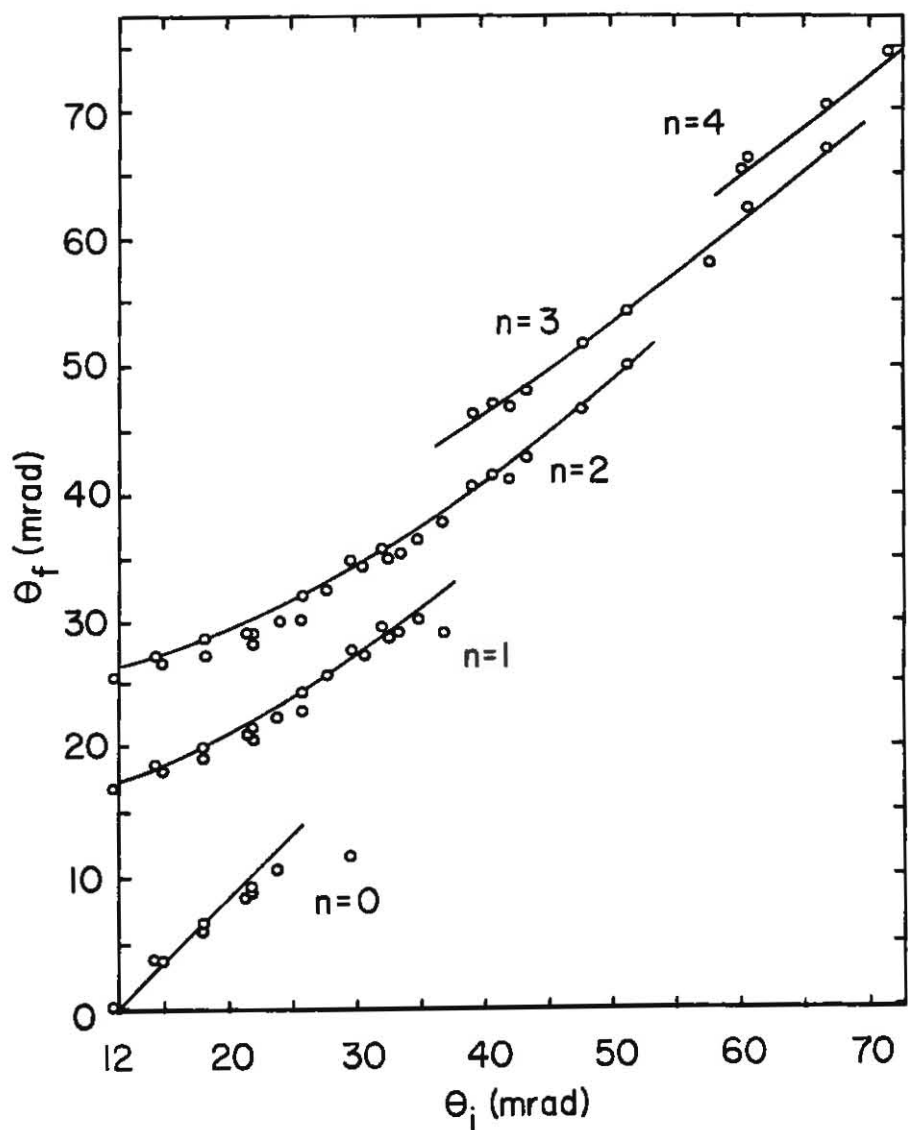


Fig. 24 Comparison to theory of splitting vs incident angle.

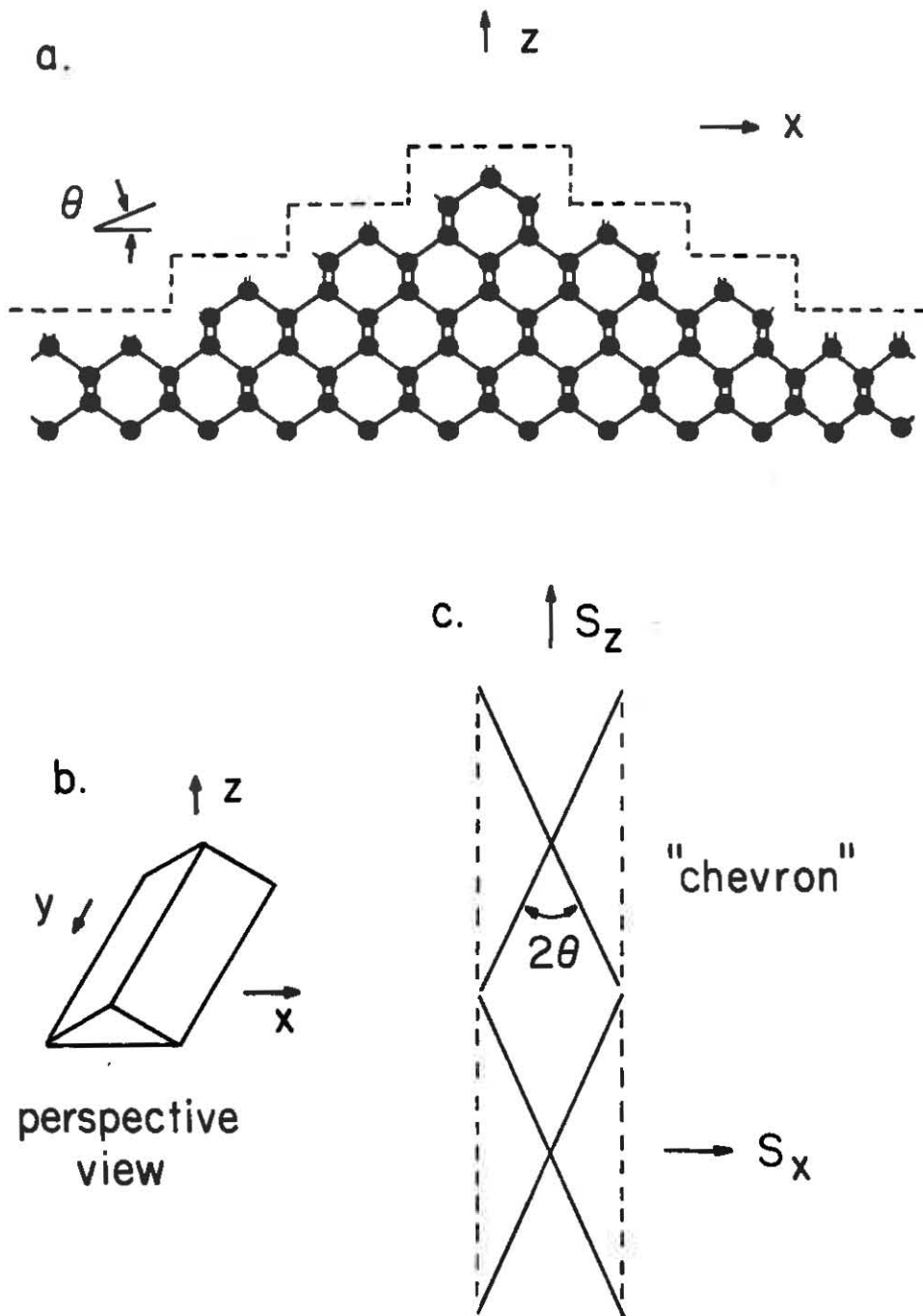


Fig. 25 Facet geometry and reciprocal space.

reciprocal lattice cross section of the asperities.

These cross sections have been reported in the literature as "chevrons", "arrowheads", or "rockets". The "chevrons" observed typically are asymmetric with the downward tails usually much stronger than the upward tails. Electron refraction has been thought to contribute to this effect [Miyake, 1938]. Experimentally, by comparing measured angles to those calculated, the preferred (hkl) face of a pyramidal facet can be obtained. This will be used in Sec. 5.3 and 5.4.

Chapter 3

Crystal Growth Mechanisms and Theoretical Results

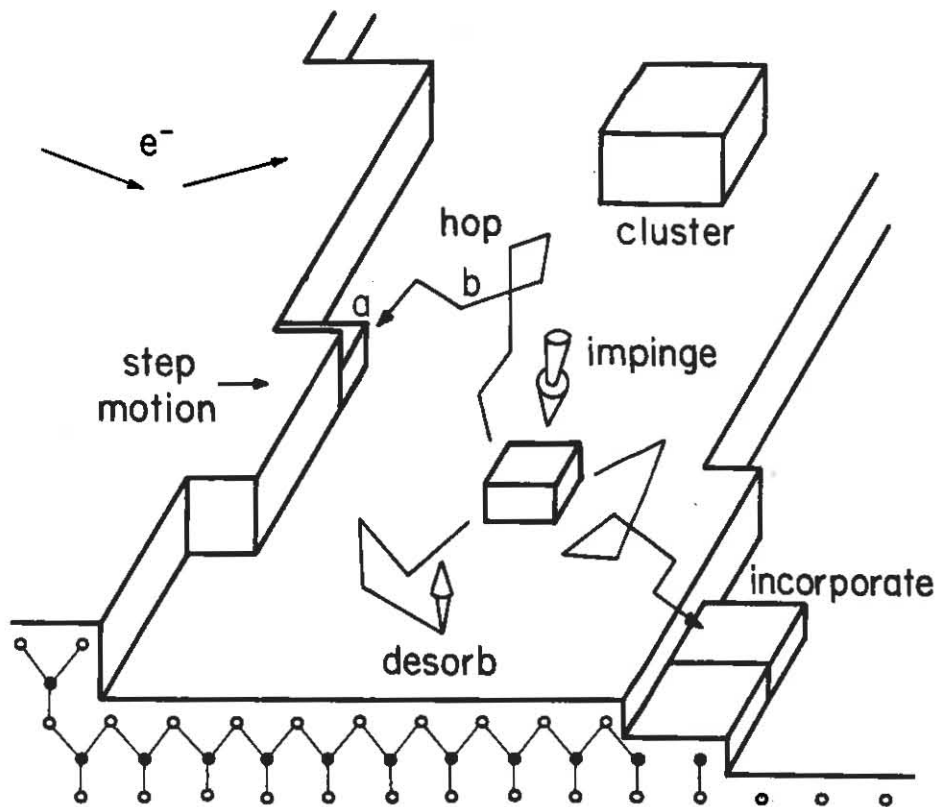
The growth of GaAs and other III-V materials by MBE has provided precise control for the fabrication of layered structures in many electronic and opto-electronic applications. This control is particularly important at the heterojunction interfaces incorporated in many of the devices. For example, the quality of an interface is influenced by the transition between dissimilar materials and the smoothness of the initial surface. MBE is able to meet these requirements as it is a low temperature process that employs fast switching (relative to the growth rate) between constituent fluxes, thereby achieving abrupt interfaces with limited interdiffusion between the layers. If the growth of the layers can be better understood the quality of ultrathin superlattices and metastable structures will likely improve.

In this section the fundamental mechanisms controlling MBE will be reviewed. We will describe how steps, clusters, and asperities (detailed in the previous section) are important in the growth process. In Sec. 3.2, the problems associated with heteroepitaxial growth and, in particular, that of polar on non-polar growth will be outlined. This will provide a basis for understanding the RHEED

measurements of GaAs/Si and GaAs/Ge growth in the results section. In Sec.3.3, we develop a model of diffusion-driven, homoepitaxial growth on a stepped surface. The solution of the partial differential equations describing the growth uncover time-dependent behavior that has some complicated dynamics. Further, using the diffraction theory outlined in the previous section, we can simulate the RHEED behavior during this process. The results of the simulation and diffraction calculation compare amazingly well with the experimental RHEED measurements of intensity oscillations on stepped surfaces. The hope is that this calculation will help in the understanding of the interactions between adatoms and steps that lead to the growth of a smooth epitaxial layer. Before this is attempted though, some basic ideas must be presented.

3.1. Molecular Beam Epitaxy

The first stage of growth from the vapor phase is impingement and adsorption of the atomic or molecular species onto the crystal surface. In this state the adatom can be considered weakly bound due to its low coordination. It can then randomly walk by hopping to an adjacent site until incorporating or reevaporating as shown in Fig.26. For an elemental material like Ge, both the gaseous and adsorbed species exist as a monomer. In the case of GaAs, less is



$$\text{substrate misorientation} = \frac{d}{\langle L \rangle}$$

◦ - As

• - Ga

Fig. 26 GaAs(100) surface showing growth processes.

known about the adsorbate stage. Pioneering work done by Arthur [1968] and Foxon and Joyce [1975] has provided an initial understanding of the adatom species involved. From these studies, it is well understood that Ga exists as a monomer and is the rate controlling step during the homoepitaxial growth. Arsenic impinges as either a dimer or tetramer depending on whether the tetramer is dissociated before arriving. Once on the surface it is believed to exist in a weakly bound precursor dimer state As_2^* that will reevaporate unless sufficient Ga is present.

The classical mechanism for crystal growth allows for the weakly bound adatoms to migrate to regions of higher coordination or deeper potential wells such as substrate step edges [Burton, 1951] or cluster step edges. This can be seen in Fig. 26, as the probability of nucleation at point b is considered to be much less than the probability of incorporation at point a. Therefore, if adatoms impinging at point b are given enough time and thermal energy to migrate to point a, a net reduction in free energy will be obtained. If the binding energies for the various sites are known then the most likely configuration can be determined.

A complicating issue is the presence of surface reconstruction. The reconstruction lowers the surface free energy and is thought to stabilize the growth front

[Giling,1985]. For example, the bulk-terminated (100) face of diamond will not change surface free energy (number of dangling bonds) with the introduction of a growth unit, neglecting next nearest neighbor interactions (i.e. reconstruction). Therefore, such a surface should grow atomically rough. However, the reconstruction of a (100) surface leads to an increased surface energy if adatoms disrupt the local bonding arrangement and form isolated growth units. Under these circumstances, the free energy change is minimized by incorporating atoms at only the step sites. Because of these reasons, for reconstructed surfaces such as (100) GaAs and Ge, the lowest energy growth process is believed to be step propagation from clusters or substrate steps.

For Ge(100) and also Si(100), a 2×1 reconstruction is observed over a wide temperature range. Because of two possible domains, this reconstruction is generally observed as a 2×2 diffraction pattern. The RHEED measurement of this pattern is detailed in Appendix A. Fig.27 shows a ball and stick model corresponding to this surface with the outward directed sticks denoting surface dangling bonds. The 2×1 reconstruction is considered to result from pairing or orbital rehybridization of adjacent atoms that are in the dangling bond, [011] direction (Fig.27b) [Tromp,1987].

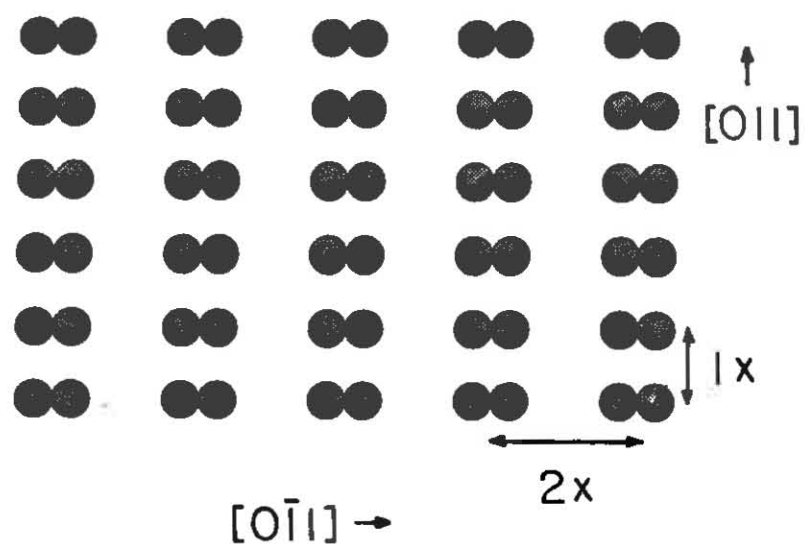
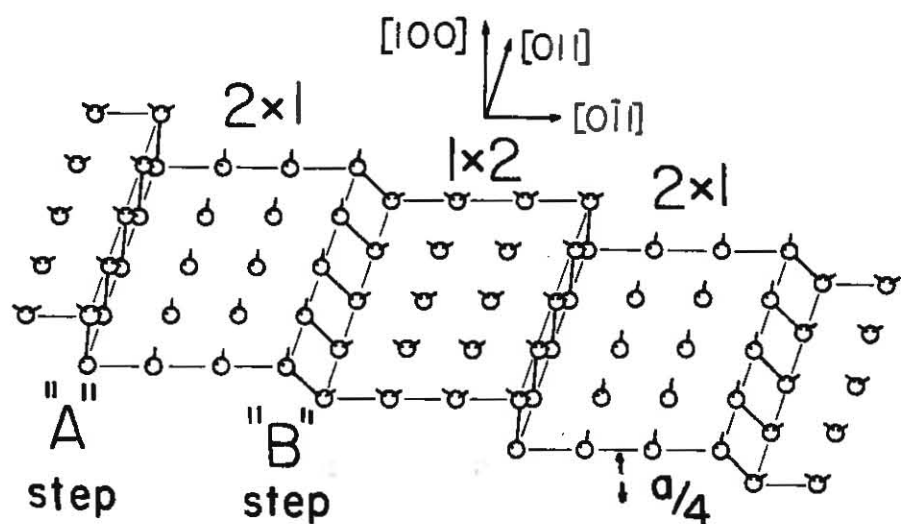


Fig.27 a. Misoriented Ge(100) surface.

b. Reconstruction of Ge surface atoms.

GaAs(100) exhibits several reconstructions. These can be separated into As-stabilized and Ga-stabilized depending on whether the surface is As rich or As deficient. The reconstructions can be obtained by varying As flux or substrate temperature independently [Cho, 1971]. Typically, growth is performed under As-stabilized conditions and a 2×4 reconstruction (see Fig.2 and Appendix A). In this case, the 2× is thought to be a pairing of adjacent As atoms similar to that of Ge. The 4× may be caused by a missing dimer [Pashley, 1987]. Fig.28 shows two types of unreconstructed, stepped, As-stabilized surfaces. The two types of domains are possible since the introduction of substrate steps reduces the crystal symmetry with respect to surface bonding geometry. This is important because while Ge(100) can show both domains at once (see Fig.27), single crystal GaAs can show only one domain or the other. This will be repeatedly referred to in Sec.5, where results of anisotropic growth mechanisms on stepped GaAs and Ge surfaces and heteroepitaxial growth of GaAs on stepped Ge and Si will be presented.

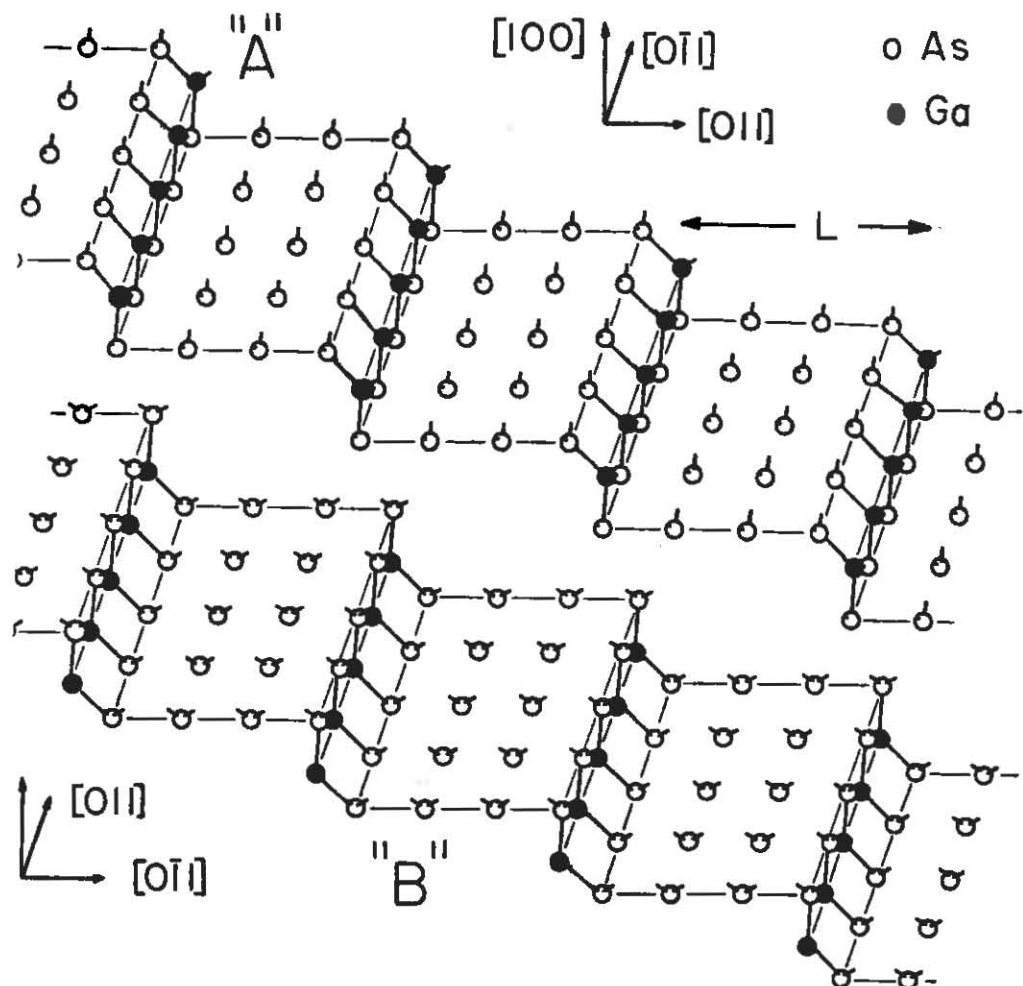


Fig.28 Misoriented GaAs surface showing
(top) Ga terminated steps
(bottom) As terminated steps.

3.2. Classifications of Growth Modes

The previous section outlines the basic surface mechanisms involved in molecular beam epitaxy. As evidenced by the lack of knowledge concerning adatom species, little predictive power exists in determining the actual growth process. Many experimental observations over a variety of growth systems (reviewed by Venables, 1984) reveals that there are several growth modes characterized by distinguishing features. Among these are layer-by-layer (Frank-van der Merwe) growth and three-dimensional (Volmer-Weber) growth. These can be further categorized as to whether they involve homoepitaxy or heteroepitaxy, elemental or compound materials, and lattice-matched or lattice-mismatched materials.

Layer-by-layer epitaxy is the preferred growth mode for several technological reasons, of which the capability of maintaining smooth surfaces and interfaces is the most important. Madhukar (1983), Dudley (1987), and Rockett (1987) have used Monte Carlo simulations to gain a better understanding of the kinetics of this growth process. However, many details of the layer-by-layer growth remain unresolved.

Three-dimensional growth by definition implies rough

surfaces consisting of asperities. The phenomenological differences between the two modes are shown in Fig.29. Why a material grows layer-by-layer or three-dimensionally is not completely understood. However, in the case of heteroepitaxial growth, it is generally accepted that if the epitaxial material would rather bond to itself rather than with the substrate, a three-dimensional growth mode will result. This is observed with several heteroepitaxial combinations but not all. The technologically important AlGaAs/GaAs is one instance where layer-by-layer growth can be achieved at all stages of heteroepitaxy.

The heteroepitaxial system that is the main thrust of this investigation is GaAs/Si and GaAs/Ge. These two systems involve all the combinations listed above and ask the same questions regarding the growth process. Additionally, the origin of antiphase domain free growth of GaAs on Ge and Si(100) is not understood [Fischer,1986]. The fundamental issues we will address are, first, the growth of a polar, zincblende lattice on a nonpolar, diamond substrate [Kroemer,1986] and, second, the observed three-dimensional nucleation of GaAs on Si [Biegelsen,1987]. Another important issue at the present is dislocation formation at the GaAs/Si interface but one that will not be investigated here. The mechanisms of antiphase domain formation will be briefly outlined next.

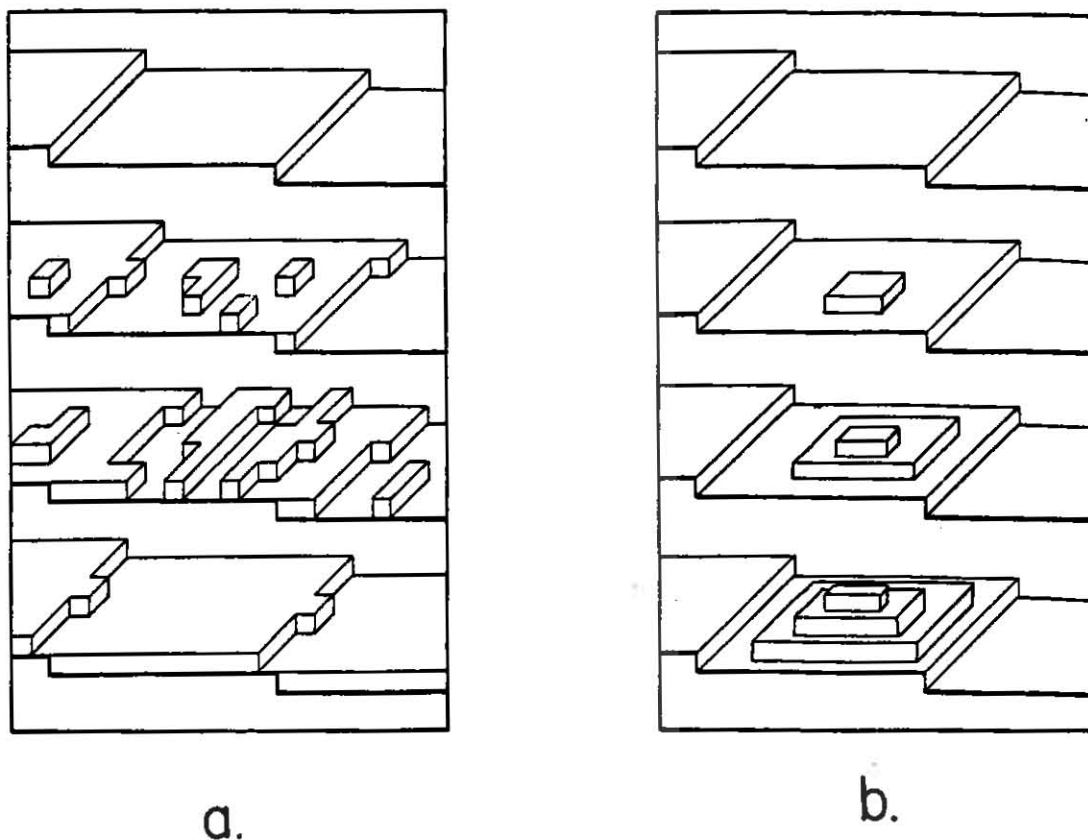


Fig.29 a. Layer-by-layer growth.

b. Three-dimensional growth.

Antiphase domain formation can be crudely explained by assuming mistakes in the epitaxial orientations during the initial stages of GaAs growth. For example, if both sublattices of the Ge or Si(100) substrate are exposed on the initial surface (as in Fig.27a) and the first layer of growth is limited to As, antiphase domain boundaries would naturally arise, as shown in Fig.30. The boundaries would line up along odd-multiple monolayer ($na/4$ where $n=odd$) step heights. Conversely, if the substrate consists of only even-multiple monolayer step heights, then antiphase domain formation can conceivably be suppressed. The two possibilities of the final GaAs domain orientation are shown in Fig.28. There is considerable electron diffraction evidence for both even-layer [Olshanetsky,1977 and Kaplan,1980] and odd-layer step heights [Neave,1983 and Saloner,1987] over a range of Ge(100) and Si(100) misorientations. However, the issue is more complicated since a Ge or Si(100) surface with odd-layer step heights can be used successfully as a template for growth of single domain GaAs [Pukite,1987 and Wang,1984]. Therefore, the mechanism of double-layer step heights is not a requirement for obtaining antiphase domain free growth. A different mechanism is clearly required.

Equally difficult to explain is the observed three-

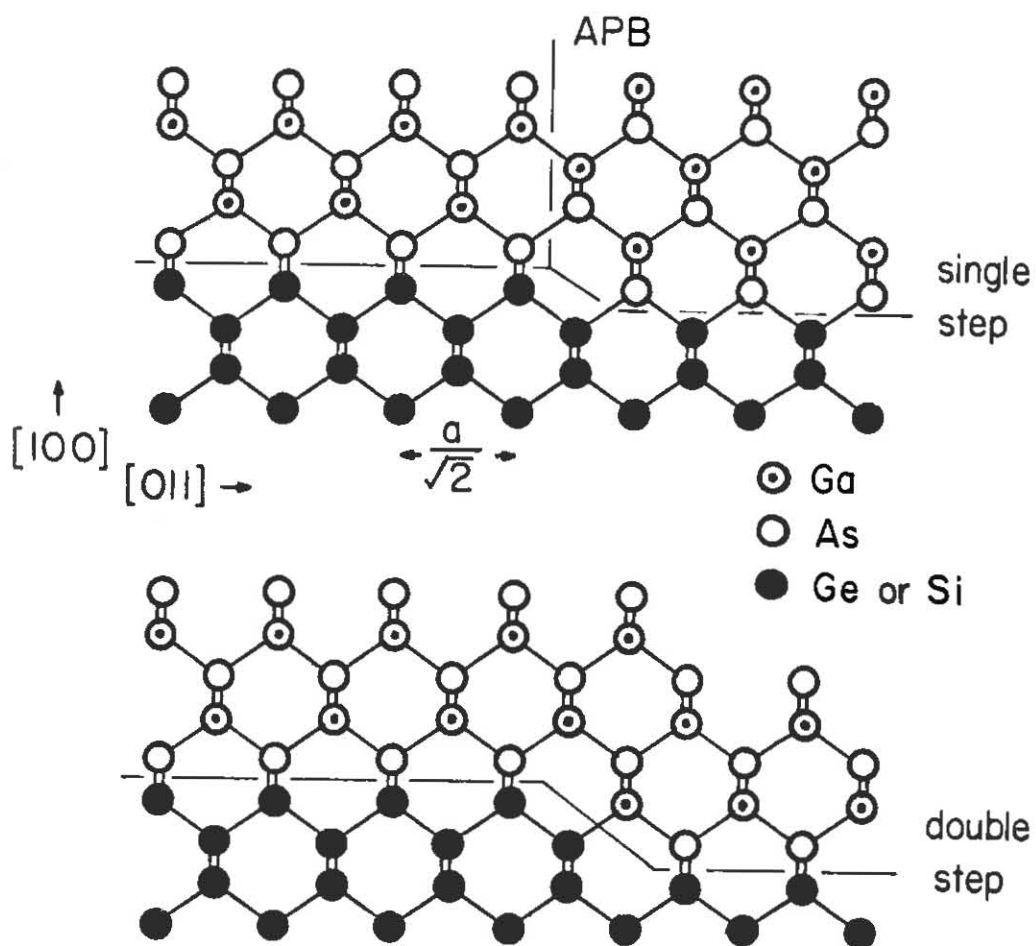


Fig.30 Antiphase domain formation on diamond (100) surface.

dimensional nucleation of GaAs on Si and Ge. The origin of this growth mode could be related to the aforementioned domain problem. Among other causes mentioned are strain (specifically due to the lattice mismatch between GaAs and Si) and polar-nonpolar electrostatics [Harrison, 1979]. As high-quality, homoepitaxial GaAs growth is known to be layer-by-layer, the technological goal is to achieve a smooth, dislocation-free, bulk-like GaAs layer as quickly as possible. If the anti-phase elimination and the three-dimensional growth can be better understood, perhaps growth techniques can be improved. The clear challenge is to transform a heteroepitaxial three-dimensional growth mode to a homoepitaxial layer-by-layer process. In the next section, we will develop a growth model for a homoepitaxial layer-by-layer growth system.

3.3. Layer-by-Layer Growth on a Vicinal Surface

3.3.A. The Time-Dependent BCF Model

In the classical view of homoepitaxial growth, the rate at which the adatoms reach low-energy step edges and kinks is dependent on surface diffusion. Burton, Cabrera, and Frank (BCF) [1951] included diffusion in a model that describes crystal growth solely by the propagation of surface steps. Within this model, the concentration gradient

of adatoms toward step edges is considered the driving force for step propagation. The solution to the BCF diffusion equation includes the approximation of low-supersaturation or close to equilibrium growth. This means that desorption or reevaporation is nearly equal to incorporation. This is far removed from the conditions typically used during MBE [Madhukar, 1983]. Several groups [Ghez, 1987 and Voigtlaender, 1986] have modified the equations to take into account the high supersaturation conditions employed during MBE. The major alteration involves including a moving reference frame into the analysis.

Figure 31 shows the stepped surface or staircase used in the modified BCF analysis. Here, surface steps of fixed height separate low-index terraces of uniform length. The step height is generally a multiple of the interplanar spacing while the terrace length is determined by the specific surface misorientation. We neglect surface evaporation, which is a good approximation for both GaAs and Ge over a certain temperature range. Then the diffusion equation can be written as,

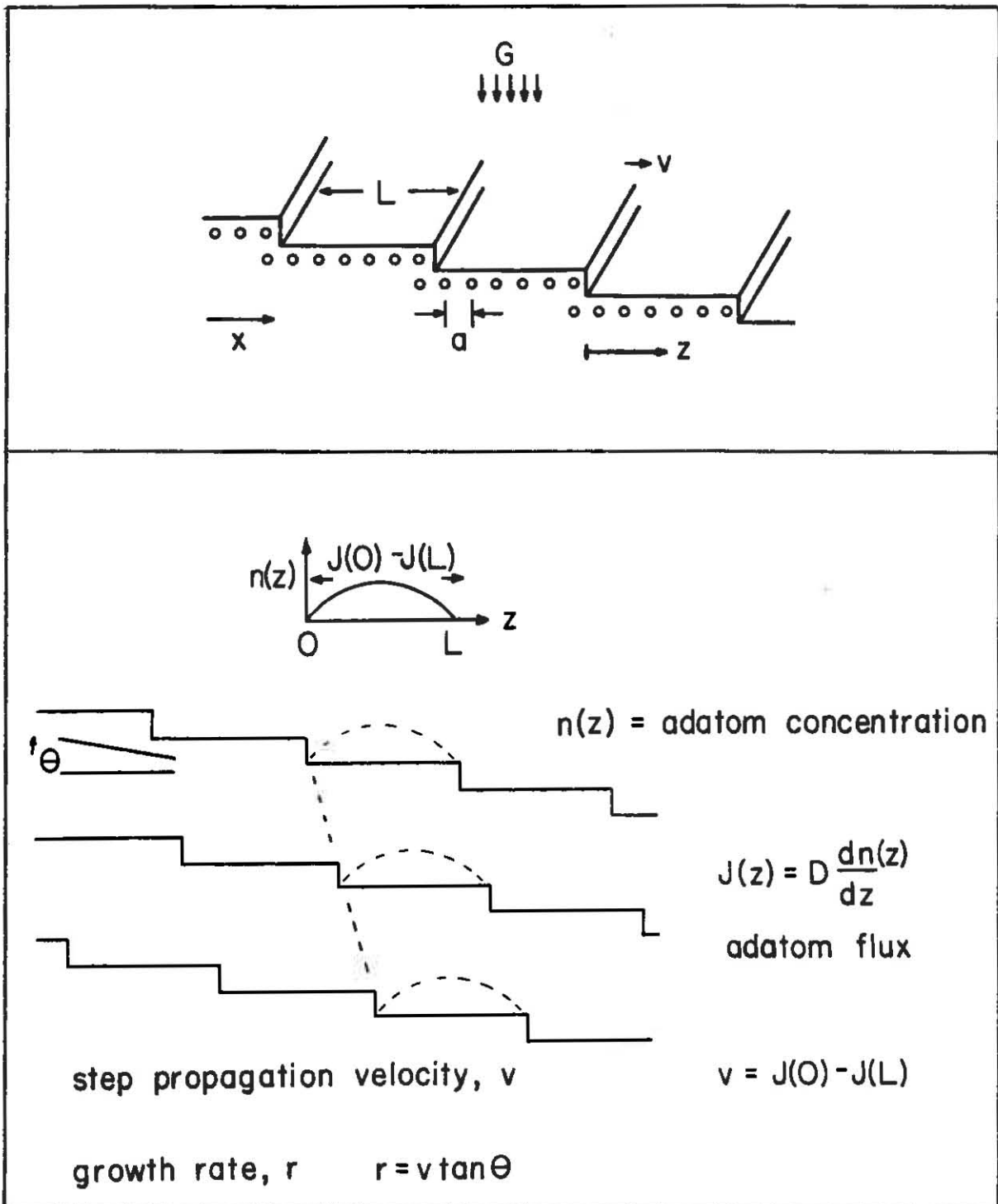


Fig.31 (top) Burton-Cabrera-Frank (BCF) model staircase.

Fig.32 (bottom) Step propagation process.

$$\frac{dn(x,t)}{dt} = D \frac{d^2n(x,t)}{dx^2} + G/a , \quad (20)$$

where $n(x,t)$ is the concentration of adatoms, D is the chemical diffusion coefficient, G is the growth rate in monolayers/sec, and a is the lattice constant. At the step edges the equilibrium adatom concentration is taken to be zero. These are the required spatial boundary conditions, $n(0,t)=n(L,t)=0$. The assumption here is that all adatoms that reach the step edge incorporate. The steady state picture looks something like Fig.32 where the concentration gradient is driving the step motion. If G/a is a step function, $G/a*u(t)$, the equation simulates the rapid onset of growth, in particular by molecular beam epitaxy. Therefore, the initial condition for MBE growth is that $n(x,0)=0$. For $t>0$, growth is initiated and $n(x,t)$ evolves to steady state. Equation 20 is then soluble in the time domain by a Fourier series analysis as follows,

$$n(x,t) = \left(1 - \frac{(2x-L)^2}{L^2} \right) \cdot \frac{GL^2}{8Da} - \quad (21)$$

$$\sum_{m=0}^{\infty} \frac{GL^2}{2D\pi^3} \cdot \frac{(-1)^m}{(m+0.5)^3} e^{-(m+\frac{1}{2})^2 \frac{4\pi^2}{L^2} Dt/L^2} \cos((m+\frac{1}{2}) \cdot 2\pi(x/L-1/2)) ,$$

where $L^2/(\pi^2 D)$ is a natural response time to reach the steady state. The progression of the step response is shown in Fig.33 with the first four terms used in the sum of Eq.21. The parameters were chosen such that $n(L/2, \infty) = 1$. Details of the solution are given in Appendix D.

The inclusion of the moving frame, $z = x - sv(t)dt$, where $v(t)$ is the step velocity modifies the equation to the following form,

$$\frac{dn(z,t)}{dt} = D \frac{d^2 n(z,t)}{dz^2} + v(t) \cdot \frac{dn(z,t)}{dz} + G/a . \quad (22)$$

This is a nonlinear differential equation, which is difficult to solve without numerical methods. In the steady state, however, where $v(\infty) = G \cdot L$, the solution is straightforward:

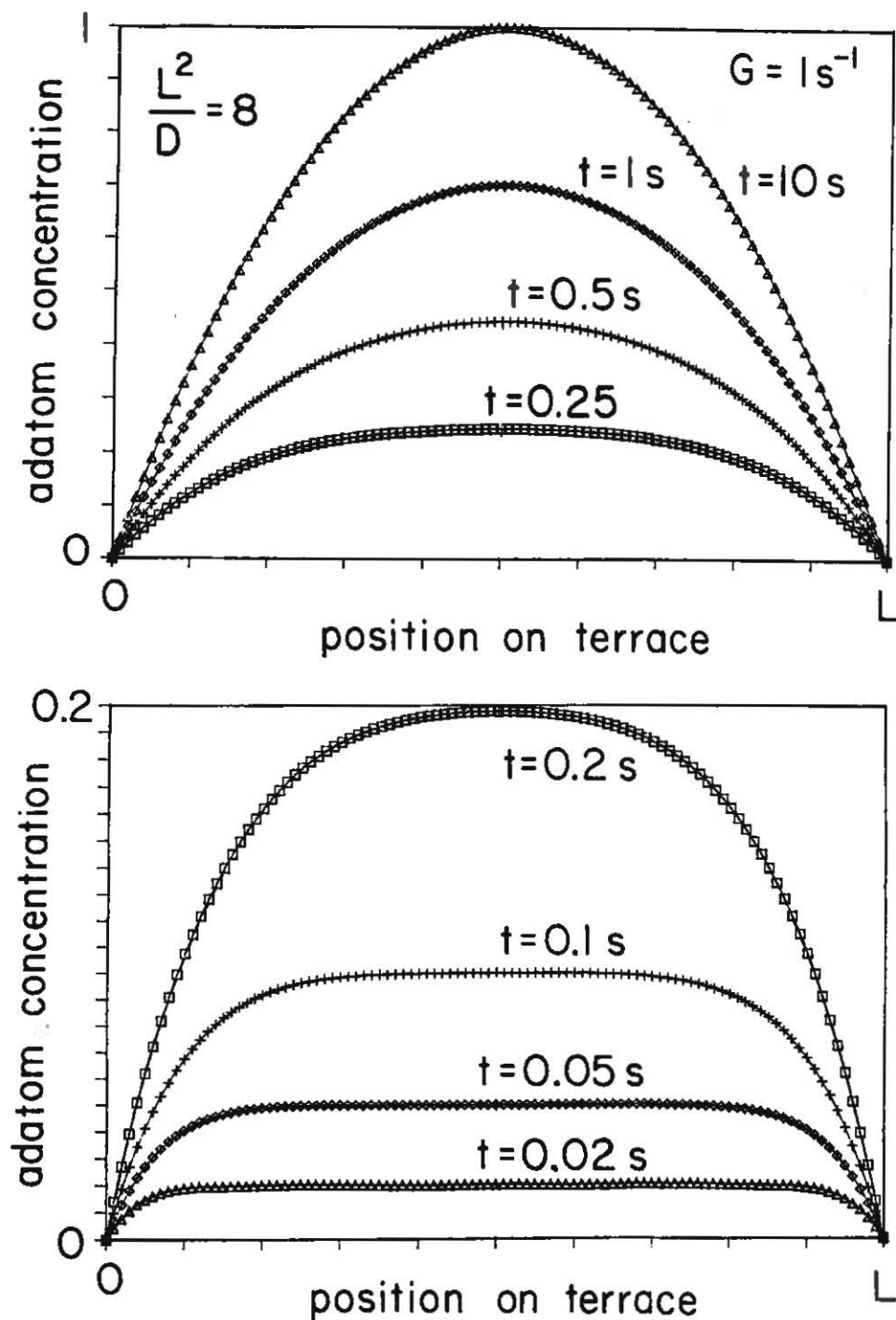


Fig.33 Time dependent solution to BCF model.

$$n(z,\infty) = n_0 \cdot \left\{ \frac{1 - \exp(-zLG/D)}{1 - \exp(-L^2G/D)} - \frac{z}{L} \right\}. \quad (23)$$

Here n_0 is the one dimensional surface site density, $1/a$. In this model the velocity of the step edges is proportional to the gradients feeding them as follows,

$$v(t) = aD \cdot \left\{ \frac{dn(z=0,t)}{dz} - \frac{dn(z=L,t)}{dz} \right\}, \quad (24)$$

or by integrating Eq. 22,

$$v(t) = GL/a - \int_0^L (dn/dt) dz. \quad (25)$$

Figure 34 shows adatom concentration profiles for various values of L^2G/D . For $L^2G/D < 1$, these profiles are identical to those obtained from Eq. 20 in the steady state. Above this value, the profiles are asymmetric. This can be explained as follows. For $L^2G/D < 1$ the maximum adatom concentration is given as,

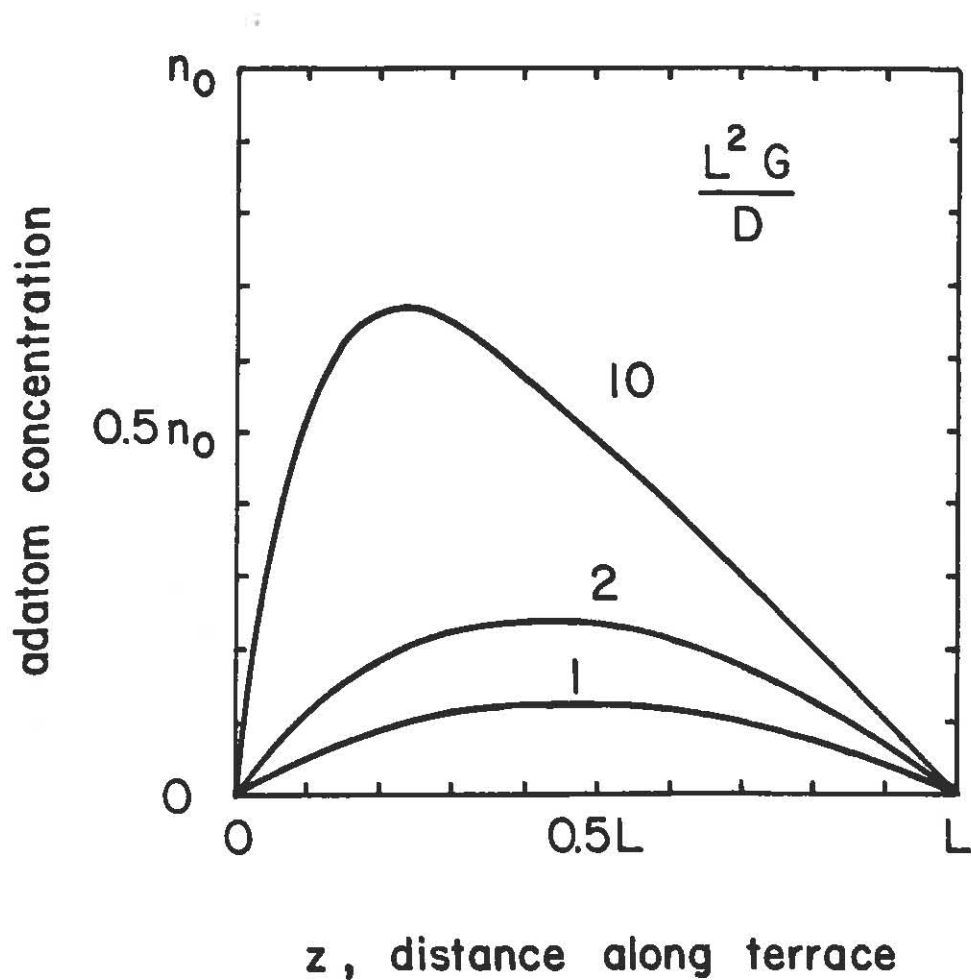


Fig.34 Steady state adatom concentration of BCF model.

$$n_{\max} \approx \frac{L^2 G}{8Da} . \quad (26)$$

Since $G = 1/\tau$ where τ is the monolayer time, one can see that a natural diffusion length can be expressed as $x_s = \sqrt{2D\tau}$. Equation 26 then can be written as the square of the ratio between $L/2$ and diffusion length. The diffusion length gives the mean distance an adatom can travel in time τ . If the diffusion length is less than $L/2$, there is a high probability for the adatoms to remain in the terrace region and be swept up by the propagating step instead of diffusing toward it. This has been referred to as growth by convection [Ghez, 1987] and is shown in Fig.35. Here, $J(0)$ is the proportion of atoms that approach the step edge from the leading edge. For progressively larger diffusion lengths, the adatoms will more likely diffuse toward a step, rather than be accumulated by convection. This leads to a more symmetric diffusion-like profile. The asymmetry of $J(0)$ vs $J(L)$ is important with respect to the stability of the propagating steps as it keeps the step-to-step distances from fluctuating too wildly. This is further discussed in Appendix E.

The step response of Eq.22 can be solved numerically if the first and second derivatives are expressed as a difference equation. Then Eq.22 can be rewritten,

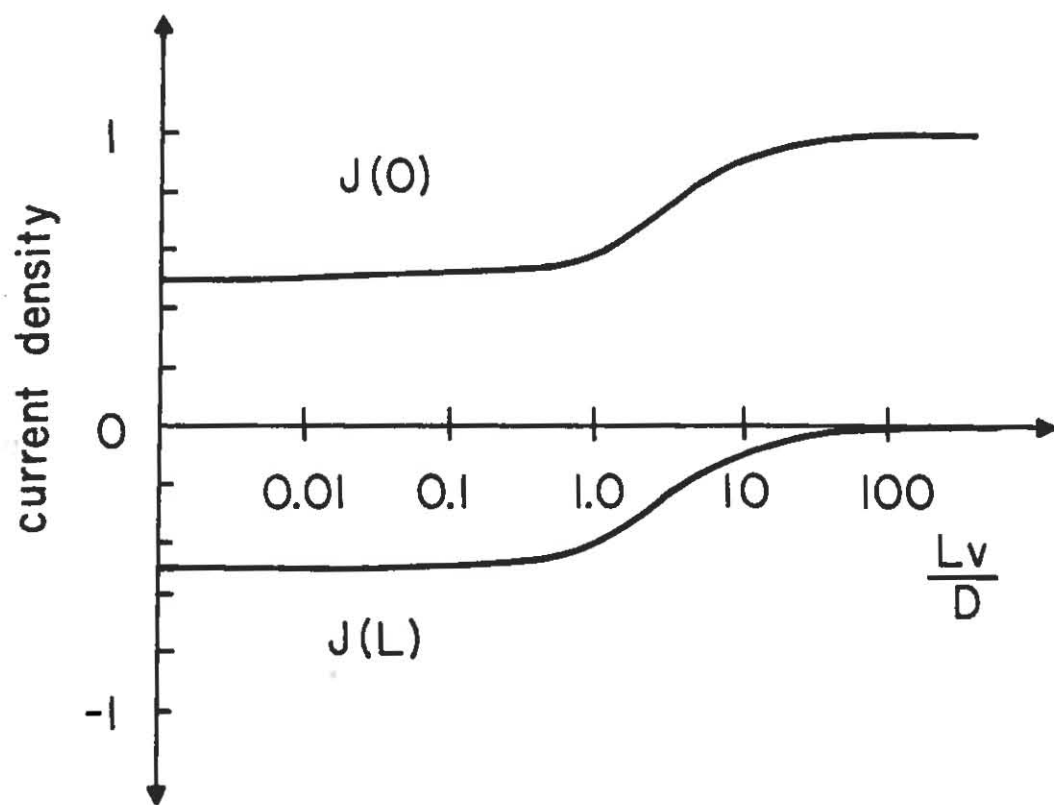


Fig.35 Left and right directed adatom flux.

$$\frac{dn_j}{dt} = -\nu \cdot (2n_j - n_{j+1} - n_{j-1}) + v(t) \cdot (n_{j+1} - n_j) + 1/\tau \quad (27)$$

and,

$$v(t) = n/\tau - \sum_{j=1}^N \frac{dn_j}{dt}, \quad (28)$$

where N is the number of lattice sites along the terrace of length L and $D=\nu a^2$. The boundary conditions are set such that $n_1=n_{N+1}=0$. To solve numerically, Δt is chosen and then Δn_j is calculated according to the difference equation. This result is used to first calculate the velocity and then to increment the accumulated adatom concentration for the next time step. To ensure convergence $\nu \cdot \Delta t < 0.5$. A listing of the Pascal computer program used for this calculation is found in Appendix F.

The results of this numerical calculation agree with Eq. 21 if the diffusion length is large relative to the terrace length. However, for small diffusion lengths, the step response of adatom concentration and velocity show damped oscillations. Figure 36 shows the oscillatory nature of the adatom concentration and step velocity for one choice of parameters. At $t=0$ seconds, growth is initiated and at $t=5$ seconds growth is stopped. In this example, the period is $\approx 1.2 \cdot \tau$. For smaller D , the period approaches the limit of

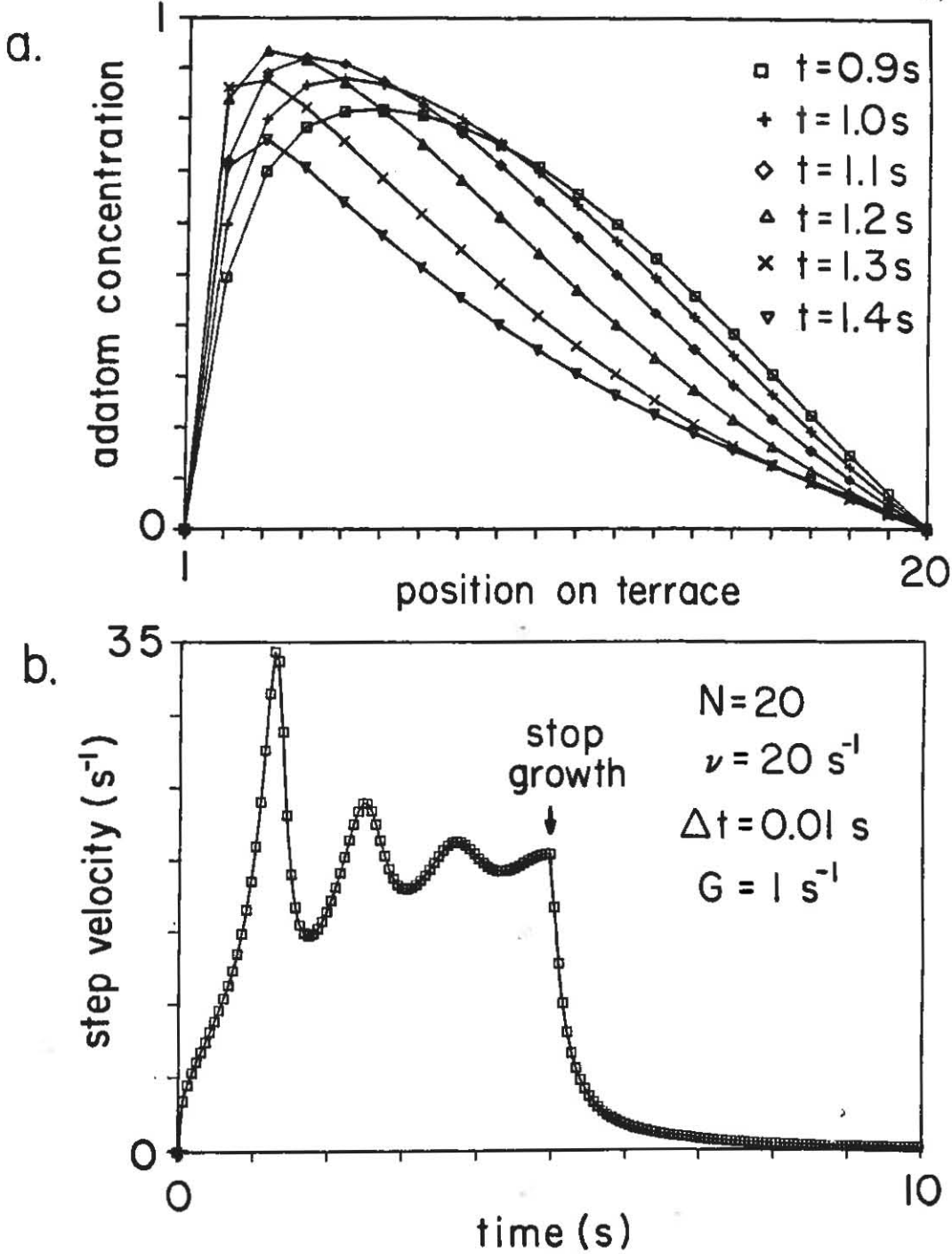


Fig. 36 a. Time dependent solution for low D.

b. Step velocity oscillations.

r. For successively smaller diffusion lengths the maximum adatom concentration greatly exceeds 1 or the limit of available sites.

The reason for these oscillations can be understood by noting that two mechanisms for growth are competing, diffusion and convection. At the initial stages of the growth, the velocity is small due to a small diffusion coefficient multiplied by a small concentration gradient. However, at a later time the step begins to advance into a region of higher concentration. The advancement forces a higher concentration gradient and, consequently, the step starts accelerating. The motion of the advancing step then literally sweeps the terrace clean by removing adatoms by convection. The cycle is repeated when the step slows down after removing a portion of the adatoms. Steady state is reached because the accelerating step cannot remove the adatoms fast enough before the next layer builds up. We will compare these oscillations to experimentally measured RHEED oscillations in Sec.3.3.C. There we will make a connection between the oscillatory adatom concentration and a smooth to rough cyclic behavior that RHEED is sensitive to.

As a caveat, the effect of cluster formation or cluster growth has not been included in this calculation of independent single particle hopping. Obviously if the peak

density of adatoms approaches the limit of available sites, the adatoms would not be free to hop from site to site without making frequent collisions with other adatoms. Clusters may then form (see Fig.26) which, if stable against dissociation, will act as new growth sites or steps as shown in Fig.29. The difference between single particle hopping (no interactions), as in the modified BCF model, and hopping with interactions, is how these clusters are treated. One empirical way of solving this problem is by assuming a diffusion coefficient that depends on concentration. Other methods involve molecular dynamics or Monte Carlo techniques that allow for any number of interaction parameters.

3.3.B. Monolayer Cluster Formation

In the previous section, the strong possibility of cluster formation was mentioned. The important point to remember is that clusters that form on the surface act as new step sites for layer-by-layer crystal growth. However, short of Monte Carlo techniques, there are no straightforward ways to include clustering or cluster growth. Described next is an intuitive approach that can help guide the experimental observations.

In general one would expect that an increase in adatom concentration would lead to an increased probability of

cluster formation. The probability increase can be thought of as an increased collision rate between adatoms in a high concentration region,

$$R_{\text{coll}} \approx n^2 \cdot \bar{v} \approx n^2 \cdot D/a , \quad (29)$$

where \bar{v} is the mean velocity of adatoms and R_{coll} is the collision rate, assuming a scattering cross section of one [Walton, 1962]. If n is given by Eq.26, then

$R_{\text{coll}} = L^4 / (64a^2 D \tau^2)$ in the center of the terrace. However, the collision of two adatoms may or may not lead to a growing cluster. The stability of a cluster is dependent on temperature. At high temperatures, the dissociation rate of clusters may be greater than the collision rate between adatoms. The growth rate of a concentration of clusters can be modelled by the following equation.

$$\frac{dn_c}{dt} = - \frac{n_c}{\tau_{\text{diss}}} + R_{\text{coll}} . \quad (30)$$

Here, n_c is the concentration of clusters and τ_{diss} is the characteristic time for dissociation. The solution to this equation is as follows,

$$n_c(t) = \frac{L^4}{64D\tau^2} \cdot \tau_{diss} \cdot (1 - \exp(-\frac{t}{\tau_{diss}})) / a^2 . \quad (31)$$

If t is treated as the monolayer deposition time, τ , two limiting cases of the above expression can be obtained:

$$n_c(\tau) = \frac{L^4/a^2}{64D\tau} \quad \tau \ll \tau_{diss} , \quad (32a)$$

$$n_c(\tau) = \frac{L^4 \tau_{diss}}{64D\tau^2 a^2} \quad \tau \gg \tau_{diss} . \quad (32b)$$

By analyzing Eq.32, one can see that the strongest effect on cluster formation is the separation of steps. From the above expressions one can see that the collision rate in the middle of a terrace increases as L^4 . By increasing misorientation, clustering should be diminished. This will be investigated more thoroughly in the results section.

The difficulty of separating two temperature dependent kinetic processes such as diffusional hopping and cluster dissociation can also be understood. In the first expression the only temperature dependent parameter is D , however in the second, τ_{diss} is also temperature dependent. An additional difficulty is that the rates of cluster formation and diffusion may depend on the addition of impurities to the surface. In this case, impurities can slow down diffusing adatoms, create nucleation sites, or occupy

preferred step sites, thereby increasing the probability of clustering.

To summarize, the calculation of adatom concentration within the BCF growth model presented here shows the interrelation of growth rate, diffusion coefficient, and step density that must extend to the MBE environment. The presence of misorientation steps have been shown by many workers to be important during the MBE process. For example, certain GaAs misorientations are relatively insensitive to impurities during growth (Radulescu, 1987) and the growth of GaAs on Ge and Si has been observed to benefit from a substrate misorientation (Fischer, 1985). By using RHEED measurements of the growth on such misoriented surfaces, the present investigation will further address these issues in Sec. 5.

3.4. RHEED Intensity Oscillations

Layer-by-layer crystal growth on a surface without substrate steps would be expected to proceed as cluster formation followed by step propagation of the cluster edges. As the clusters meet and coalesce, a smooth surface is recovered. The next layer would repeat the cycle. If a RHEED beam is monitored during this process the intensity would be observed to follow a similar cyclic behavior of monolayer

period. This is the basis for RHEED intensity oscillations [Van Hove, 1983 and Neave, 1983].

The simplest explanation for the diffracted intensity behaviour was outlined in Sec.2.2.A. The diffracted peak intensity is the highest for a smooth surface. The growth is initiated when the vapor source shutter is opened. At this point, growth clusters are formed on the surface. The diffracted beam broadens and decreases in intensity due to the decrease in correlation length on the surface. At 1/2 coverage in a two level system, the surface roughness reaches its maximum and this corresponds to the minimum value in peak intensity. Beyond this point, the surface becomes smoother and the peak intensity recovers.

The oscillations described are related to those calculated in Sec.3.4. For example, if the intensity from the surface of Fig.36 is calculated as a function of time and evaluated at $S_x = \pi/L$ (see Appendix G), the oscillations of Fig.37a would result. If the diffusion length were increased, so that fewer adatoms were allowed to build up on the terrace, Fig.37b would result. This comparison has to be used judiciously, as the effect of clustering was not included in the calculation.

The intensity oscillations have been observed in many

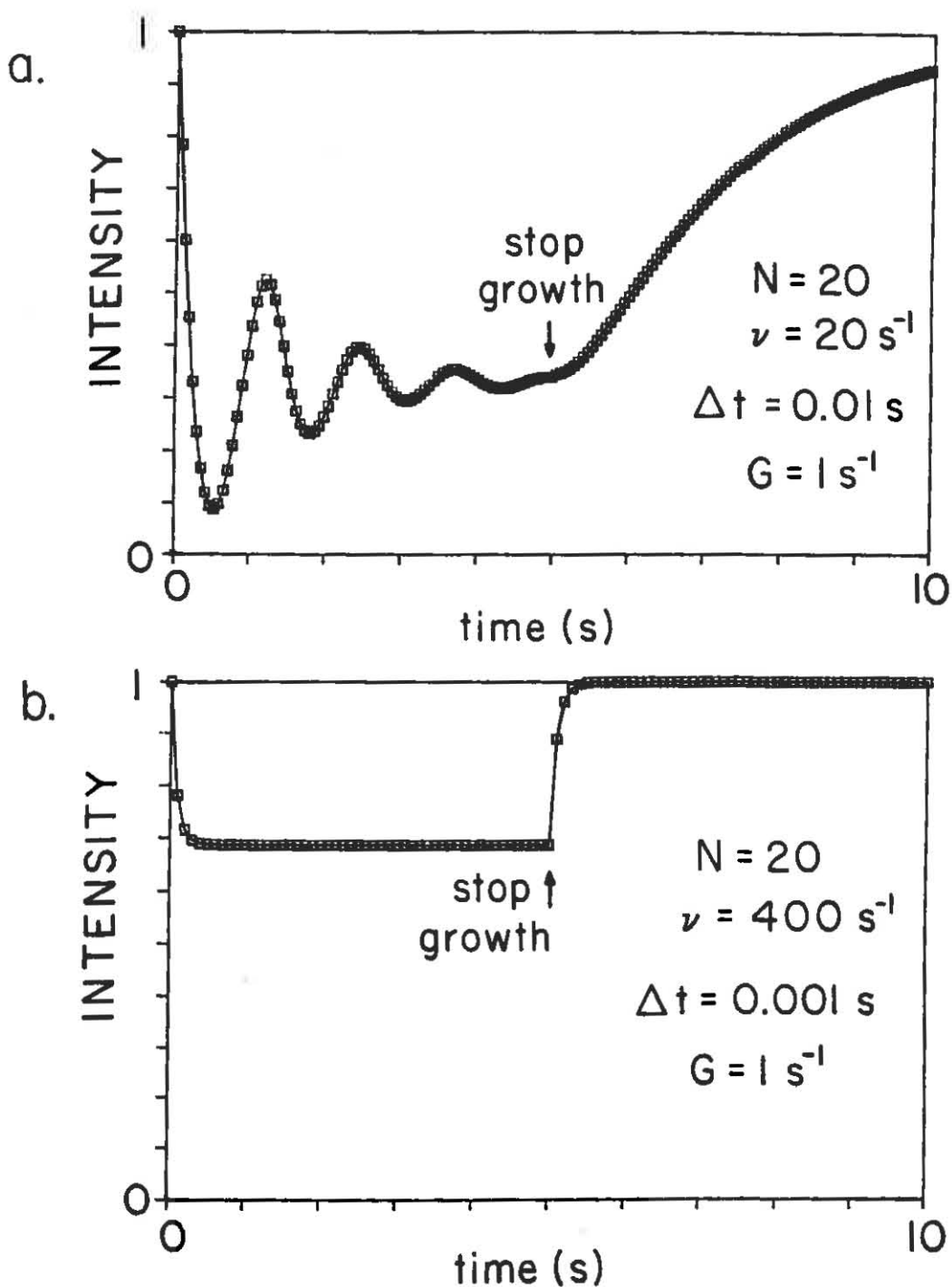


Fig.37 a. RHEED intensity oscillations from Fig.36.

b. RHEED intensity for larger D.

growth systems, including metals [Purcell, 1987]. In the results section, we will use the oscillations in conjunction with the other diffraction analyses presented earlier to understand the homoepitaxial and heteroepitaxial growth of GaAs and Ge(100).

Chapter 4

Experimental

4.1. Diffraction and Growth Apparatus

The MBE system consists of three chambers as shown in Fig.38 (Perkin Elmer PHI 400). The sample is loaded via the introduction chamber and is transferred into the analysis chamber (Auger analysis) and then to the main growth chamber. Within the growth chamber are BN evaporation sources for depositing Ga, As₄, As₂, and Ge. The As₂ source includes a Mo tube for cracking the As₄. The sources are individually shuttered to provide control of layer thicknesses.

A schematic of the diffraction apparatus is shown in Fig.39. The diffractometer consists of a 10 keV electron gun that is focussed at the phosphor screen. A highly collimated and narrow beam is important for beam profile analysis so that magnetic shielding was used liberally. The glancing incident angle could be varied by a combination of sample motion and beam deflection. The incident azimuth could be varied by rotating the sample about the normal. The light from the phosphor screen was imaged onto a slit or pinhole aperture. The light through the aperture was detected by a photomultiplier. The scattering angles were determined by

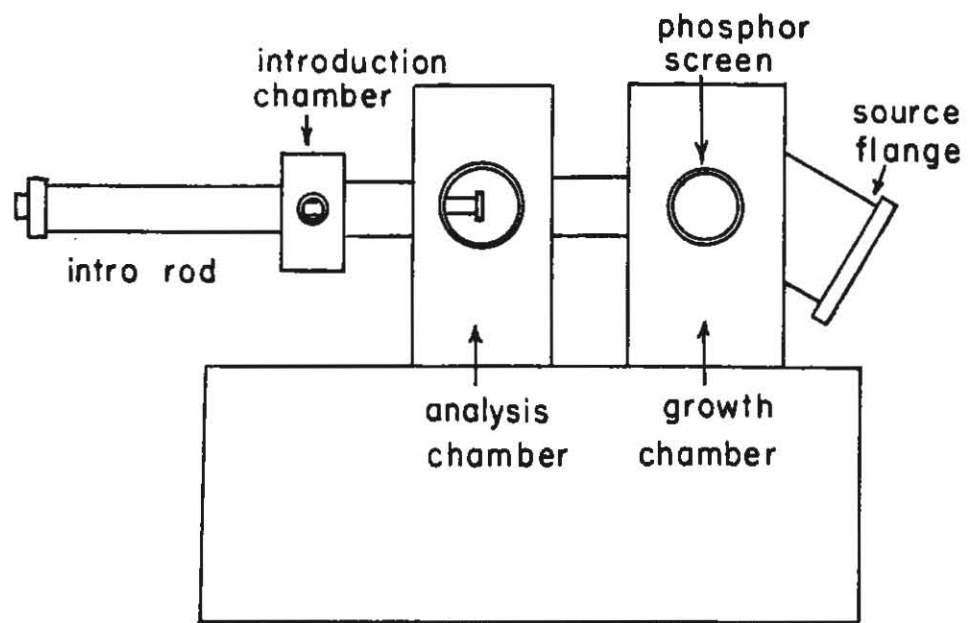


Fig.38 MBE system.

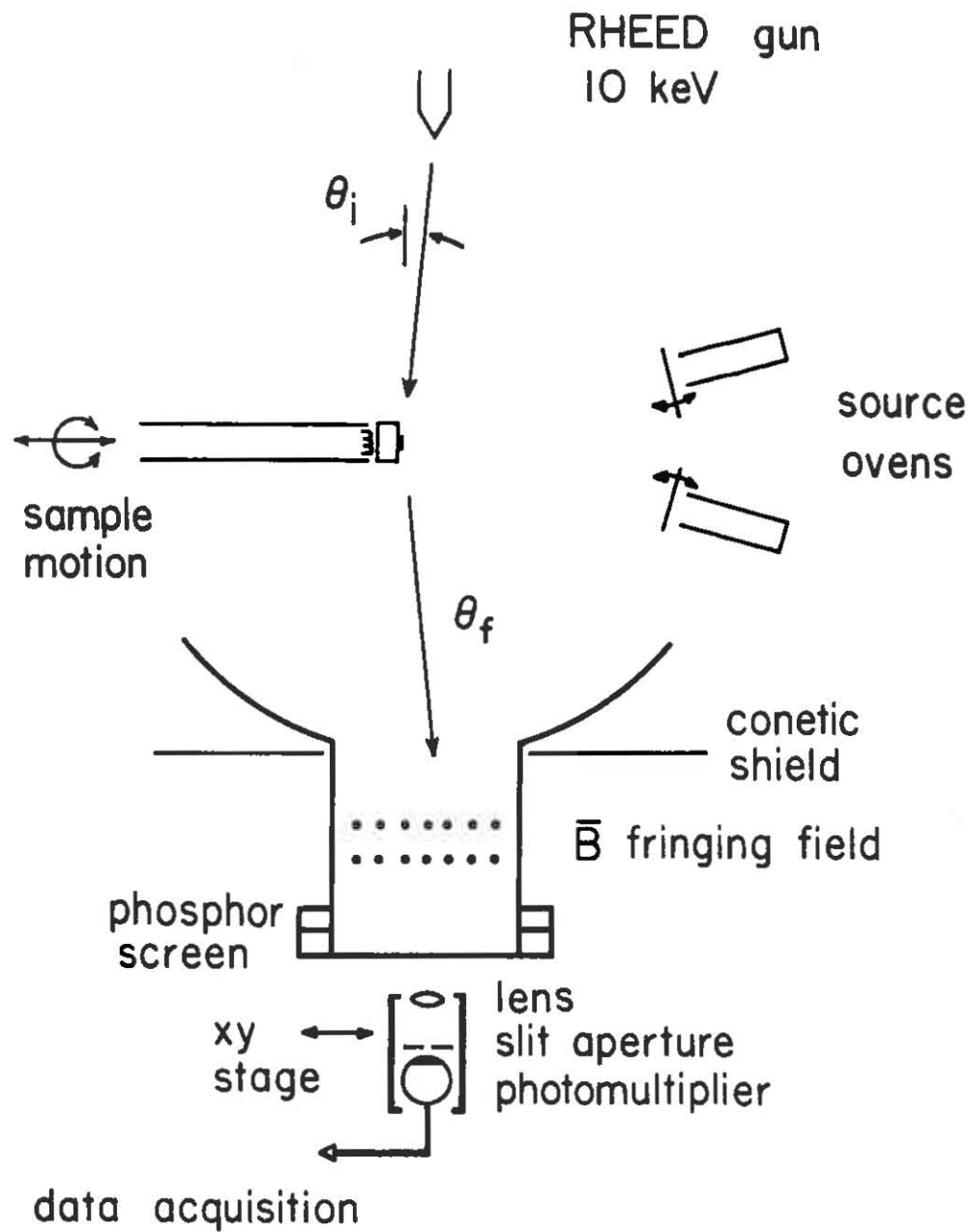


Fig.39 Growth chamber and RHEED geometry.

measuring the azimuthal position of the sample relative to symmetry directions and from the separation between the specular beam, primary beam, and shadow edge.

The detector assembly was positioned using x-y micrometer controls. Absolute angles were known to within 1 mrad. To avoid nonuniformities in the phosphor, the detector was left fixed and angular profiles were obtained by moving the diffraction pattern with a pair of electromagnetic coils. The angular profile of a diffracted beam at an in-phase angle gave the instrument response. This full width at half maximum (FWHM) was 0.1 mm, which corresponds to the lowest resolvable $\Delta\theta_f$ of 0.35 mrad (spot diameter divided by sample-to-screen distance). Important to achieving sharp in-phase profiles is to use flat, small (1mm \times 1mm) substrates which subtend a small range of angles and do not bend easily. Bowing of the lattice planes or random up and down steps among many levels can mask the intrinsic response of the diffractometer. To achieve the greatest sensitivity to the steps, all of the measurements were taken at an incident angle corresponding to the out-of-phase condition.

The temperature of the substrate was measured by a thermocouple pressed against the back of the sample holder. To ensure the reproducibility of the temperature measurements, the thermocouple was calibrated once by

measuring the Si/Al eutectic temperature. This was then compared to the 2×4 to "1 \times 1" phase transition of GaAs. All subsequent measurements used this phase transition as the calibration temperature. To accurately compare different surfaces, more than one sample could be mounted at one time.

4.2. Preparation and Growth of GaAs

Epitaxial GaAs and Ge films were grown in the same chamber. GaAs(001) surfaces were prepared by MBE using standard techniques. A thin wafer was first chemically etched and then cleaved into 1mm \times 1mm sections. A section was soldered to a Mo block with In before introduction into the vacuum system. Then the surface oxide was desorbed by brief heating to 620°C under an As flux, and a 1/3 μ buffer layer was grown on the surface. GaAs can be grown under a variety of surface reconstructions [Cho, 1971], but the best regions of growth for device needs are the 2×4 and "1 \times 1" As stabilized reconstructions (\approx 550–650°C). These are also the regions for obtaining the sharpest diffraction patterns. In this study, a typical substrate temperature was 580°C, a typical growth rate was 1/3 μ /h, and a typical As/Ga flux ratio was 20:1. Flux ratios and growth rates were measured by RHEED intensity oscillations.

The misorientation of a substrate was measured by x-ray

$\Theta-2\Theta$ goniometry. This was checked against RHEED results. The surfaces monitored during the growth of GaAs were either misoriented towards the (111)A or (111)B directions (see Fig. 28). The (111)A type misorientations have Ga terminated steps while (111)B misorientations have As terminated steps. These two surfaces corresponded to respective sides of the same wafer. The RHEED pattern was used to distinguish between the two as follows. The diffraction pattern for the 2x4 GaAs surface reconstruction shows quarter-order reflections if the beam is directed towards the [011] and half-order reflections if the beam is directed towards the [011] direction [Cho, 1971]. These determine the "B" and "A" directions, respectively (c.f. Appendix A). The [011] direction was then compared to the staircase direction to determine the step termination.

4.3. Preparation and Growth of Ge and GaAs/Ge

Ge substrates were etched with the same technique as GaAs prior to loading. However, Ge films were typically grown on GaAs(100) substrates, as no differences were detected in the quality of the layers using GaAs substrates. This was expected as Ge and GaAs are closely lattice matched (<0.1% difference in lattice constant). Ge(100) growth is possible over a wide temperature range corresponding to the 2x1 reconstruction, but annealling above 600°C after growth

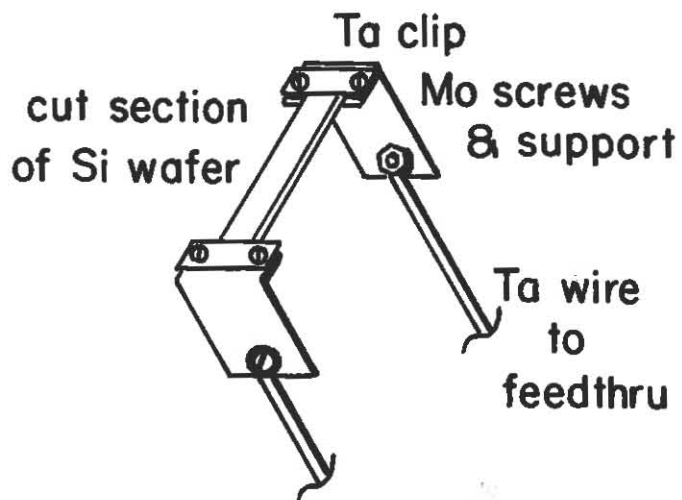
gave the sharpest diffraction profiles. Growth rates of Ge were determined by RHEED intensity oscillations. For Ge, another important consideration is the background level of As within the growth chamber. To keep this reproducible, shutters and other parts coated with As were kept cold. The background pressure during growth was typically 5×10^{-9} Torr.

Prior to growth of GaAs on Ge, the surfaces were prepared by growing a 1000 Å layer of Ge onto misoriented GaAs or Ge substrates. Then As in the form of either As_4 or As_2 was applied to the surface as a pregrowth step. The flux was set to give an As incorporation rate of 1.5 monolayers/s for GaAs at a substrate temperature of 500°C based on RHEED As oscillations [Lewis, 1986]. Then GaAs growth was initiated as the Ga shutter was opened. Initially the growth temperature was 500°C and growth rate 0.1 μ/h. After 200 layers were deposited, these were increased to 580°C and 0.8 μ/h respectively. The final GaAs thickness was 2 μ in all the films.

4.4. Preparation of Si Substrates for GaAs Growth

The Si(100) substrates used in this study were B doped, 0.01 Ω-cm and misoriented by $2.5 \pm 0.1^\circ$ toward a <011> direction as determined by x-ray goniometry. Chemically etched wafers (following the technique of Ishizaka, 1986)

were cleaved into pieces 2cm × 2mm × 0.5mm and loaded onto a sample holder (shown below) by Ta and Mo clips. The Si was then heated by passing a direct current through its length. This enabled much higher substrate temperatures than the conventional In bonding approach. Sample temperature was determined by pyrometer, which was calibrated to the GaAs 2×4 to "1×1" phase transition (this was done after the GaAs was grown) [Van Hove, 1985].



The Si oxide was removed by heating to 850°C for < 15 minutes. This was verified by the simultaneous observation of the 2x2 Si(100) RHEED pattern. Alternatively the Si surface was cleaned by exposing to a Si evaporation source located in the analysis chamber. This consisted of another resistively heated strip of Si. The advantage of this technique is that much lower temperatures (750°C) are required and an In bonded sample could be used. After this stage, a Si buffer layer could be grown from the same source. No observable differences were detected in the RHEED results reported here with or without this buffer layer. The subsequent GaAs growth was initiated at 430°C with a growth rate of 0.1 μ/hr. The rate was then increased to 1 μ/hr and temperature to 580°C after the first 0.1 μ of growth. This follows the two step "As prelayer" recipe [Fischer, 1986]. The As₄ flux was held fixed during growth at 1.7 equivalent layers/s.

Results

In this section RHEED measurements of the growth of GaAs and Ge on stepped substrates of GaAs(100), Ge(100), and Si(100) will be presented. We first examine the homoepitaxial growth processes of GaAs and Ge. Particular attention will be paid to the differences in step structure and anisotropy on each surface. We find that As as an intentional impurity has a strong interaction with Ge. The heteroepitaxial growth of GaAs on Ge(100) and Si(100) is then presented. The RHEED results obtained indicate that the substrate step distribution is crucial to the subsequent growth mode and that the step distribution is changed by reaction with an As flux.

5.1. GaAs Surface and Growth Characterization

The RHEED pattern from stepped or vicinal surfaces often shows splitting of the diffracted beams. This results from destructive interference between electrons scattered from spatially separated terraces on a staircase of steps. The measurement of the diffracted beam positions and shape gives quantitative information on the step heights and terrace lengths. Furthermore, the time-dependent behavior of the diffracted beam intensity gives information on the

homoepitaxial growth mechanisms. In the following section, these measurements taken together will allow us to formulate a realistic picture of the single-crystal vicinal GaAs surface. In the subsequent sections, the transformation of the initial substrate surfaces of Si and Ge to bulk-like layers of GaAs by heteroepitaxial growth will be compared to this picture.

The measurements described in Sec.2.2.C assume that the GaAs (or any surface) staircase is sufficiently ordered that sharp splitting is obtained. In fact, the order of the GaAs staircase depends on surface reconstruction [Pukite,1985] and on growth conditions [Cohen,1986]. The sharpest splitting is usually obtained in the "1×1" regime, where evaporation at kinks is important. Further, it will be shown that the type of steps present is important in establishing the staircase order. For GaAs, either Ga or As terminated steps are possible. These correspond to misorientations toward the [011] or [01 $\bar{1}$] direction as shown in Fig.28. The measurements described previously in Sec.2.2.C were from steps in the [010] direction (i.e., kinked with both As and Ga terminated step edges).

Figure 40 shows angular profiles from surfaces misoriented by 2° with Ga (Fig.40a) and As (Fig.40b) terminated steps. In both cases, the beam was directed close

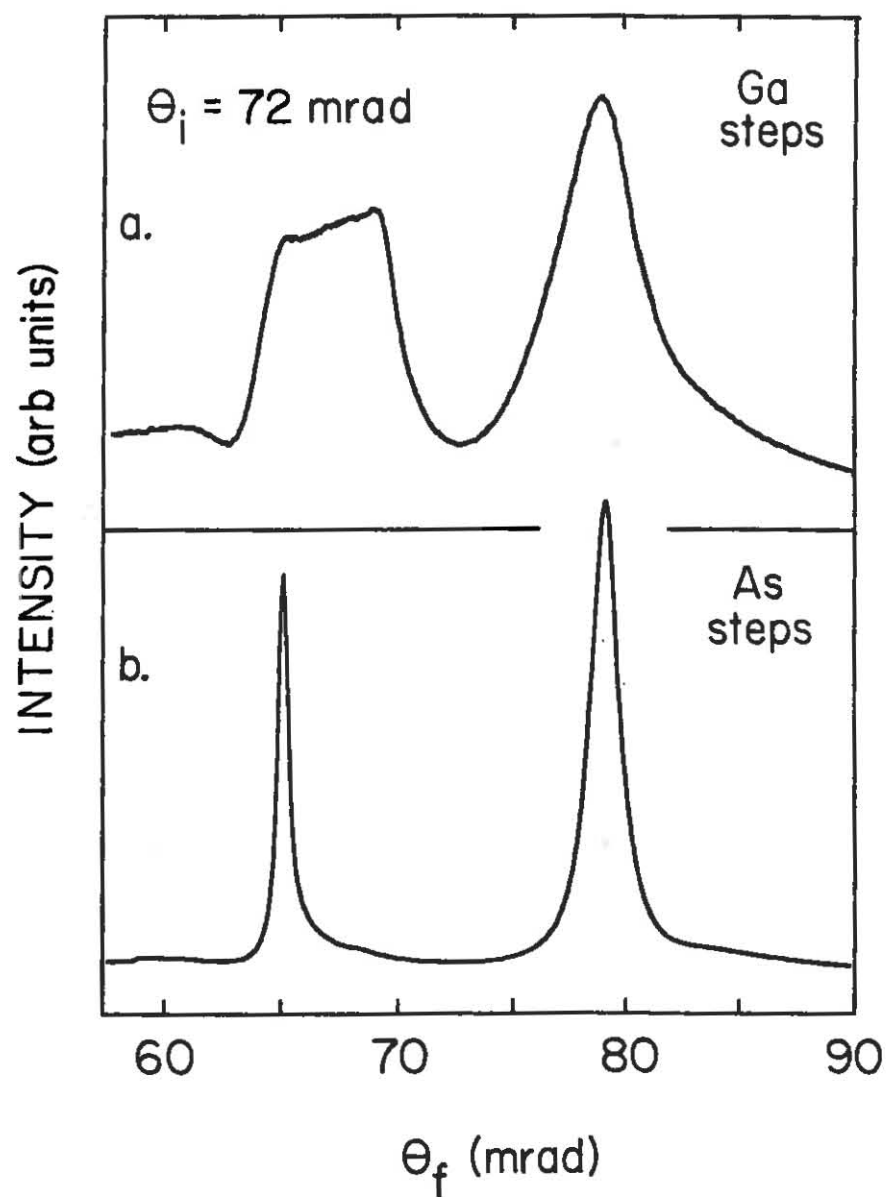


Fig.40 RHEED profiles from 2° GaAs misorientaion.

to down the staircase at an out-of-phase angle. The surface was static and under a 2×4 reconstruction with only As flux supplied. Note that the As terminated step-edged surface gives a very sharply split diffracted profile while the Ga terminated step-edged surface is broadened considerably. The latter profile can be obtained reversibly. Heating the Ga terminated step-edged surface into the "1 \times 1" reconstruction sharpens the profile until it approaches that of Fig.40b. Upon cooling to the 2×4 reconstruction, the broadening is recovered. Growing GaAs on the surface also sharpens the profile. The broadening is then due to a large fluctuation in the equilibrium (non-growth) terrace lengths [Pukite,1987c].

Figure 41 shows the rms fluctuation in terrace length, $\sigma = (\langle L^2 \rangle - \langle L \rangle^2)^{0.5}$, that would be expected to give a certain broadening for a 2° surface at $\theta_j = 72$ mrad. A delayed geometric distribution of terrace lengths was used in the calculation (see Appendix C and [Pukite,1985]). The difference between Ga and As terminated steps is a near doubling in rms deviation in terrace lengths.

One mechanism that could cause fluctuation in the terrace lengths is a high kink density. Conceivably, a measure of the kink density can be determined by aligning the electron beam perpendicular to the staircase direction

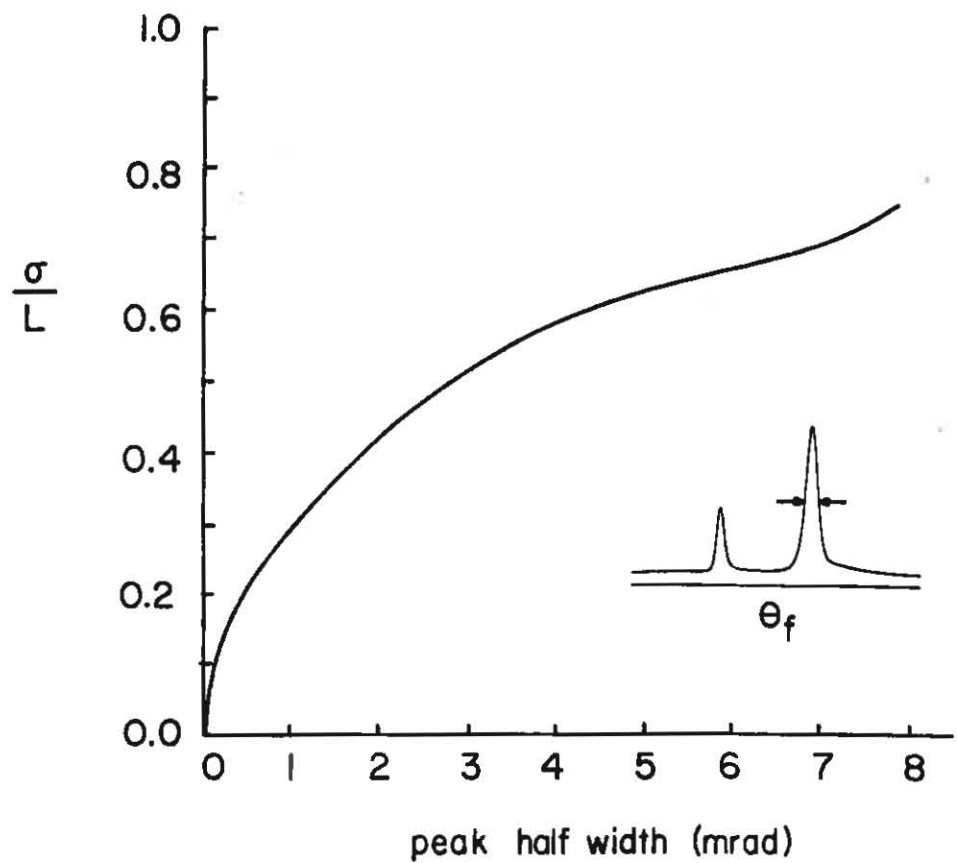


Fig.41 Peak half width (inset) vs terrace length disorder.

and taking scans along the streak. If the steps are very straight over long distances, the profile is narrow due to the long correlation length in the beam direction. In the limit of straight steps, the pattern in Fig.21 at 90° should be observed. However, if the step edges meander with the introduction of kinks, the electron would effectively traverse more up and down steps along its path. The correlation length would then decrease and cause the beam to broaden. Figure 42 shows the $\Delta\Phi_f$ -integrated angular profiles perpendicular to the staircase direction at an out-of-phase angle for Ga (Fig.42a) and As (Fig.42b) terminated steps. Clearly, the Ga terminated step edges meander less. This implies that the disordering of the Ga terminated staircase in the 2×4 reconstruction is not solely the result of an increased kink density. Figure 43 gives a conceptual view of the differences between these two surfaces. The chemical or electronic differences at the two types of step edges must play a role in determining the respective degrees of disorder.

The density and character of both substrate and cluster steps is expected to be important during growth. Since the (100) is not a cleavage face, all surfaces with this orientation are expected to contain substrate steps. This is mainly a result of the difficulty of orienting, cutting, and polishing with the aim of eliminating steps entirely.

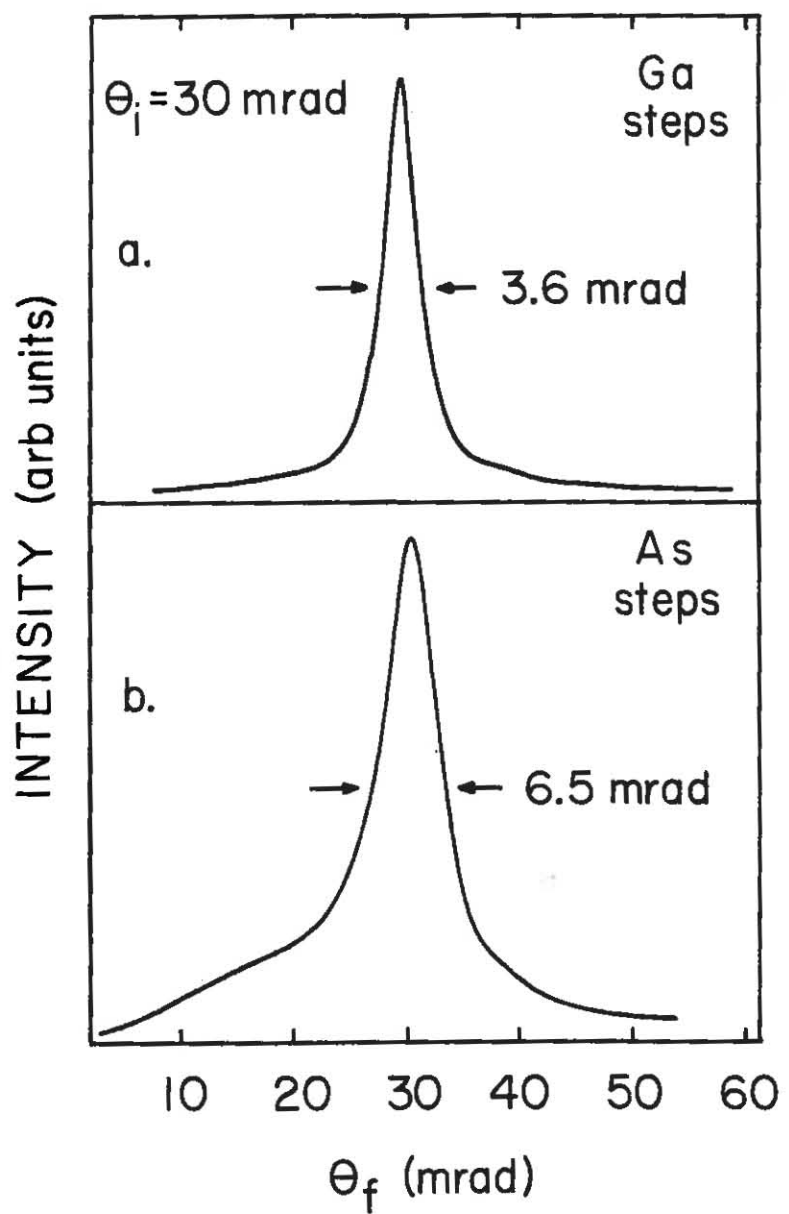


Fig. 42 Perpendicular GaAs RHEED profiles.

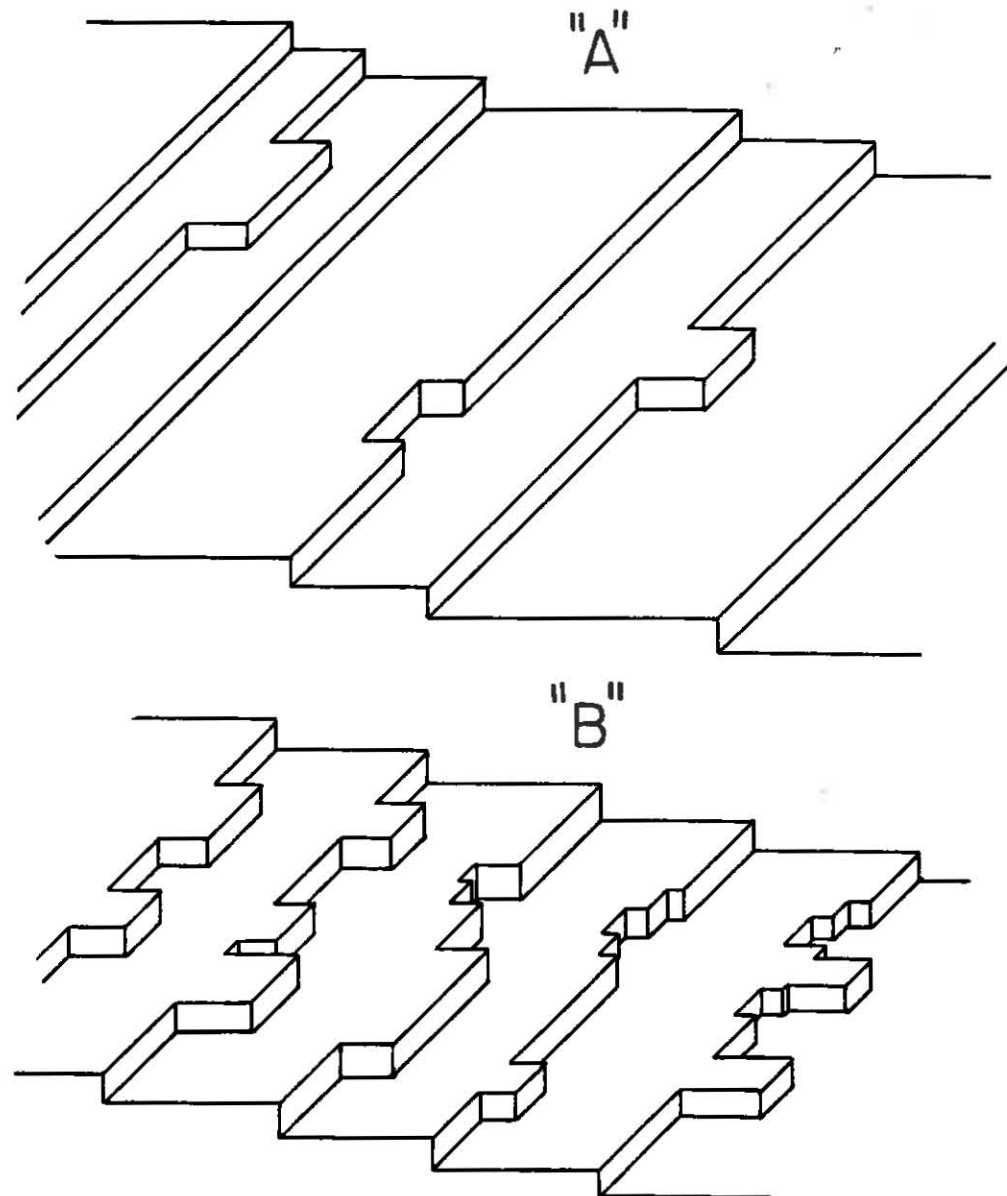


Fig. 43 Conceptualization of GaAs "A" and "B" misorientations.

One should realize that even a misorientation of 1 mrad from the (100) will contain on the average 3000 Å between surface steps. This is within the region that RHEED is sensitive to steps. The RHEED studies of GaAs growth on such surfaces has focussed on the shape of the diffracted beam as a function of growth conditions [Lent, 1984 and Van Hove, 1985]. This technique is expected to give information on the distribution of cluster steps.

The main result of these measurements has been a determination of the correlation length of clusters during the initial stages of growth. The correlation length was determined at nearly half coverage, i.e. at the minimum of an intensity oscillation. Here, the full-width at half maximum of the angular profile is inversely related to the correlation length. The correlation length was observed to increase as a function of temperature, particularly as the surface reconstruction passed from the 2×4 to the "1×1" reconstruction [Van Hove, 1985]. The activation energy associated with this temperature dependence was 3.8 eV. The implication of this was that some non-diffusion bond breaking process was occurring. Other measurements have indicated that evaporation of GaAs is important only in the high temperature "1×1" reconstruction [Van Hove, 1985].

These measurements have been extended to misoriented

surfaces. Figure 44 gives a comparison of growth oscillations on a 1 mrad and a 35 mrad misorientation. The lack of strong oscillations on the 35 mrad surface has been attributed to the high density of step sites available for step propagation [Pukite, 1984b]. For the 35 mrad surface, the average terrace length is 80 Å. Recalling from Sec. 3.3 that the average number of collisions in the middle of a terrace goes as L^4 , this number can be reduced by a factor $\sim 10^6$ by reducing the average terrace length from 3000 Å to 80 Å. This reduction is directly observed in the weakness of the oscillations. In the limit of pure step propagation, no oscillations should be observed as there is no cyclic variation in roughness. The weak oscillations observed on the 35 mrad surface are from the few adatoms that form critical clusters before reaching the propagating step edges. We should note that sharp splitting is maintained throughout the growth. This implies that the staircase does not undergo severe fluctuations in terrace length distribution and perhaps an ordering mechanism similar to that described in Appendix E is operative.

Neave and coworkers (1985) have estimated the Ga diffusion coefficient by adjusting the growth rate and substrate temperature until the oscillations completely disappear on a 2.5° misoriented surface. In effect, this modifies the adatom concentration according to Eq. 26 (which

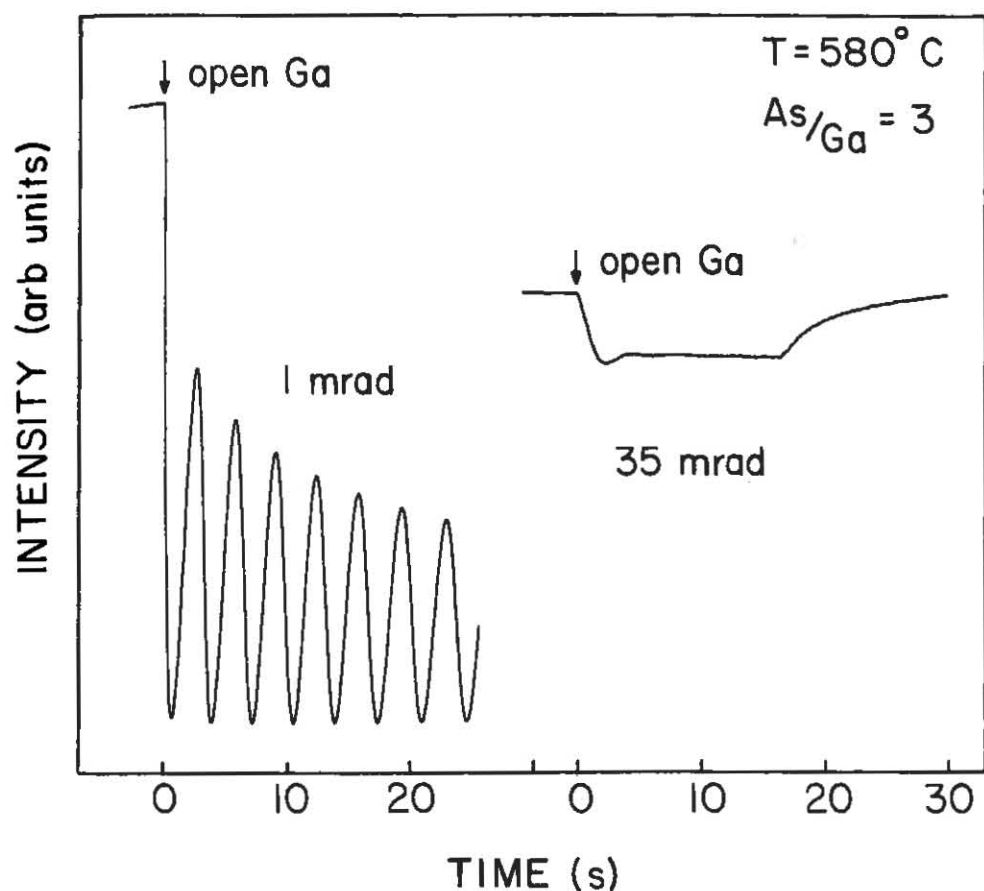


Fig. 44 GaAs RHEED oscillations on flat and stepped surfaces.

neglects clustering or ad-ad interactions) or that of Eq.32a,b which somewhat crudely includes collisions. Since the diffusion coefficient is a temperature activated process, where $D=D_0 \exp(-E_d/kT)$, the goal is to record the growth rate needed to barely detect oscillations as a function of temperature. A one-to-one correspondence can then be set up between growth rate and diffusion coefficient at each temperature. This can be seen in the denominator of Eqs.26 and 32a,b. In these equations, an increase in temperature or equivalently D can conceivably be corrected for by a decrease in τ . As an example, Fig.45 shows the amplitude of the oscillations at a fixed growth rate as temperature is varied. These measurements have been extended over a larger temperature range.

Figure 46 is a plot of the temperature needed to completely extinguish oscillations as a function of growth rate, for both the "A" and "B" type misorientations. At low temperatures within the 2×4 reconstruction the Neave analysis may apply, however near the transition to the " 1×1 " reconstruction the cutoff point is less sensitive to the growth rate. This again implies that a different bond breaking process may be occurring. It is possible that the energy changes in a way similar to that from Eq.32a to Eq.32b. For Eq.32a, the temperature dependence should be $\exp(-E_d/kT)$, while Eq.32b gives a dependence like

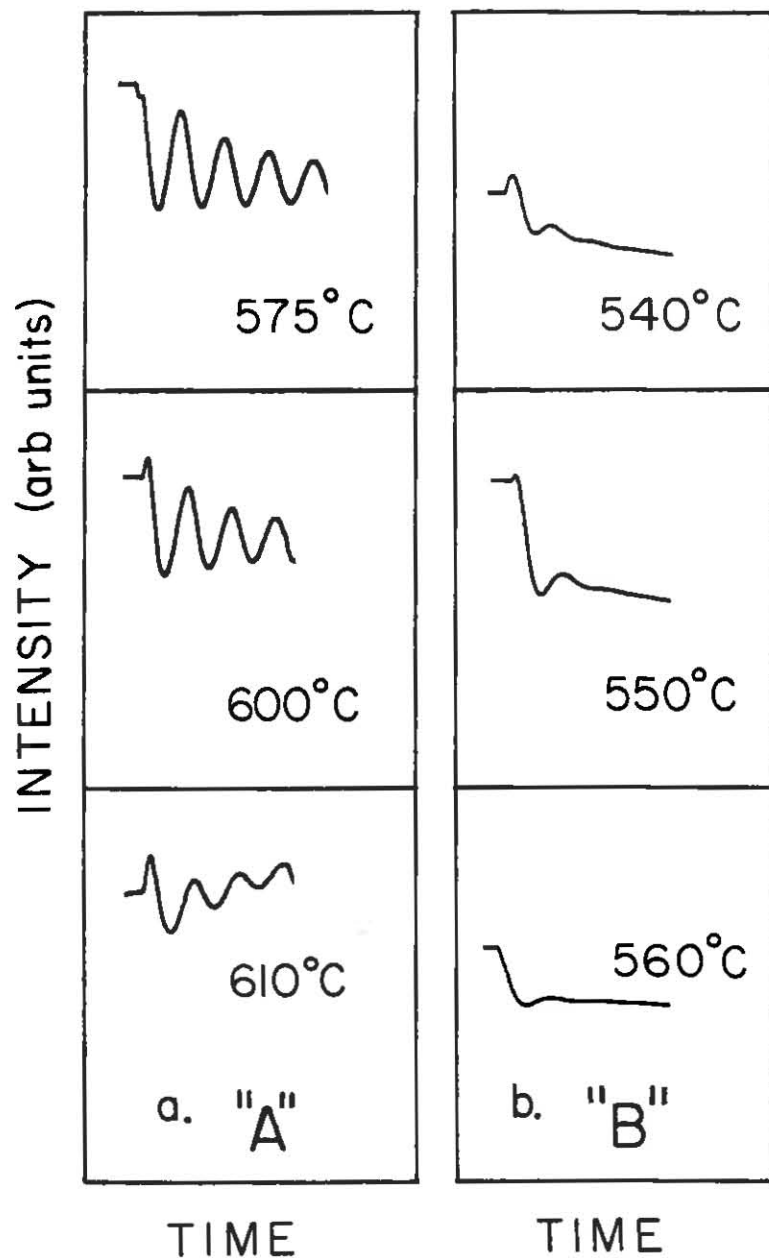


Fig.45 GaAs oscillations on "A" and "B" misorientations.

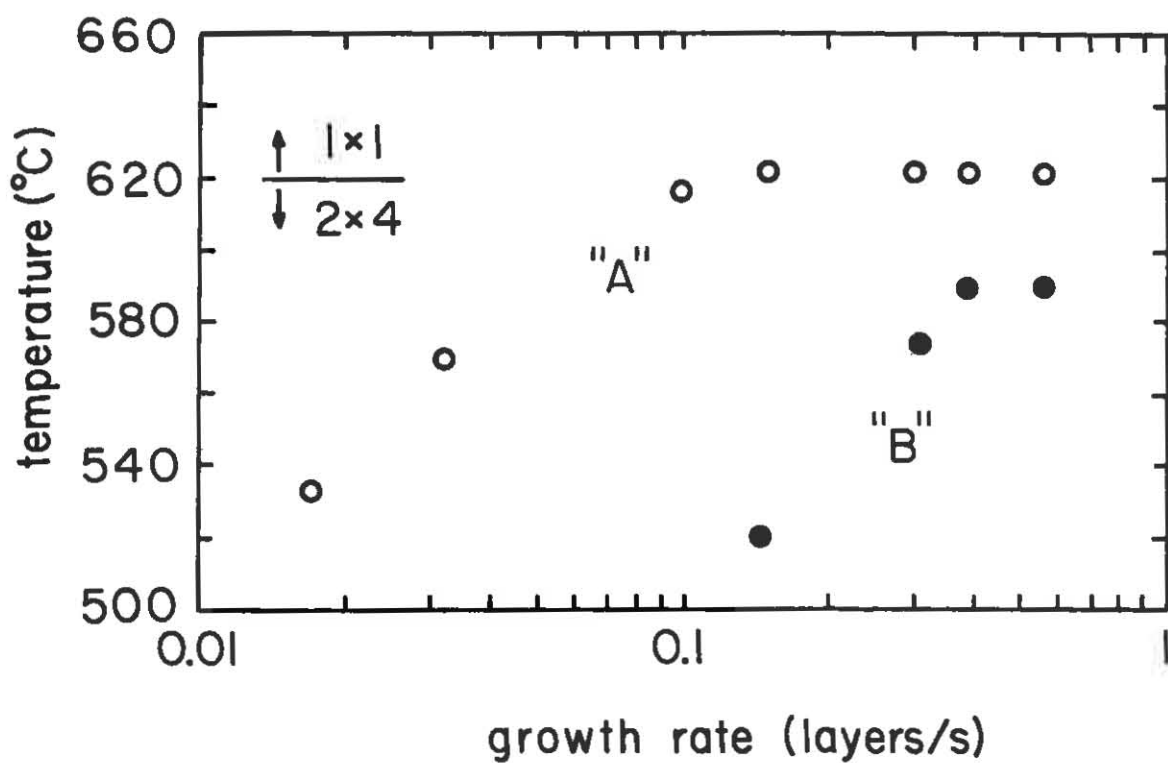


Fig.46 Maximum temperature of oscillations vs growth rate.

$\exp(-(E_d + E_{diss})/2kT)$, which includes fast cluster dissociation kinetics.

We have found that the direction of misorientation is important in this analysis. In Fig.45, growth oscillations on two types of step edges are shown. Recall that if the surface is misoriented in the four-fold direction, As terminated step edges are revealed. If the surface is misoriented 90° to this, in the two-fold direction, the step edges are Ga terminated. For the misorientation with Ga terminated steps, much stronger oscillations are observed. In fact, the As terminated stepped surface often exhibited no oscillations over the entire temperature range. A plausible explanation is that the diffusion rate is higher in the [011] direction, i.e. the direction of the two-fold reconstruction. If this were the case, the diffusing adatoms have a lower probability of cluster formation before reaching the As terminated steps. However, it is difficult to separate faster diffusion toward steps from a decreased reflectivity at step edges. In the latter, the Ga terminated step edges would need to reflect a fraction of adatoms impinging, thereby increasing the probability for cluster formation at the center of a terrace. From an impurity incorporation standpoint, Radulescu [1987] has shown that the "B" misorientation is much more reactive to residual impurities during GaAs growth.

Results on the growth of AlGaAs on "A" and "B" misoriented surfaces have also been reported by Tsui (1985). In those studies, much rougher growth morphologies were observed if the step edges were As terminated ("B"). RHEED measurements [Saluja, 1987] of the growth instability have involved monitoring the widths of the components of the split diffracted beam (initially in the "1x1" reconstruction) as a function of growth time. The onset of beam broadening and loss of integrated intensity during the measurements was used to indicate how quickly the roughening proceeded (see Fig.47). In the RHEED measurements, the "B" surfaces were also observed to roughen much more quickly. Many theories as to the cause of the roughness have been suggested, including the segregation of Ga or a residual impurity. This may pin a step as shown in Fig.48 and cause terrace length fluctuations. Also mentioned as a factor is a lower Al diffusion length [Heiblum, 1983].

The anisotropy between "A" and "B" misorientations is important from the standpoint of growth of GaAs on Si and Ge. In this heteropepitaxial system, either stepped domain can be prepared depending on the substrate pregrowth preparation [Pukite, 1987a,b]. In the next section, the initial Ge surface characterization will be described.

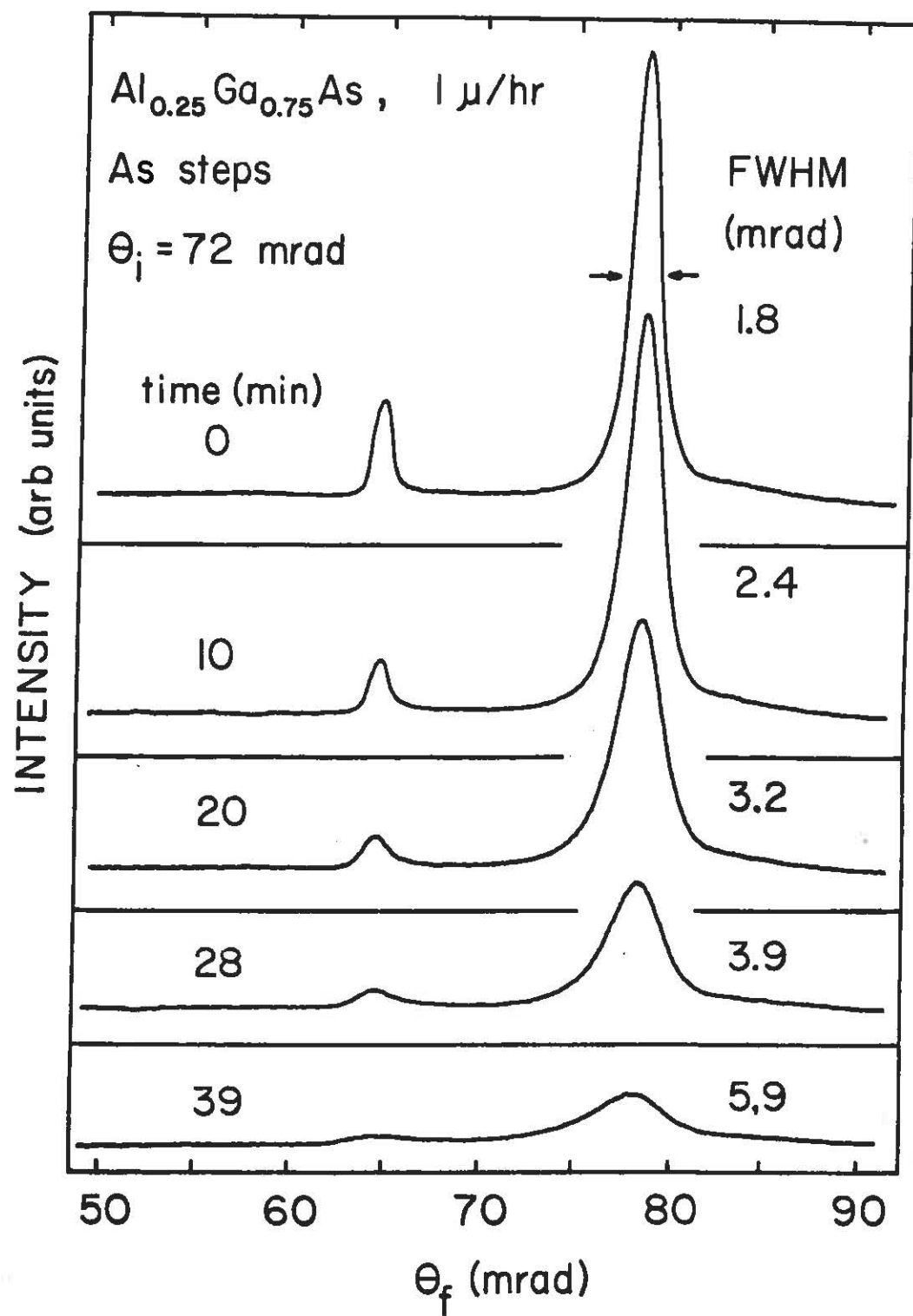


Fig.47 AlGaAs growth roughening on "B" misorientation.

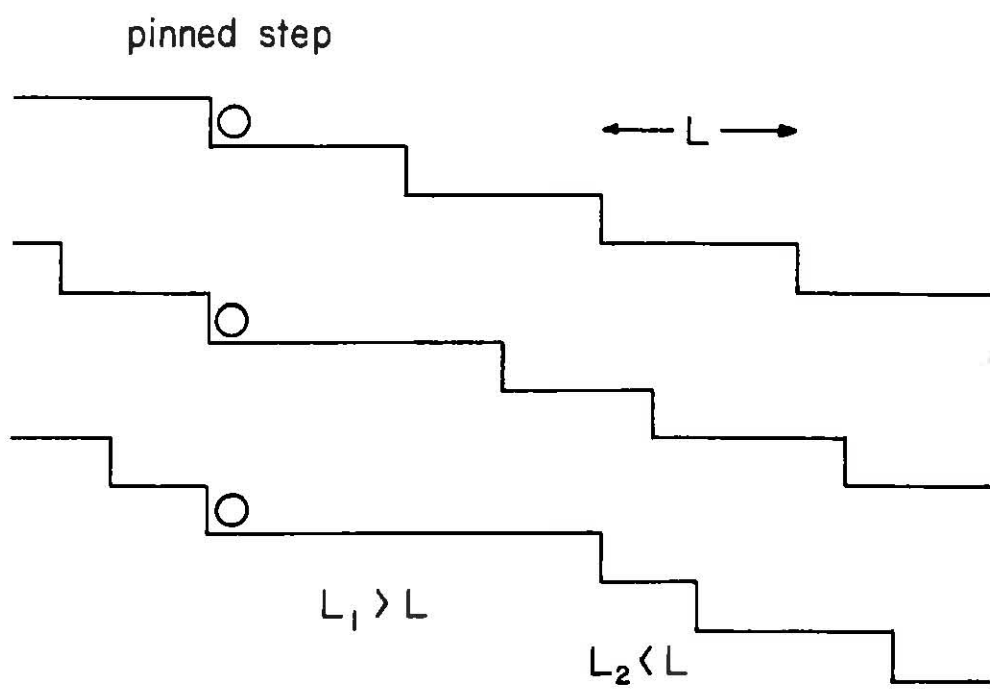


Fig.48 Step pinning mechanism.

5.2. Ge Surface and Growth Characterization

Many of the same growth mechanisms that are observed on GaAs are also observed on Ge. Understanding the growth mechanisms and surface anisotropies of Ge(100) should help the interpretation of GaAs growth and, in particular, the heteroepitaxial growth of GaAs on Ge. As an example of one measurement, Figure 49 shows Ge RHEED oscillations on a 1 mrad and a 7 mrad surface. Aside from the superimposed bilayer period which will be discussed shortly, one should note that the high density of steps on the 7 mrad misorientation diminishes cluster formation on the terraces, much like that on GaAs.

The extinction point of these oscillations was measured as a function of growth rate. Under constant background conditions this occurred at a fixed temperature independent of growth rate [Aarts, 1986]. However with the fluctuation of residual As levels (which was the main impurity) the extinction temperature varied [Pukite, 1987c]. The trend was to higher temperatures with higher background levels. Figure 50 shows RHEED oscillations with unintentional and intentional As flux applied. Clearly the addition of As is enough to enhance clustering. Before we attempt to understand this clustering though, it is important to understand how RHEED is sensitive to the diamond(100)

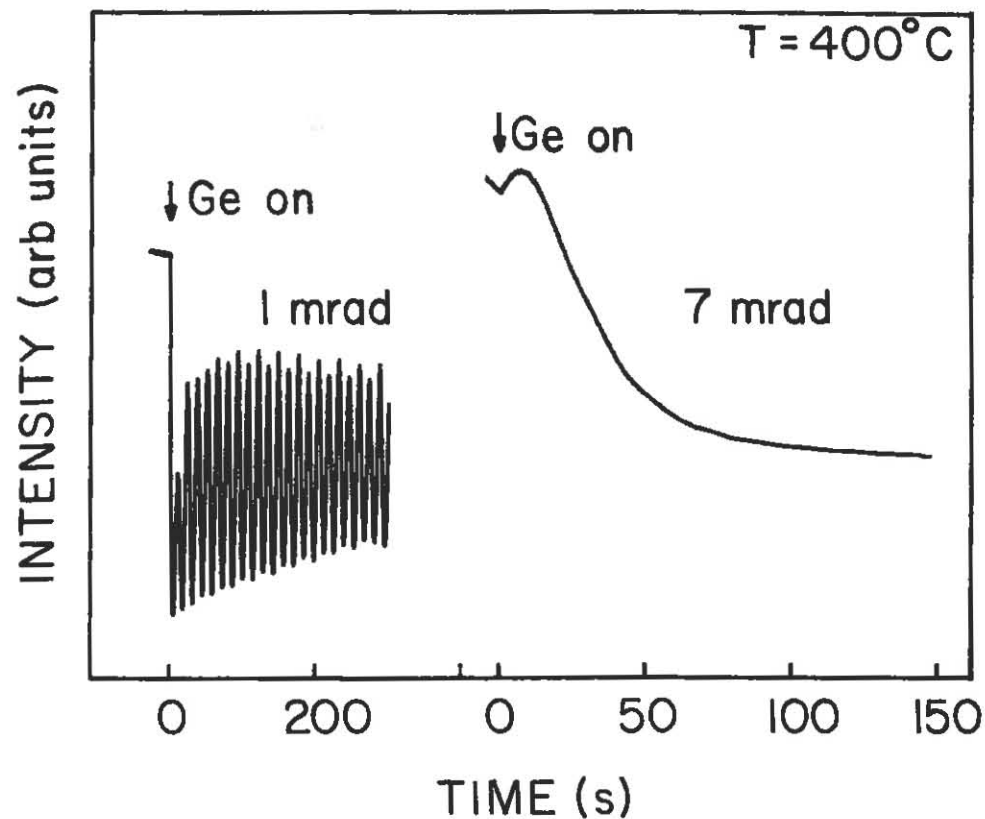


Fig.49 Ge(100) oscillations on flat and stepped surfaces.

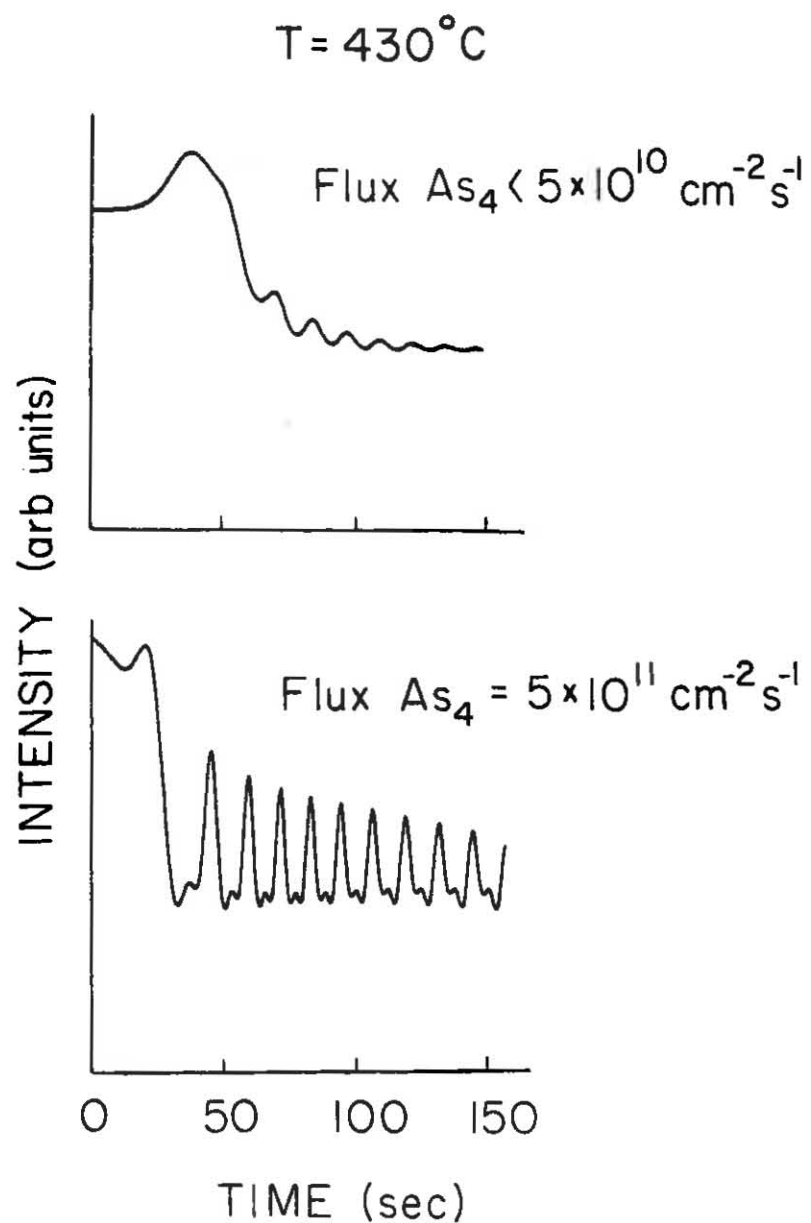


Fig.50 Dependence of Ge oscillations on As background.

crystal surface.

On the Ge(100) surface, two distinct types of steps may occur on the surface at the same time [Pukite, 1987d]. This distinction in steps is somewhat related to the "A" and "B" steps found on GaAs. In the following, we will demonstrate how the steps are distinguished by diffraction and then observe the relative propagation of the two types of steps as a function of growth conditions.

Ge(100) substrate steps are distinguished by the tilt of the dangling bonds relative to the step edge orientation. The terraces are also distinguishable, belonging in effect to sublattice "A" and sublattice "B" of the diamond structure (see Fig. 27). Since multiple scattering is sensitive to the atomic geometry of the surface relative to the beam direction, the two types of terraces would be expected to give different diffracted intensities at an arbitrary azimuth. The only azimuth where the multiple scattering is the same from terrace "A" and terrace "B" is the [010] direction [Sakamoto, 1986]. To distinguish step related effects from diffraction related effects all measurements should be made at this azimuth.

Experimentally, the existence of both terraces is confirmed by a two domain ($2 \times 1 + 1 \times 2$) diffraction pattern

(see Appendix A). To obtain physically distinguishable steps requires a misorientation towards a $\langle 011 \rangle$ direction. Figure 51a shows the angular profile from a Ge(100) surface misoriented by 4 mrad toward a $\langle 011 \rangle$ direction. The angle of incidence corresponds to a single-layer step ($d=a/4$) out-of-phase. There are three items to note here. First, two domains are confirmed by a double domain diffraction pattern. Secondly, the separation between the strong satellite peaks matches to the 4 mrad misorientation and single-layer steps. Finally, there is a small peak at the specular condition that is sensitive to Ge growth conditions.

Figures 51b and 51c shows how the central peak responds to the growth of Ge. The growth temperature is set above where intensity oscillations are observed. Importantly, in Fig 51c, the double domain diffraction pattern becomes a nearly single domain 2×1 with the dimers aligned parallel to the step edges [Kaplan,1980]. The origin of the central peak then becomes clear. In real space the staircase is transformed from a singly stepped staircase of average terrace length $L \approx L_A \approx L_B$ to one that is doubly stepped with terrace length $L = L_A + L_B$. The diffraction senses this as the single-layer out-of-phase angle becomes the double-layer in-phase angle,

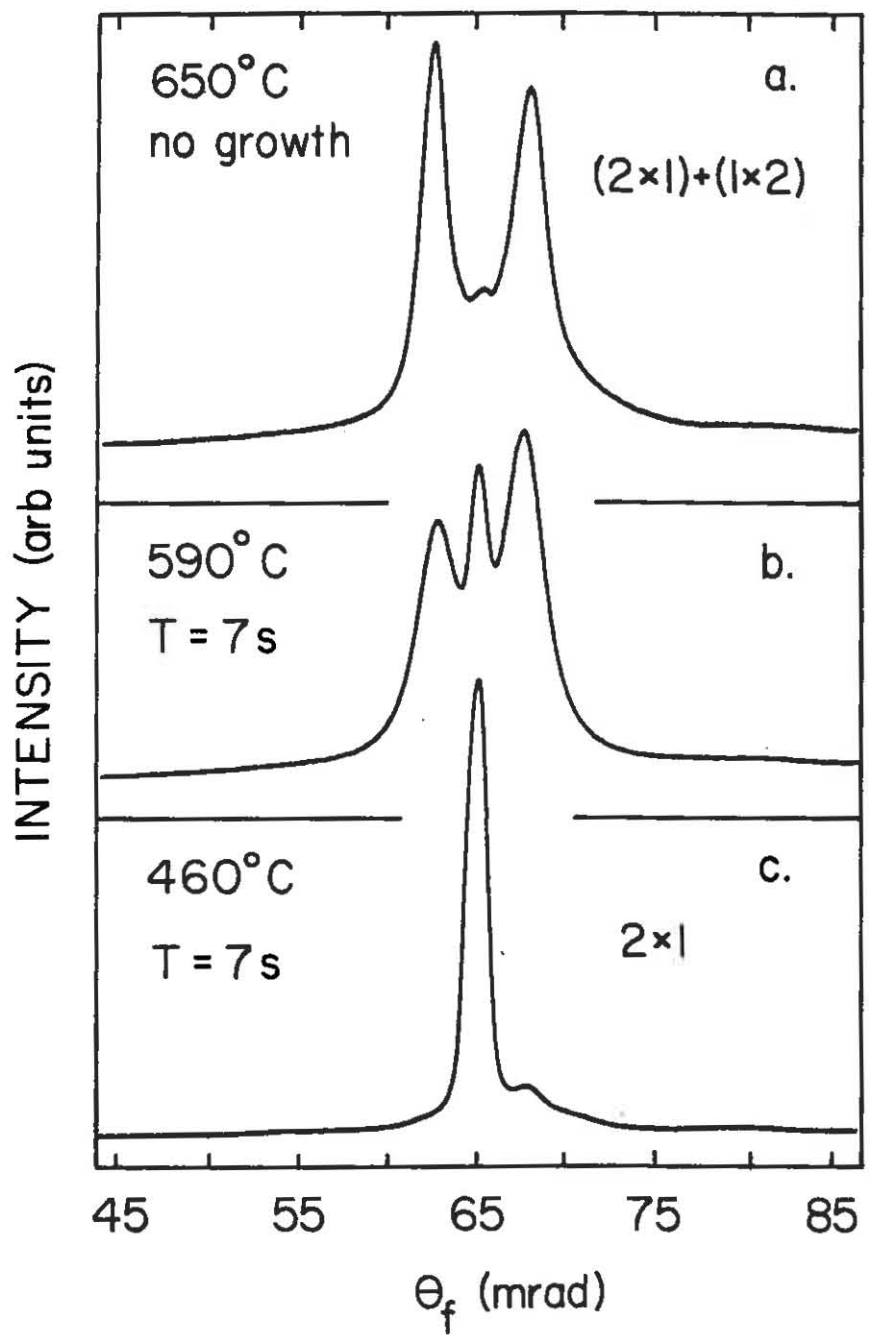


Fig.51 Growth induced $(2\times 1)+(1\times 2)$ to 2×1 transition on Ge(100).

$$\theta_i = 1.5\pi/(k \cdot d) \text{ (out-of-phase)} = 3\pi/(k \cdot 2d) \text{ (in-phase)} \quad (35)$$

where the central peak becomes the sharp in-phase peak. The relative intensity of the central peak gives an indication of the areal coverage of one type of terrace compared to another. This dependence can be expressed as

$$\frac{I_{\text{central}}}{I_{\text{satellites}}} = \frac{(1-2n)^2}{4n(1-n)} \quad (36)$$

where the intensity is the integral within each beam and n is defined as $L_B/(L_A+L_B)$. This ratio is equivalent to the ratio between $C'_{ii}(S_x)$ and $\delta(S_x)$ obtained for the two-level system at an out-of-phase condition (see Eq.8). Furthermore, the fixed separation of the satellite peaks means that $L_A+L_B = \text{constant}$. This implies a long-short alternation between L_A and L_B on successive terraces [Pukite, 1987a]. Assuming that initially the two terraces were of equal length, the decrease in length of terrace "B" with time must equal the increase in length of terrace "A".

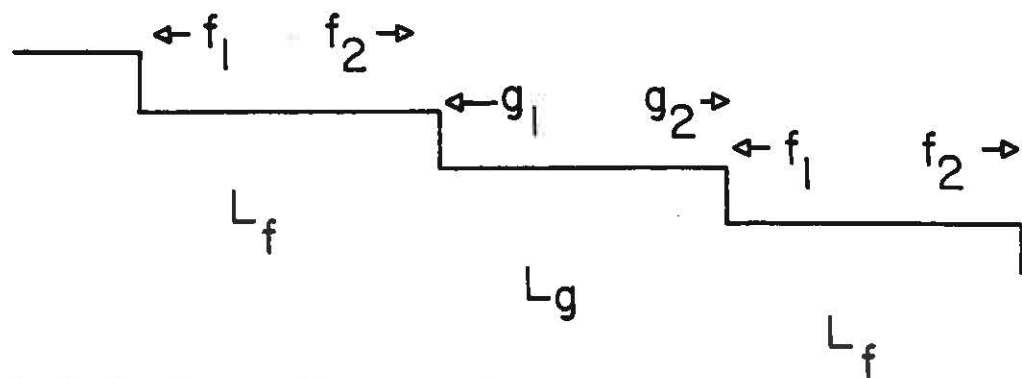
The single domain transformation is kinetically controlled. For example, if growth is stopped and the substrate is heated to 600°C, the two domain pattern and Fig.51a is recovered. This implies that single layer steps are the equilibrium configuration. The growth kinetics are

most likely related to that discussed for GaAs. The two possibilities discussed previously were anisotropic diffusion and different reflectivities at step edges. In either case, the relative propagation of the two types of steps during growth leads to the metastable arrangement. This is shown in Fig.52.

Next, we will address the issue of Ge growth clustering briefly mentioned at the beginning of this section. In particular, how As influences the Ge clustering is important to understand from the point of view of heteroepitaxial growth of GaAs on Ge. In this growth system, the interaction between As and Ge may influence the initial stages of growth.

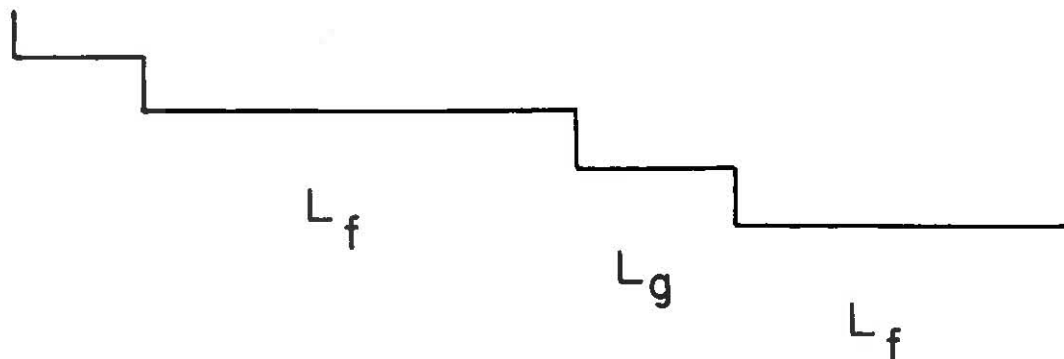
The diffraction pattern from a surface devoid of steps consists of sharp beams at each of the integral-order beam positions. When growth is started on such a surface, short-range correlations are increased and the diffracted beams broaden. As during GaAs growth [Van Hove, 1985] the broadening is also observed during Ge growth and is enhanced by As. In particular, diffraction from the two-dimensional clustering as described in Sec.2.2.B is evident.

The cluster formation shows up dramatically in the RHEED pattern. If the electron beam is directed along a



I. Calculate flux ratios,

$$\text{if } \frac{g_1}{g_2} > \frac{f_1}{f_2} \text{ then } L_f > L_g$$



2. steady state: ratios equal,
lengths alternate

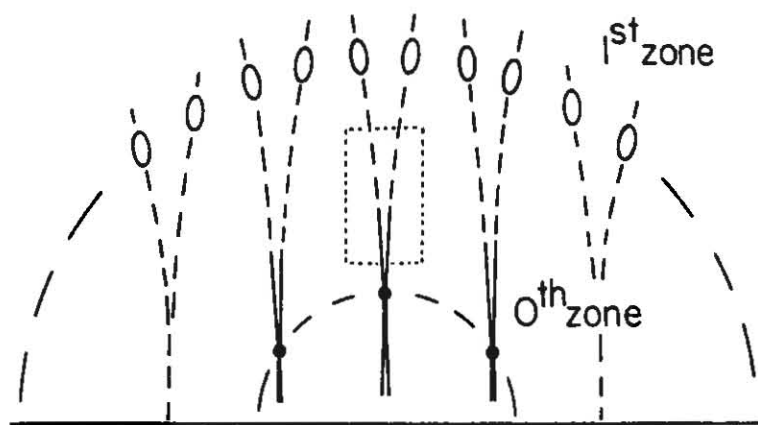
Fig.52 Model for Fig.51.

[010] axis, diverging streaks are observed to emanate from each of the diffracted beams. Diffracted beam profiles across these streaks are shown in Fig.53. This plot should be compared against that of Fig.17. The separation in $2\Delta\phi_f$ is plotted as a function of final angle in Fig.54 along with that expected from Fig.18. Comparing to the calculation of Sec.2.2.B, clearly the effect of clusters with straight edges along <011> directions is being observed. The diffraction behavior is simply a geometric shape effect featuring square or rectangular clusters.

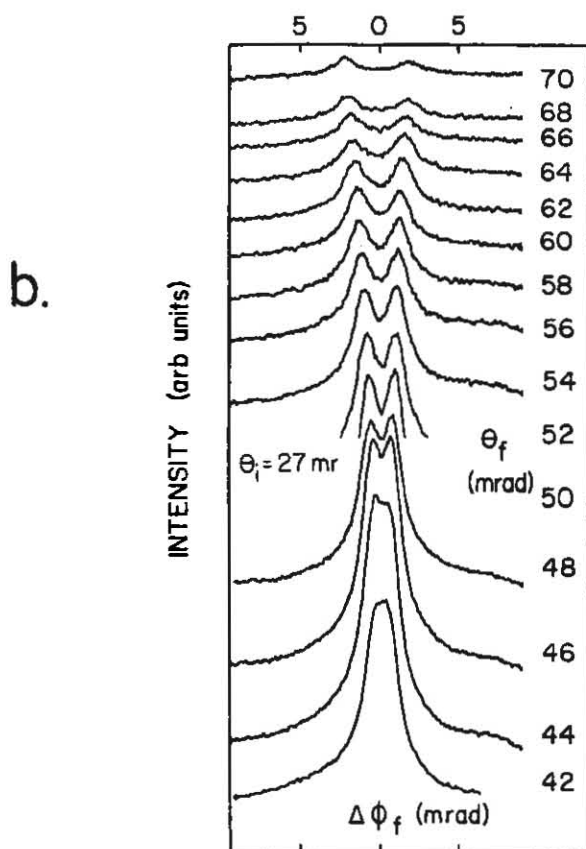
The fact that the superstructure 2×1 reflections show broadening along only one axis indicates that the clusters are rectangular. The short axis of the rectangular cluster corresponds to the reconstructed, 2×, direction (see Fig.55). The superposition of the two possible domains makes the diffraction pattern symmetric about $\Delta\phi_f=0$ for the integral order beams. Fig.56 shows the comparison to data given that the clusters are geometrically distributed with average terrace lengths of 100 Å in one direction and 50 Å in the other direction (see Appendix B for further details).

The square shape of the clusters is likely governed by energetics. Having edges along <011> directions minimizes the number of dangling bonds for a given area cluster [Giling,1985]. More difficult to explain is the elongation

[010] azimuth



a.



b.

Fig.53 a. RHEED pattern from growing Ge(100) surface.

b. Beam profiles taken across the streak (dashed box).

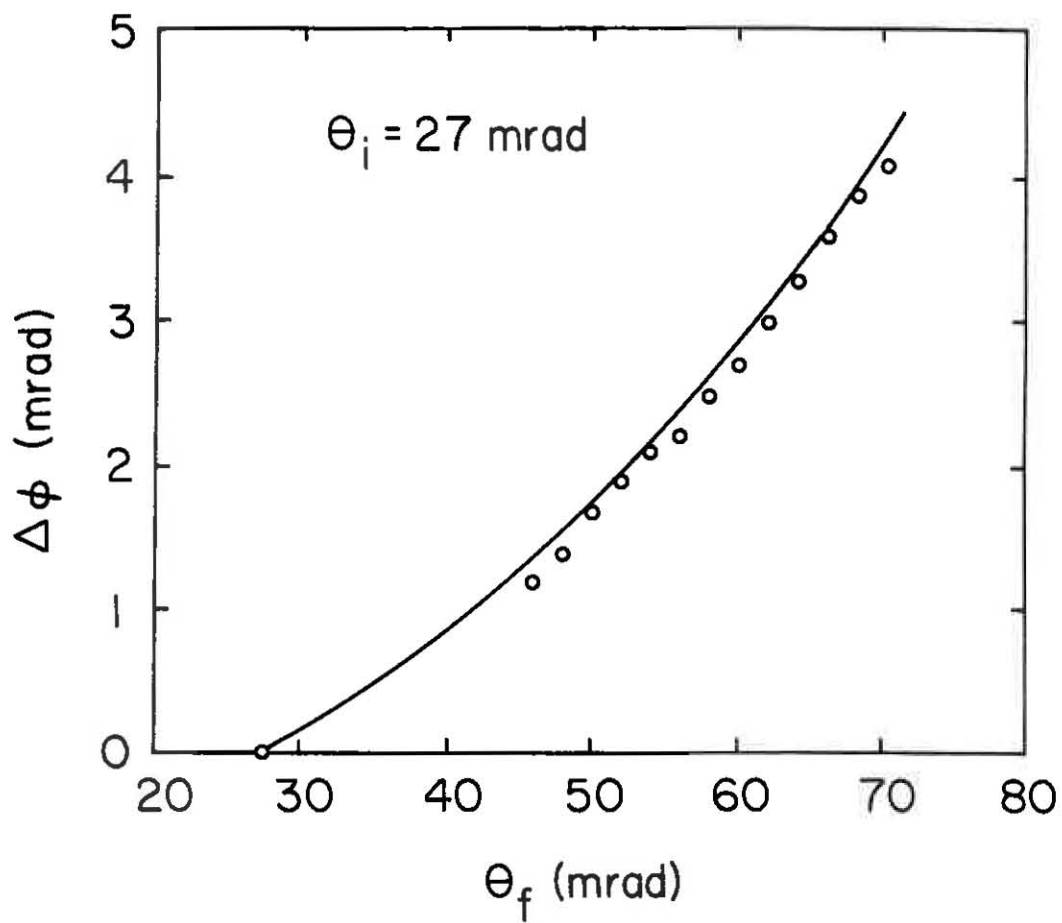


Fig.54 Streak separation vs final angle in Fig.53.

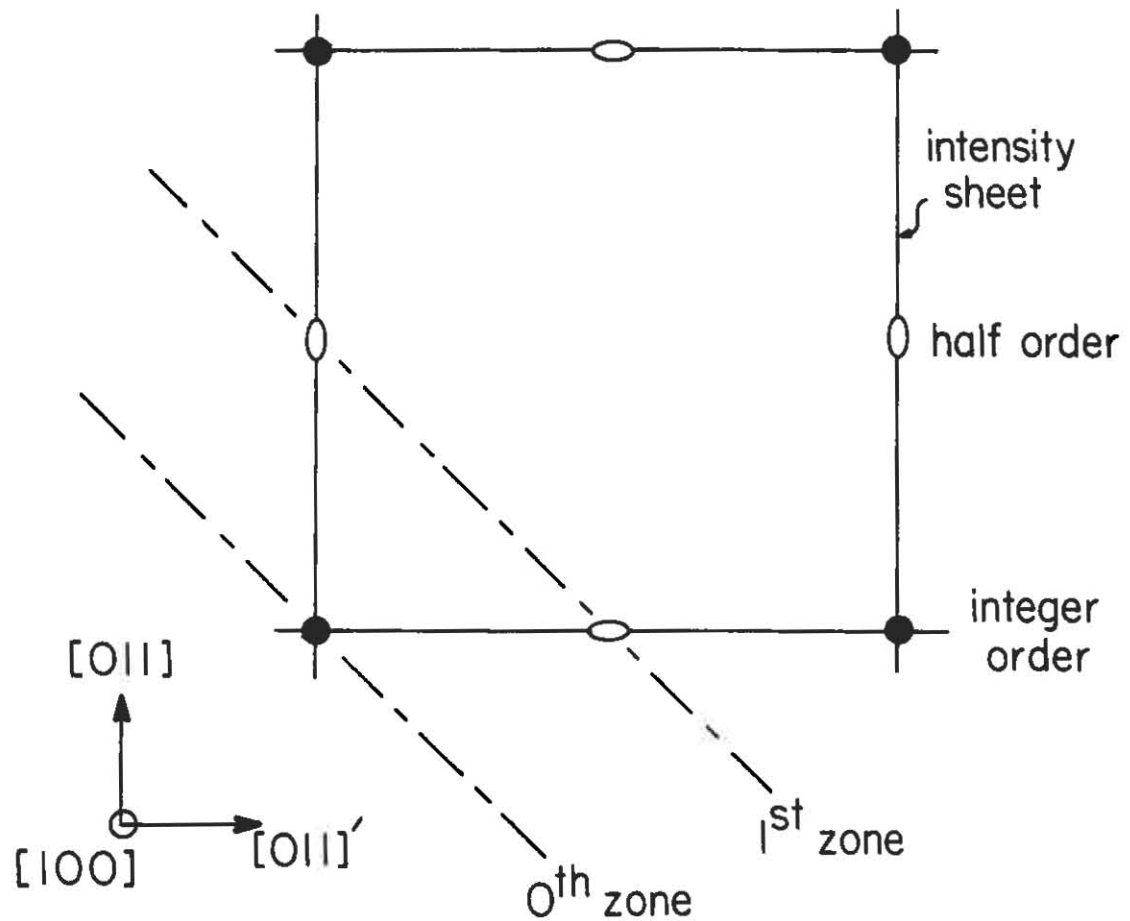


Fig.55 Top view of domain broadening.

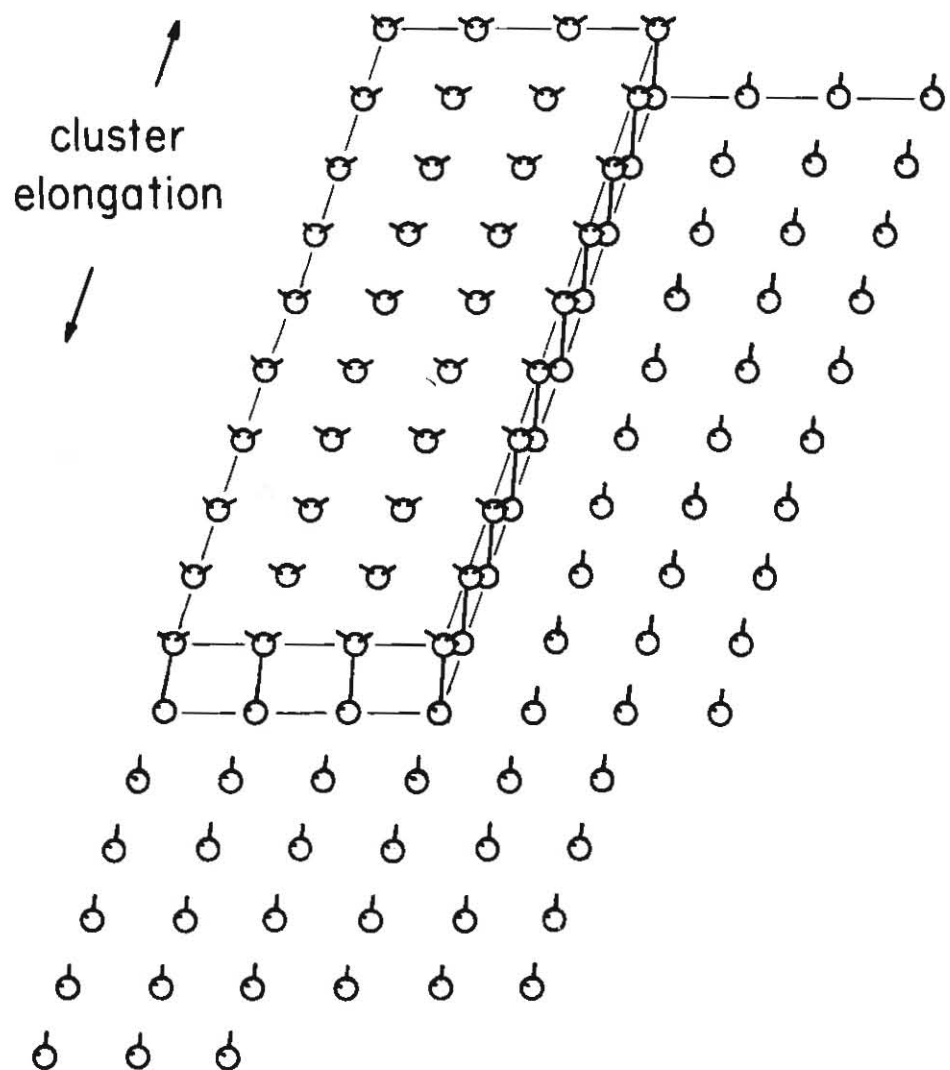


Fig. 55 Continued

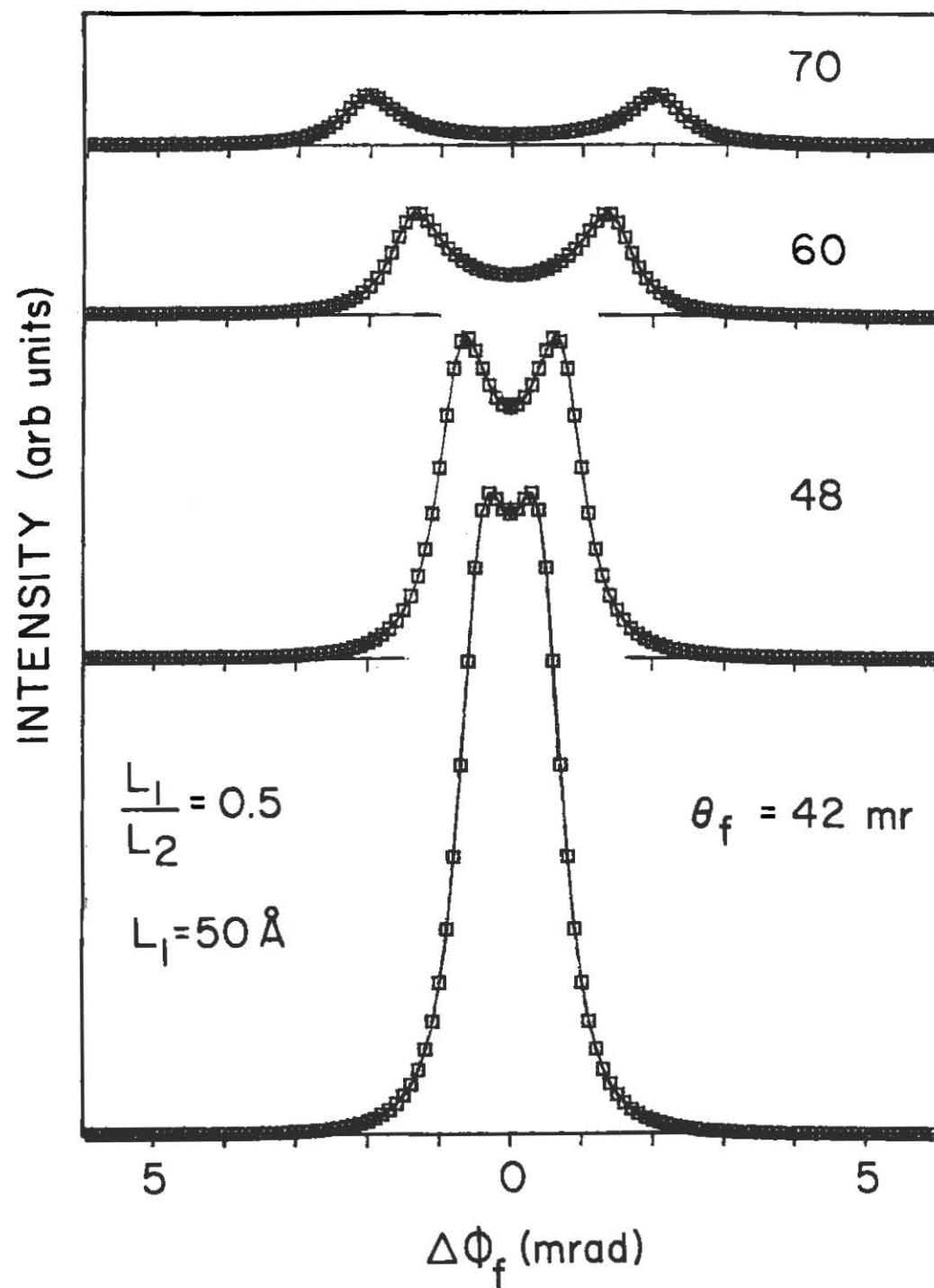


Fig.56 Fit to Fig.54 showing asymmetric cluster sizes.

of the clusters. A monolayer high cluster that is square contains two types of step edges. These are distinguished by whether the dangling bond is pointed along or perpendicular to the step edge. Arsenic is known to cause a mass migration of atoms when applied to a stepped surface of Ge (see next section). This was attributed to the As occupying (111) sites at only one of the types of step edges and pinning its motion. Alternatively, anisotropic diffusion could also play a role in the elongation [Rockett, 1987].

The clusters are stable when growth is stopped. The streaking only disappears when the substrate temperature is increased to a level where normally no oscillations are observed ($>550^{\circ}\text{C}$). Presumably, at this point the dissociation rate of critical clusters greatly exceeds their formation rate. Growth strictly by step propagation then occurs.

Finally, we would like to comment on the bilayer oscillations. Sakamoto et al [1986] have observed these on the Si(100) surface, and we find the same dependence on diffraction conditions. Figure 57 shows bilayer oscillations in the [011] azimuth and monolayer oscillations in the [010] azimuth. The bilayer oscillations in essence are directly attributable to the alternating sublattices of the diamond structure. This means that growth is proceeding monolayer by

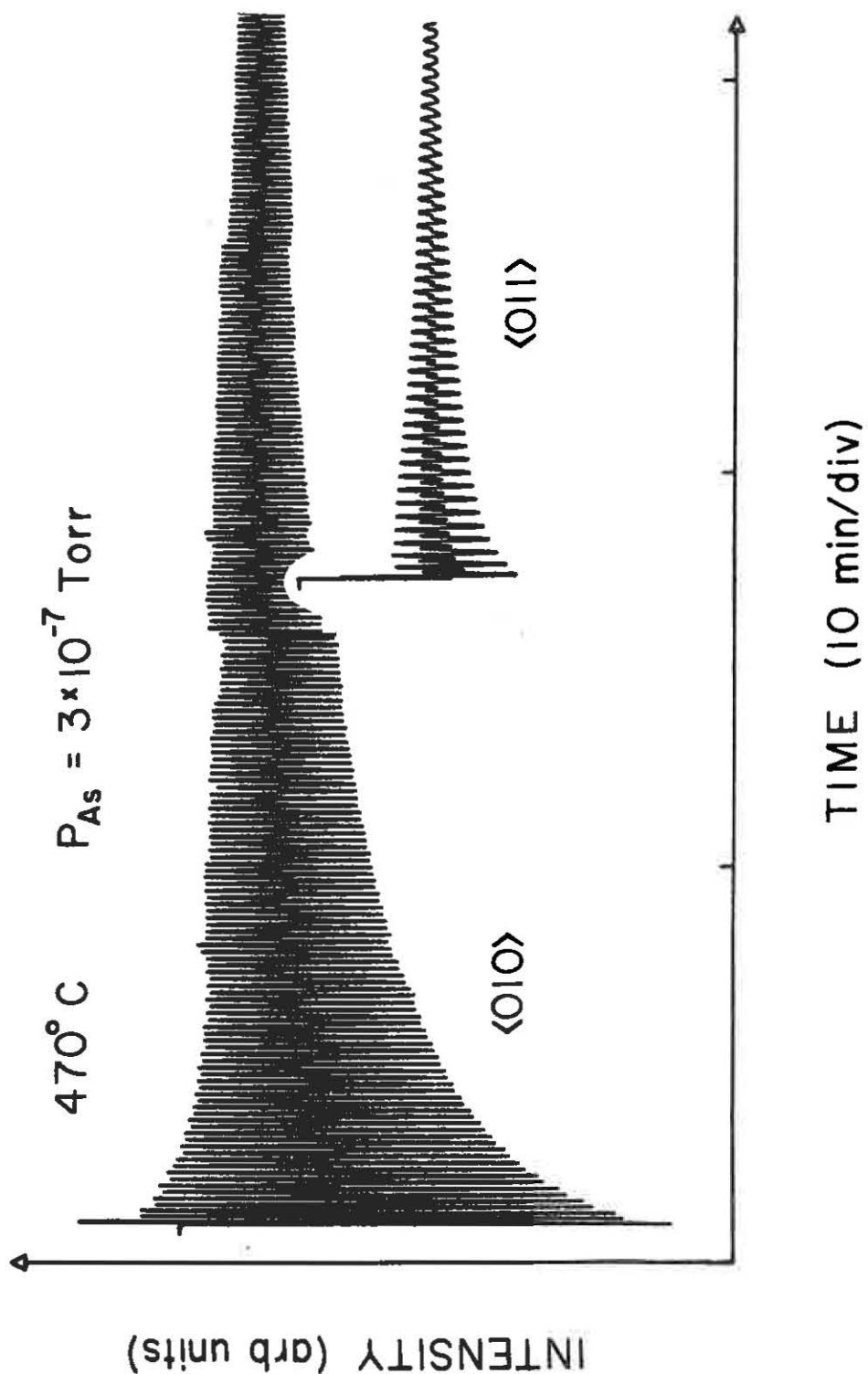


Fig. 57 Ge(100) RHEED oscillations in <010> and <011> azimuths.

monolayer but the diffraction senses the repeat period of two monolayers, i.e. of the two distinct sublattices. This is maximized for the [011] azimuth where the scattering factor difference is greatest and minimized for the [010] azimuth where there is no scattering factor difference between successive layers [Moritz, 1987]. It appears that the anisotropic growth processes observed in this study can only help make the two sublattices more distinct, particularly if it provides a difference in areal coverages of the two sublattices.

5.3. GaAs on Ge(100) growth

The characterization of the growth of GaAs on Ge follows three stages: initial clean surface, As-exposed surface, and nucleation of GaAs on Ge. In the following, RHEED is used to investigate the surface at each stage.

As others have reported [Fischer, 1985], the best growth of GaAs on Ge has been observed on substrates misoriented by a few degrees from the (100). We have followed this approach and used substrates misoriented toward the [011] and [010] directions as shown in Table 1. For a Ge(100) $2^\circ \rightarrow [011]$ surface, Fig. 58a shows the diffracted intensity along the length of the streak with the electron beam 10° from the [011] direction. The separation of the more intense peaks

| Substrate misorientation | | As species | Four-layer | GaAs domain |
|-----------------------------|--------|-----------------|--------------|---|
| ϵ | ϕ | | step period? | |
| 6° | [011] | As ₄ | Yes | [01̄1] \perp to ϕ |
| 6° | [011] | As ₂ | Yes | [01̄1] \parallel to ϕ |
| 2° | [011] | As ₄ | Yes | [01̄1] \perp to ϕ |
| 2° | [010] | As ₄ | No | Two domains |
| 0.25° | [041] | As ₄ | No | [01̄1] 69° to ϕ + weaker domain [01̄1] 31° to ϕ |

Table 1 GaAs domain orientations on Ge substrates.

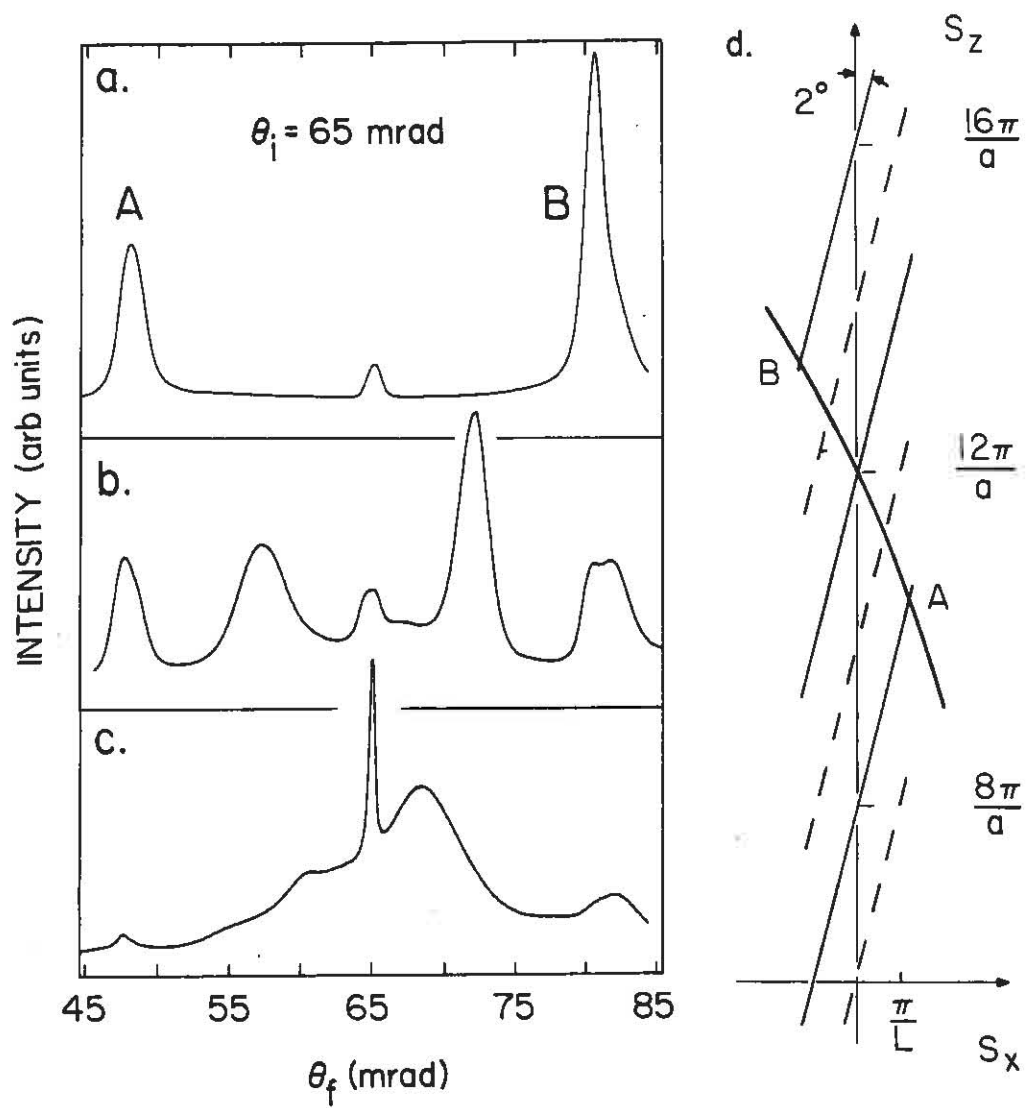


Fig.58 a. Clean Ge(100)2°[011] diffracted beam profile.
 b. After adsorption of As.
 c. Ge(100)2°[010] after As adsorption.
 d. Ewald sphere intersection for a. and b..

indicates diffraction from a surface staircase consisting of single-layer, $a/4$, steps. The Ewald sphere - reciprocal lattice intersection is shown in Fig.58d for the given incident angle (65 mrad). A similar single-layer periodicity is observed for the other misorientations. In each case a 2×2 (2×1 and 1×2 orthogonal domains) Ge reconstruction is observed in equilibrium. Special growth procedures were used to achieve a single domain 2×1 reconstruction of Ge (described in Sec.5.2), but care was taken as this was not stable at high substrate temperatures ($>500^\circ\text{C}$).

Referring to Fig.58a, the weak central peak corresponds to a less pronounced double-layer periodicity which is also occurring on the surface. Most likely, the different sublattices provide a scattering factor change which the diffraction detects as a double-layer periodicity. This is prominently seen in Fig.2c, where the [011] azimuth shows a strong double-layer splitting. As described in Sec.5.2, only for [010] beam azimuths are these scattering factors the same. In addition, a long-short arrangement in terrace lengths as described in the previous section could be occurring. This gives a similar scattering factor change but one that is the same for every azimuth. The single-layer steps we observe on the Ge(100) vicinal surface is in contrast to the double-layer steps that Olshanetsky (1977) reports for non-epitaxially prepared surfaces misoriented

toward a [011] direction.

A major reorganization of the Ge step structure occurs on each of the surfaces if exposed to an As flux. A longer range periodicity is detected by RHEED as shown in Fig.58b. The position of the new peaks as a function of scattering angle for both the 2° -[011] and 6° -[011] surfaces result in a periodicity corresponding to four-layers. The largest periodicity observed on the surface has doubled, giving rise to constructive interference conditions which are halfway between the already established peaks. The extra reciprocal lattice rods are shown in Fig.58d as dashed lines. During this step redistribution, the fractional-order peaks remained at the 2×2 positions.

The transition from single-layer steps to a four-layer periodicity is reversible as shown in Fig.59. At high As fluxes and low substrate temperatures the four-layer structure is predominant. At high temperatures, the As is desorbed and the single layer steps are recovered. Auger analysis confirmed the lack of As at high temperatures and adsorption of As at low. The phase boundary has an activation energy of 5 eV, signifying a first-order phase transition. The width of the transition region is $\leq 10^\circ\text{C}$.

The simplest interpretation to the four-layer

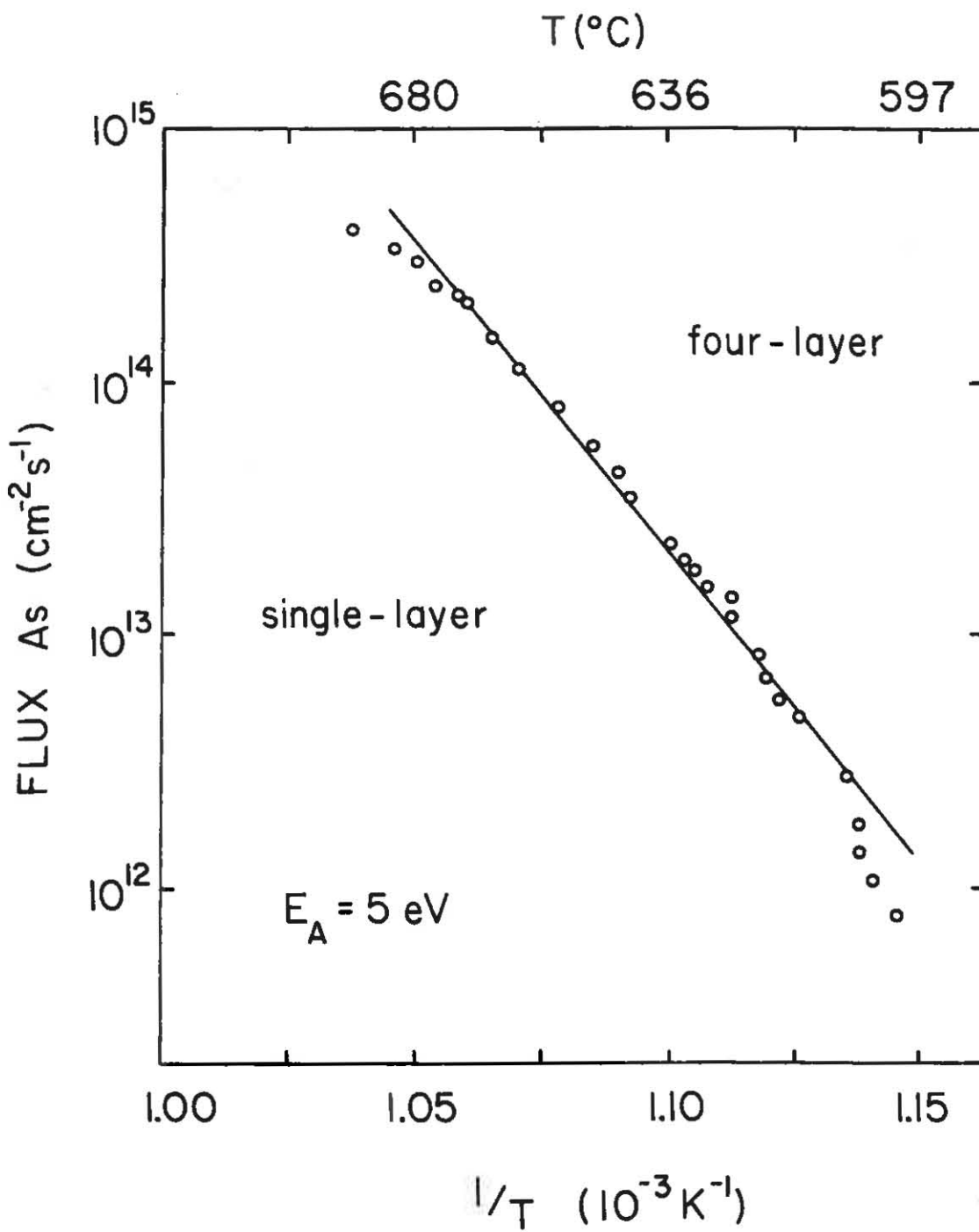


Fig.59 Phase diagram for As adsorption.

periodicity observed would be to attribute it to strictly four-layer high steps. However, both the exact shape of the diffraction profile and the appearance of a two-domain reconstruction leads one to a more complicated picture. First, the symmetry of the diffraction profile in Fig.58b shows a weak central peak and stronger satellite peaks on both sides. This suggests a large proportion of odd-layer step heights. Additionally, the two domain 1×2 observed requires odd-layer steps. A predominantly single domain 1×2 (with the 1/2 order pattern stronger in the direction perpendicular to the staircase) can be obtained by crossing through the phase boundary very slowly. The symmetry of the diffraction profile measured here (large central peak) suggests larger numbers of even-layer steps.

A simple step structure giving a two domain reconstruction and a four-layer periodicity is one that strictly alternates triple- and single-layer steps. Neglecting the alternating scattering factor effect, calculated diffraction profiles (see Fig.60) from this surface are very close to what is measured. To explain a transition from alternating triple- and single-layer steps would require an ordered mass migration of atoms. This in turn would require a high mobility of Ge adatoms and a site specific attachment of As atoms. Fig.61 illustrates a model for an As induced transition from single steps to a triple-

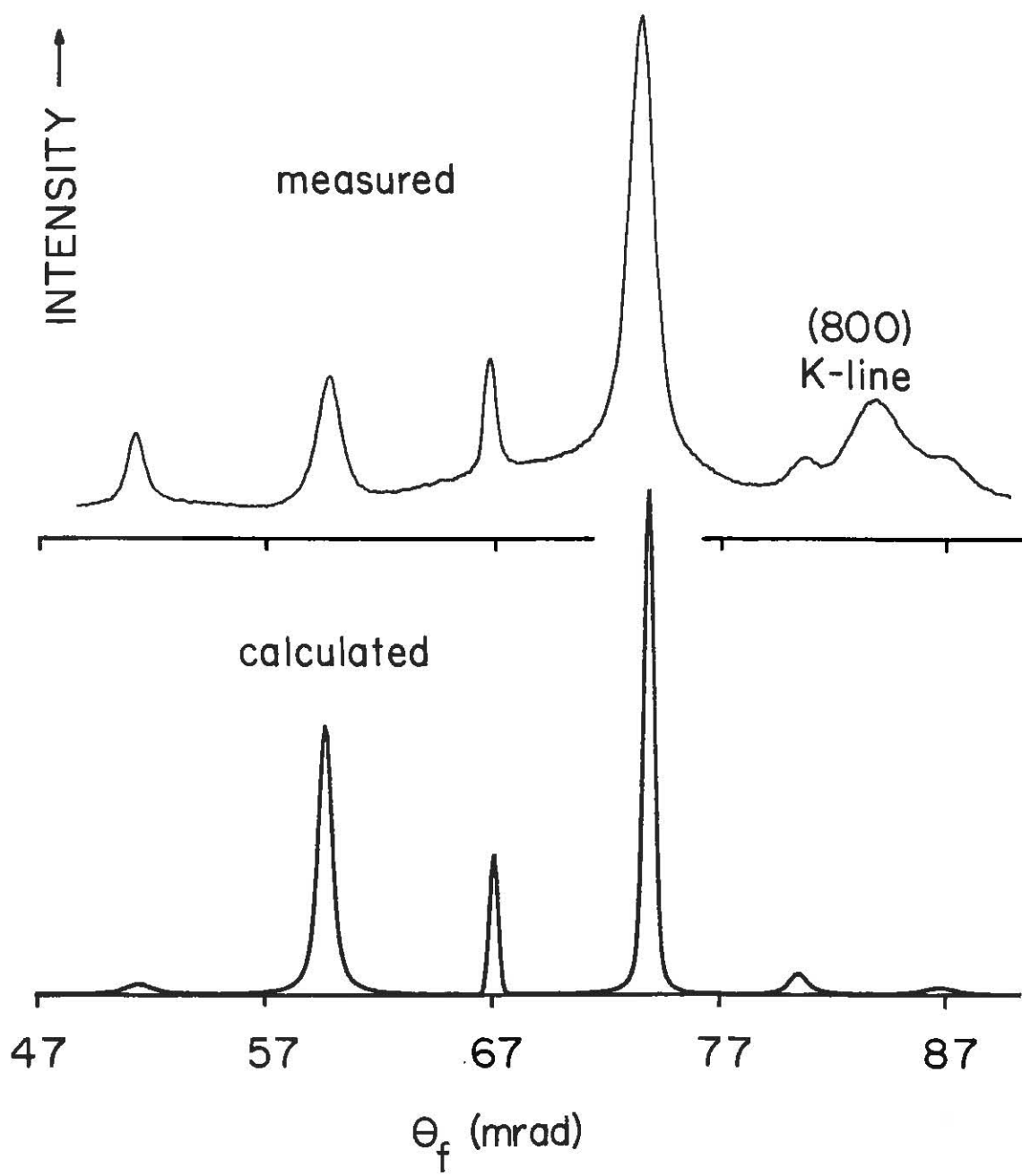


Fig. 60 Multilayer stepped surface fit to angular profile.

and single-layer alternation incorporating these ideas.

Fig.61a is the Ge(100) vicinal surface consisting of single-layer steps. A specific site adsorption of As atoms can be achieved by allowing As atoms to exchange sites with Ge atoms along only those step edges shown in Fig.61b. This in effect saturates the (111) sites along step edges. When this reaction takes place, the Ge atoms located to the right of the As sites are more weakly bound due to only a threefold coordination of As with Ge [Bringans,1986]. This allows the Ge "islands" to migrate over the surface to a lower energy configuration. The arrow in Fig.61c illustrates one path that allows the weakly bound islands to coalesce and form an alternating triple- and single-layer step periodicity. From RHEED studies of ordering rates from deliberately roughened surfaces as detailed in the previous section, a substrate temperature of $>500^{\circ}\text{C}$ is high enough to allow an average adatom migration of length 40 Å to proceed quickly.

On surfaces misoriented towards the [010] direction a mass migration is also observed as shown in Fig.58c. However, based on the diffuseness of the satellite peaks the mass migration is not ordered. From the previous model, the lack of ordering is expected from the indistinguishability of adjacent terraces and their step edge sites to As adsorption. During this transformation, curved streaks are observed (see Fig.2d) indicating steps that have tried to

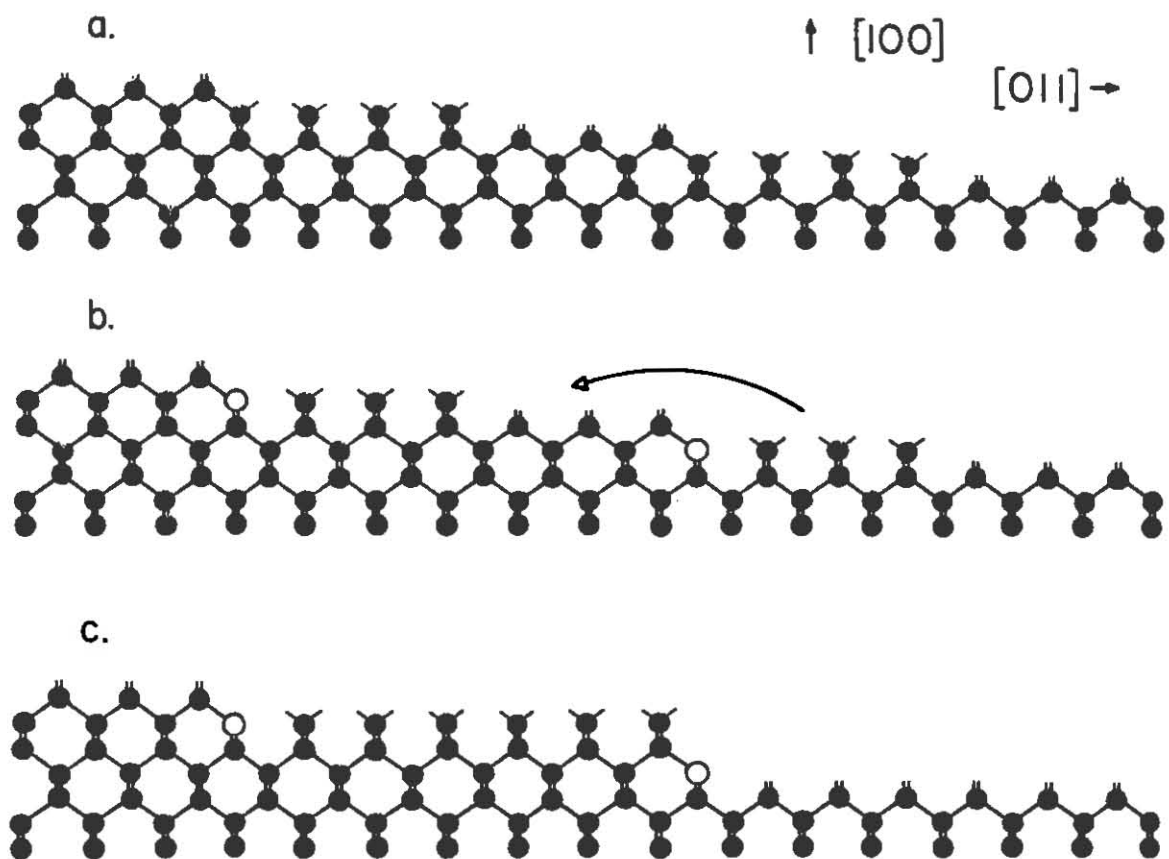


Fig.61 a. Clean Ge(100) surface staircase.

b. After As adsorption.

c. Final configuration.

straighten out along [110] axes. A schematic of this surface is shown in Fig.62 and recall from Sec.2.2.B the effect of cluster shape effects on diffraction.

To summarize, for each of the misoriented Ge surfaces studied, the adsorption of As causes a large rearrangement in the static Ge surface configuration. How this influences the initial GaAs growth will be described next.

The growth of GaAs on Ge initially follows a three dimensional process [Petroff,1977]. This is confirmed by the appearance of a transmission cross-section diffraction pattern. No RHEED oscillations are observed (this is opposite to the initial growth of Ge on GaAs). Initiating GaAs growth with an As_4 flux on a surface misoriented toward the [011], we have observed clear chevrons superimposed on the bulk spots if the electron beam is directed perpendicular to the staircase. The chevrons as described in Sec.2.2.D are due to pyramidal facets. The measured angle of the chevrons with respect to the [100] direction indicates that the diffraction is occurring from pyramidal (311) facets (see Fig.63). Within 1000 Å of growth, these chevrons fade and 1/4 order streaks are observed, establishing the facets as (311)A. With the electron beam directed down the staircase, weak 1/2 order streaks superimposed on a transmission-like pattern are observed quickly after the

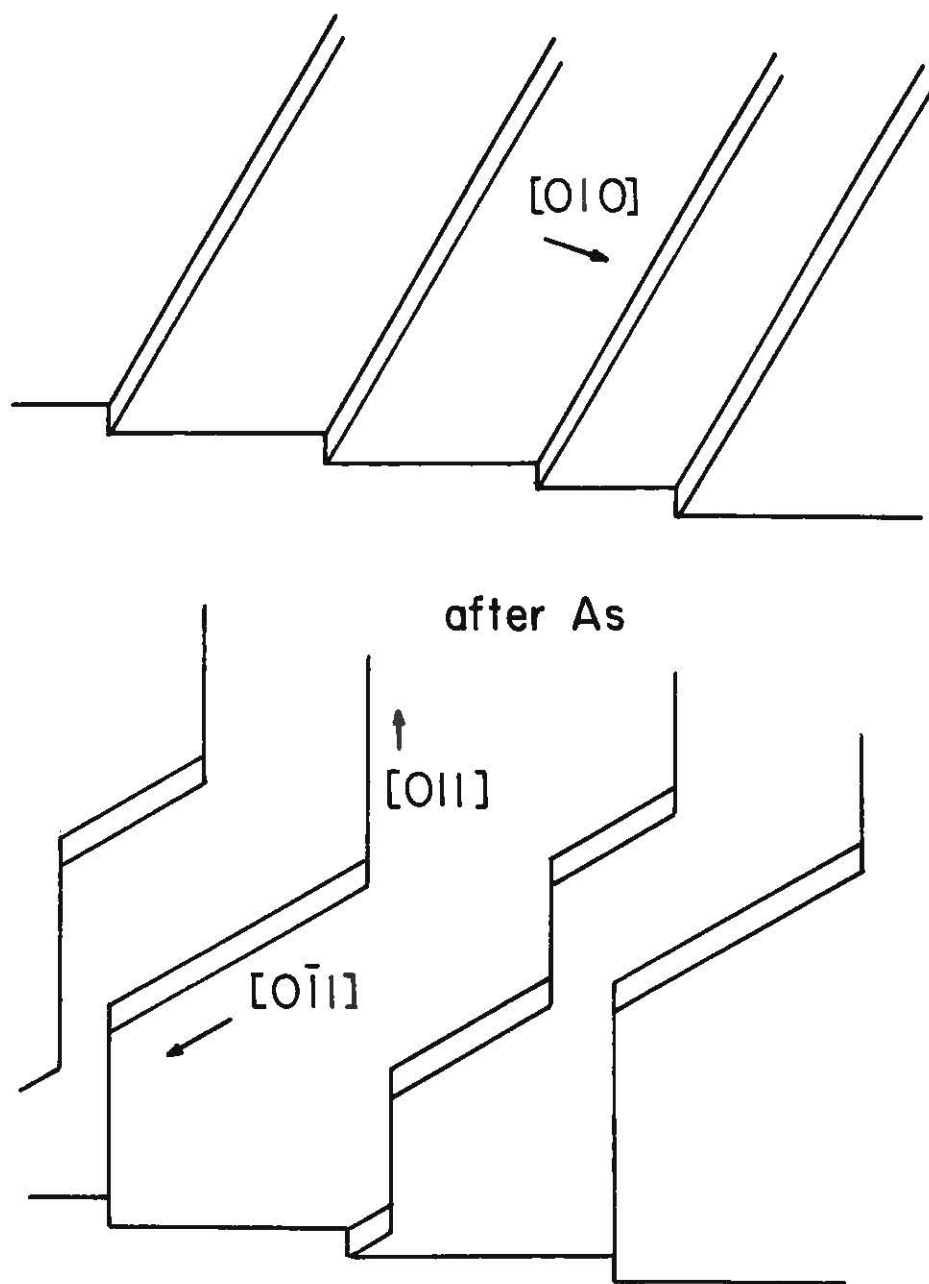


Fig. 62 Ge(100) 2° [010] step transition.

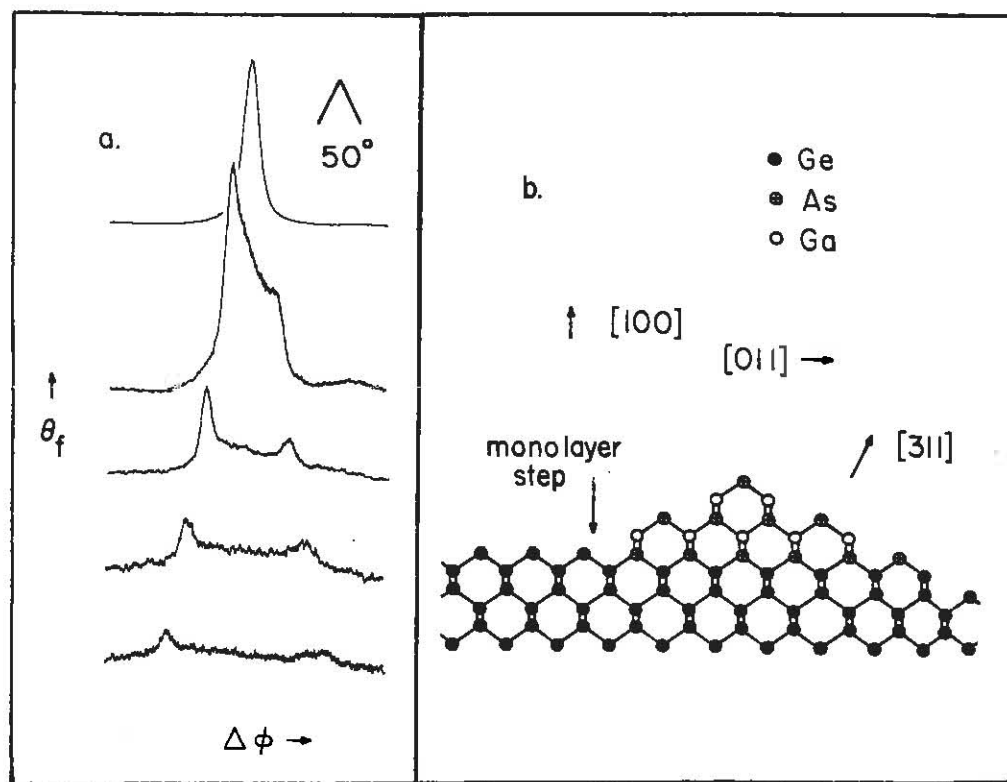


Fig. 63 GaAs on Ge(100) chevron profile.

start of growth implying an immediate orientation of the overgrowth. Further growth on such a surface results in split diffraction spots characteristic of a misoriented GaAs surface with only bi-layer As-As steps. An optical micrograph of the film shows a texturing on the surface with the lines in the texture perpendicular to the staircase in the [011] direction.

If As_2 is used to initiate growth, the GaAs domain observed is rotated 90° from the previous case, i.e. $1/2$ order streaks are observed if the electron beam is directed perpendicular to the staircase. Optically the surfaces are rougher than if As_2 is used. A cloudy appearance with none of the asymmetric texture is observed.

A similarly rough surface is observed if GaAs is grown on a surface misoriented by 2° toward the [010] with As_4 . Under the same growth conditions as the previous As_4 samples, a superposition of two orthogonal 2×4 diffraction patterns was obtained after growing a thick layer, indicating the presence of antiphase domains on this surface.

From some of the observations which are summarized in Table 1, it is clear that the domain orientation can be controlled and antiphase domain formation suppressed. Prior

to the growth of GaAs, the formation of multi-layer steps could effectively eliminate antiphase domains if either Ga or As attaches preferentially to a specific step edge site. Since adatoms adsorbed to larger steps may find a deeper potential well, the initial formation of the three dimensional nuclei at these sites could be important. The appearance of the faceted asperities may be the result of the difficulty of nucleating layer-by-layer with a polar material. Although the (311) face is polar, no charge accumulation or dipole is associated with the (311) pyramidal facet [Harrison, 1979]. Since the domains for GaAs grown by As_4 and As_2 are rotated by 90° , it is possible that the initial formation of the nuclei may be a stereochemical effect given the differences in shape and sticking coefficient of the two molecules. In other words, the way a nuclei is oriented at a step edge is dependent on the detailed bonding arrangement at the step site. The lowest energy configuration or perhaps the fastest forming configuration is the one that grows at the expense of the others.

For surfaces misoriented toward the [010] direction, the cloudy surface texture observed is likely the result of the two domain growth of GaAs on Ge. Since an ordered array of steps was not formed upon As adsorption, the nucleation of the GaAs is likely not restricted to the larger step

heights with a particular form as in Fig. 61c. The two domain growth of GaAs is also expected from symmetry arguments given the [010] direction of the misorientation. For example, if one type of multi-layer step edge was more prevalent than another, it would have a mirror reflection equivalent about the [010] axis. This would lead to a 50% chance of either domain forming throughout the surface. The rough growth is then in part caused by the disorder introduced at these antiphase domain boundaries.

To check the importance of multi-layer steps on the orientation of the GaAs domain, GaAs was grown on Ge surfaces that were exposed to As₄ at a much lower temperature. Here, not enough thermal energy was provided to effect a mass migration of atoms. However, the same result was observed --- immediate orientation of the GaAs overlayer and no antiphase domains if the misorientation was toward a [011] direction. This indicates one of the two types of single layer steps is preferred as a nucleation site.

What is not understood during the growth on the odd-layer stepped surfaces is how the GaAs overgrows the other non-nucleated step. There is no firm evidence that the shape of the facet is not associated with this overgrowth. One possibility is that the growth proceeds vertically and then bridges over laterally to another nuclei with the same

orientation. In this model, the closer together the steps are, the less bridging will occur. Similarly if only one domain of Ge were formed initially, no bridging would be required. Preliminary measurements indicate that forming a single domain Ge surface by growing Ge at low temperature and then exposing to As at low temperature helps but does not eliminate the initial faceted, rough growth.

There is further evidence that the formation of antiphase domains may be kinetically allowed under certain circumstances, but not energetically favorable. For a misorientation of 0.25° toward a [041] direction (15° from a [010]), a two domain 2×4 reconstruction is observed during growth at 580°C with As_4 . After raising the temperature to 650°C following Wang [1984], one of the orthogonal domains becomes more predominant, with the [011] domain direction having a stronger component perpendicular to the staircase direction as expected from Table 1. We can relate this to the previous arguments. Since the misorientation is not exactly in a [010] azimuth, one of the Ge multi-layer step edges should be more prevalent after the As induced mass migration. Raising the temperature allows the GaAs domain which initially is more prevalent to dominate, thereby eliminating energetically unfavorable antiphase domains. However, how the antiphase domains disappear is not understood.

5.4. GaAs on Si(100) Growth

The analysis of the initial surface of Si and the subsequent growth of GaAs was structured very similarly to that given in the previous section for GaAs on Ge. However, no pregrowth of homoepitaxial Si was done apart from using a Si strip evaporation source to occasionally clean the surface and/or grow a buffer layer. Substrates misoriented by a few degrees toward the [011] were found to give the fewest antiphase domains [Akiyama, 1986]. The analysis followed this outline.

(1) The sublattice and lattice domain orientations of Si and GaAs were obtained from the reconstructions observed. Si(100) reconstructs in a 2×1 unit cell, which is similar to Ge (both have a diamond lattice). This is typically observed as a 2×2 diffraction pattern if both sublattices are exposed at the surface, see Fig.27a. Steps between sublattices "A" and "B" are then odd multiples of $a/4$ high. Under every condition reported in this study, including heating to $\approx 1050^\circ\text{C}$ for 2 minutes, both 2×1 and 1×2 domains were observed with nearly equal intensity. A similar analysis was applied to the GaAs film. Since GaAs(100) reconstructs in 2×4 symmetry under As stabilized conditions, the presence of antiphase domains is signalled by a 4×4 diffraction pattern.

(2) The step structure of the surface is obtained by analyzing the shape of the specularly diffracted beam. The beam splits if there is a regularity in step heights and terrace lengths. Because the Si(100) surface has two sublattices, a more complicated interference effect arises. In this case, terraces separated by monolayer ($a/4$) steps belong to different sublattices (A and B) and consequently have different electron scattering factors. This difference can be explained by a strong dependence of RHEED intensity on azimuthal angle of incidence. Since "A" and "B" sublattices are effectively rotated in azimuth by 90° , the dependence on azimuth is observed as an alternation in scattering factor intensities. This is, not surprisingly, the same mechanism as for Ge.

(3) If the surface is rough with small asperities, a transmission cross-section diffraction pattern is observed. From the nature of the spots, the shape of asperities on the surface can be obtained.

The initial Si(100) characterization is shown in Fig. 64a where we plot an intensity profile along the length of the (00) streak. The incident beam is directed 20° from the [011] azimuth, which for this surface was nearly pointing down the staircase formed by the misorientation.

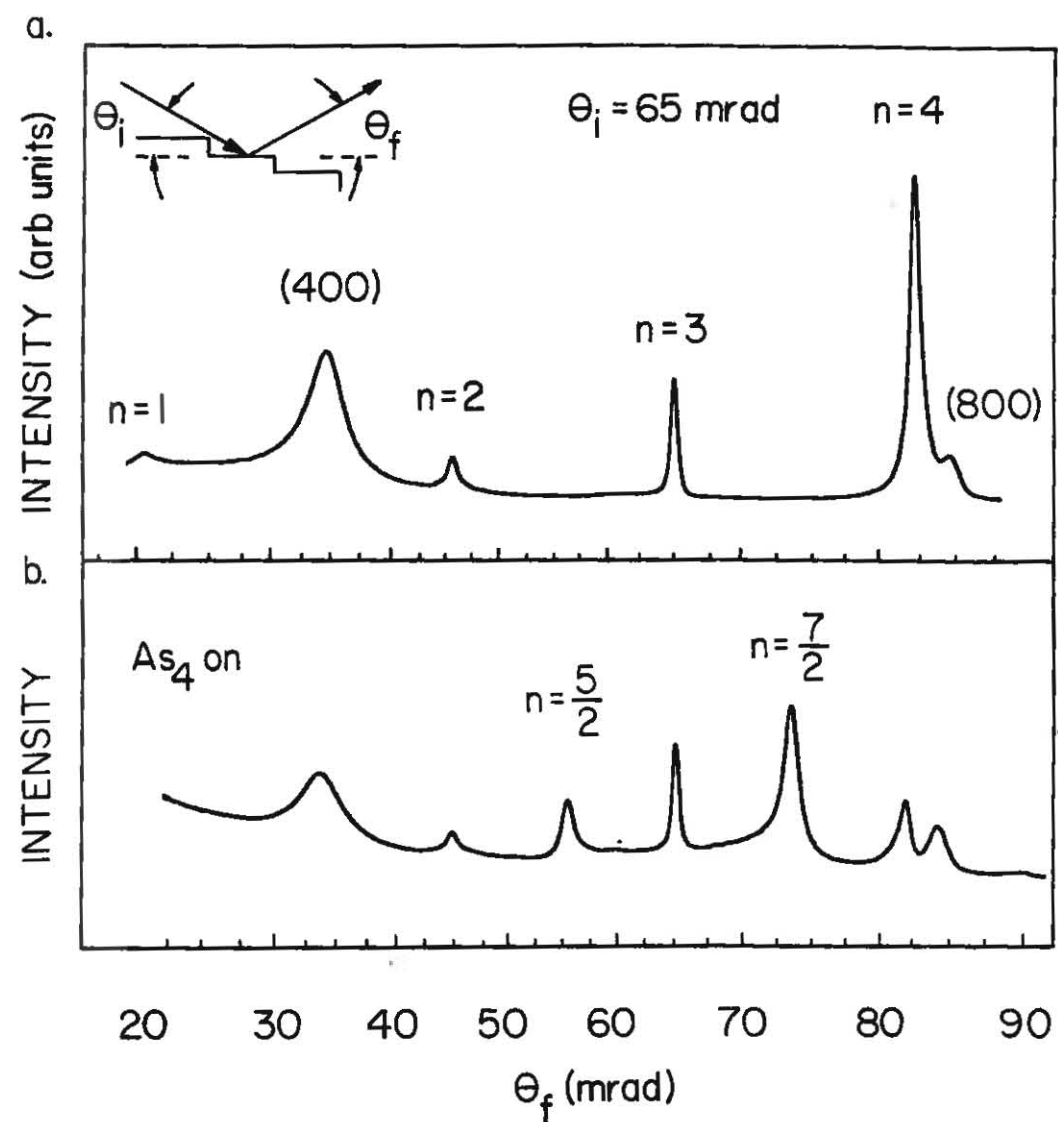


Fig.64 Clean and As adsorbed misoriented Si(100) profiles.

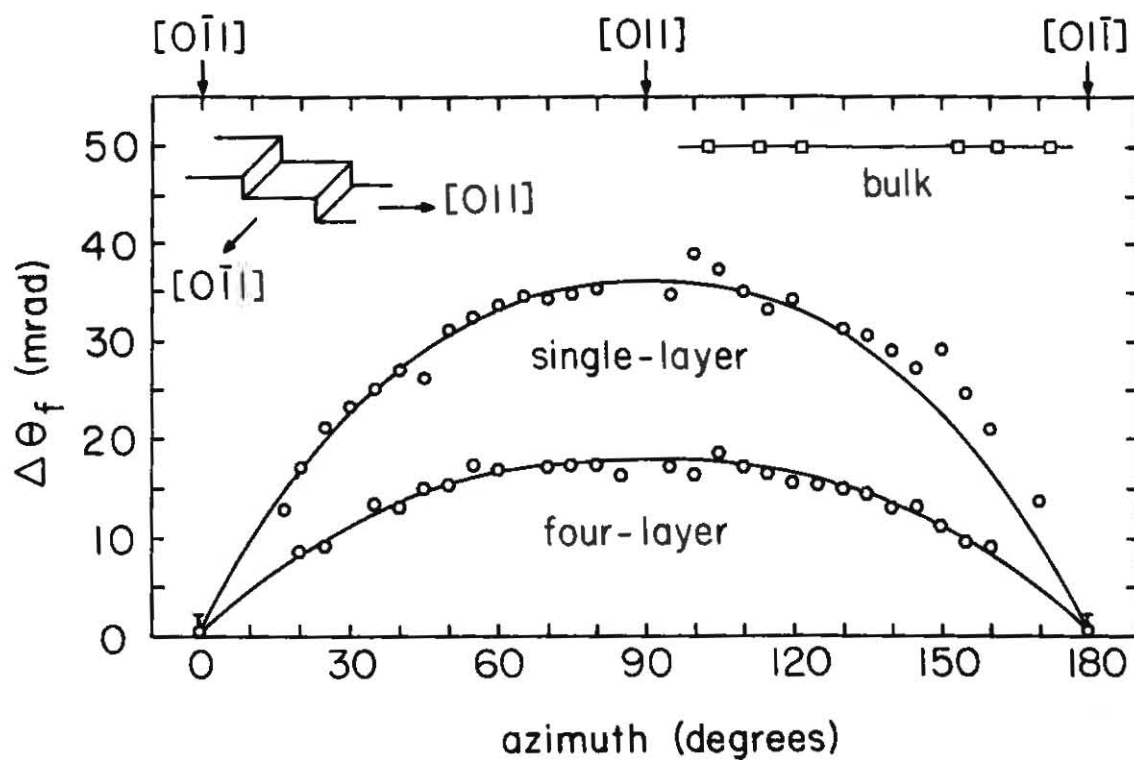


Fig. 65 Azimuthal measure of Fig. 64 splitting.

The inset shows the scattering geometry, with the incident and final glancing angles, θ_i and θ_f , measured with respect to the low-index terraces. The curve in Fig.64a was measured with a fixed incident angle of 65 mrad. The data is interpreted to indicate that the peaks labelled (400) and (800) are bulk, Kikuchi features, the peaks labelled $n = 1$ and 3 to arise from the difference in the scattering factor of type "A" and "B" terraces, and the peaks labelled $n = 2$ and 4 to result from single (mono)layer ($a/4$) steps. Understanding these features is important, as the diffraction profile changes markedly when As is adsorbed. Each is discussed briefly below.

The peaks labelled (400) and (800) are clearly distinguished as bulk-enhancement features by the Kikuchi lines which intersect the (00) streak. By contrast there is no Kikuchi line crossing the remaining peaks, so that one suspects that they are entirely step related. For $\theta_i = 65$ mrad, the specular (or $n = 3$) peak and the $n = 1$ peak correspond to a double-layer periodicity since at these θ_f 's, electrons scattered from adjacent terraces separated by a monolayer step are one half wavelength out of phase. It is essential to note that since both the 1×2 and 2×1 reconstructions are observed with near equal intensity, it is incorrect to say that the surface contains primarily double-layer steps. In fact these peaks mainly correspond to

the double-layer period resulting from the alternation of the scattering factor between type "A" and type "B" terraces on a singly stepped staircase. This is very similar to the results obtained for Ge(100).

The monolayer steps that dominate the clean Si(100) surface undergo a major rearrangement when exposed to an As flux above $\sim 650^{\circ}\text{C}$. This is indicated in Fig.64b, where new peaks, labelled $n=5/2$ and $n=7/2$, appear in the diffraction profile. To fit these peak positions, a step periodicity of four monolayers must be assumed. Thus, a multilayer step transition is caused by the addition of As. After the rearrangement, both the 2×1 and 1×2 reconstruction domains remain. A simple model consistent with both the requirement of odd-layer step heights and also of four-layer periodicity is that this surface consists of alternating triple- and single-layer steps. The model is identical to that proposed for Ge(100):As which was more fully described in the previous section.

At still higher temperatures the monolayer stepped surface is recovered. This is determined by the disappearance of the As induced peaks in the profile. Based on what was observed for Ge, this indicates the desorption of As. As a function of As flux and temperature, the reversible transition boundary is shown in Fig.66. The

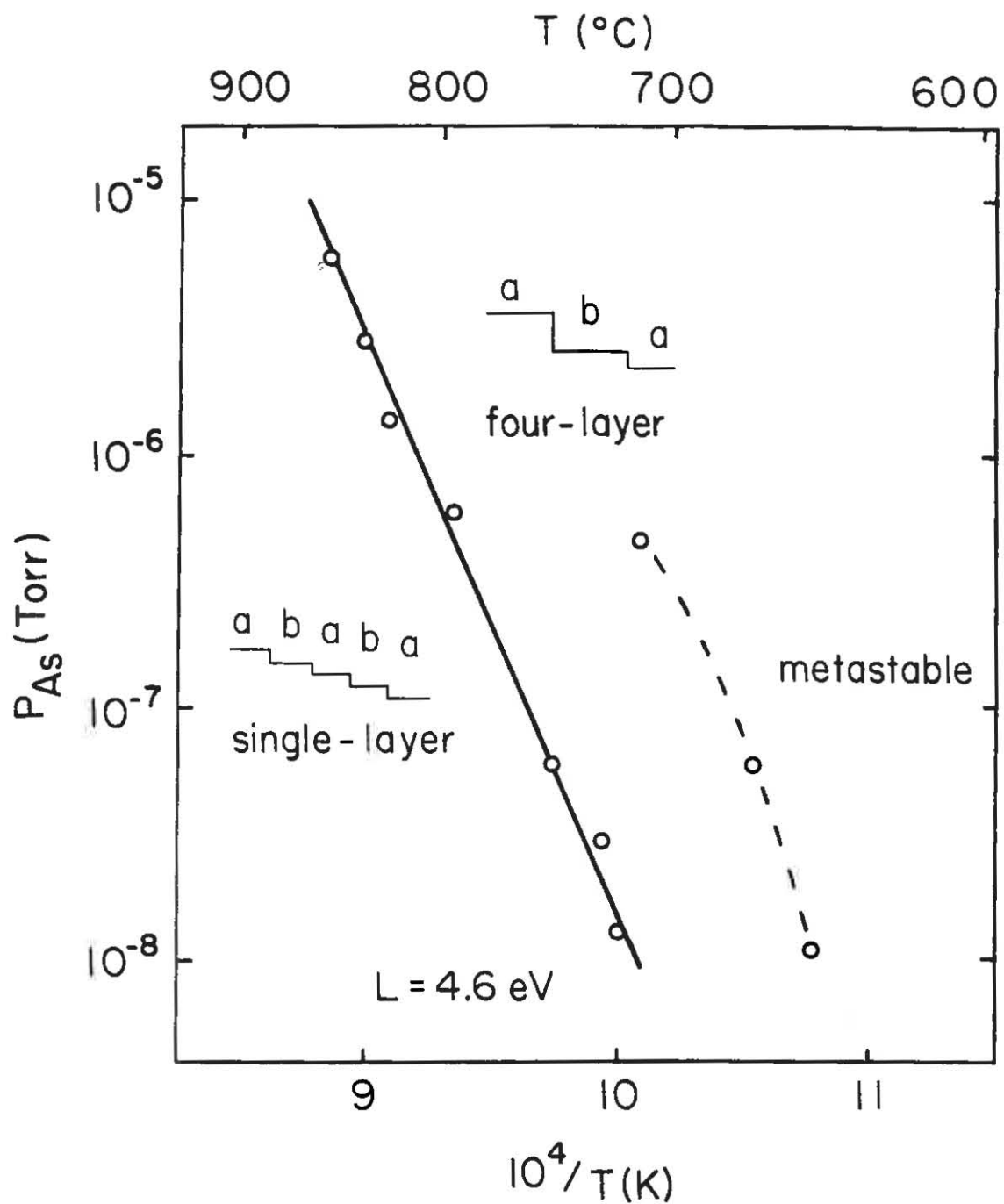


Fig. 66 Phase diagram for As adsorption on Si.

(first-order) transition has a latent heat of 4.6 eV with a hysteresis region of <15°C.

The multilayer transition is kinetically hindered at lower temperatures. If the sample temperature is below ~650°C when the As is introduced, no change in the diffraction is observed and monolayer steps are retained. This is illustrated in Fig.66 as a dotted line. However, any increase in temperature beyond this boundary results in the formation of the multilayer structure. The transition is not reversible. Therefore, we find that either the monolayer or multilayer Si(100) surface can be prepared for the GaAs growth by appropriate choice of As ambient and temperature cycling.

The last stage of growth is the nucleation of GaAs on the Si(100) surface. Similar to growth on Ge, GaAs nucleates on Si in the form of three dimensional clusters [Biegelsen,1987]. RHEED was used to determine the shape of the clusters by interpretation of the electron diffraction from the small asperities. If the clusters are asymmetric in shape, we can relate the pattern observed at different azimuths to the orientation of the staircase. As described below, the results of nucleation on the multilayer steps is markedly different than nucleation on the single-stepped staircase.

By initiating growth on the two domain, multilayer stepped surface a chevron-like diffraction pattern is observed from the small clusters. If the electron beam is aligned along the staircase direction, strong chevrons are observed. The angle of the chevrons with respect to the (100) reveals their origin as either (311) or (411) pyramidal facets. After 0.2 μm of growth, the chevrons fade and 1/4 order streaks are observed. With the electron beam directed in the orthogonal [011] azimuth, transmission spots are observed that are connected by weak lines of intensity, indicating (111)_B facets. As these spots fade, 1/2 order streaks develop. Further growth results in split diffraction spots characteristic of a misoriented GaAs surface with bilayer As-As steps [Pukite, 1984a,b]. Because of the domain orientation with respect to the staircase direction the steps are labelled as (111)_B or As terminated.

By contrast, if the two domain, monolayer stepped Si surface is used as a substrate under identical growth conditions (low temperature and slow growth rate), the domain formed is rotated 90° from the previous case. Chevrons which evolve into 1/4 order streaks are now observed if the electron beam is aligned perpendicular to the staircase direction. The 1/2 order streaks that eventually form in the orthogonal azimuth confirm the

presence of a single 2×4 GaAs domain, but the domain rotation forces (111)A or Ga terminated steps.

The domain orientation of the GaAs is established within the first few layers of growth — in spite of the two sublattice Si surface. The conclusive RHEED evidence is the observation of chevrons in only one of the $\langle 011 \rangle$ azimuths. Furthermore, the presence of both sublattices of the Si substrate implies that the GaAs is preferentially nucleating at one type of step, and then overgrowing the other type of step. Changing the initial step distribution from monolayer steps to multilayer steps and in turn altering the GaAs domain orientation supports this idea. It is important to note that the monolayer steps separating sublattice "A" from "B" are distinguishable from those separating sublattice "B" from "A", as shown in Fig. 27a. Therefore, a more realistic description of GaAs domain formation can be made as follows. Given that two types of steps are equally distributed on a misoriented Si(100) surface (or Ge surface), the GaAs must establish a preferred orientation at one of the two step sites before growing as a single domain film. The choice of step site and orientation for the nuclei is governed by the most energetically favored configuration. Figure 67 gives examples of two possible nuclei orientations.

The improvement of the GaAs layer surface quality with

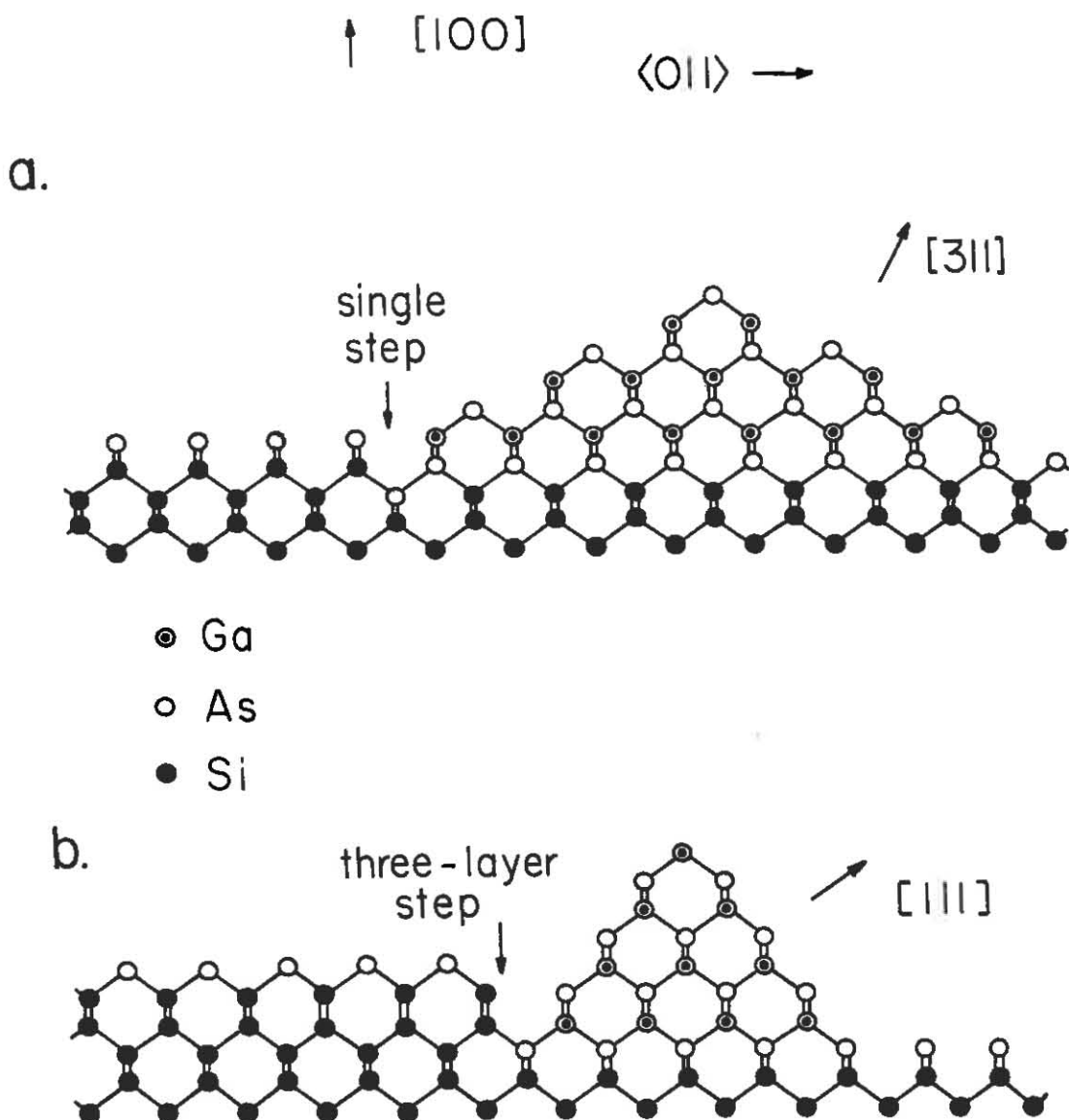


Fig. 67 a. Possible "A" domain nuclei configuration.
b. Possible "B" domain nuclei configuration.

film thickness is shown in Fig.68. The increase in the sharpness of the splitting indicates the staircase becomes ordered with time. It is possible that an ordering mechanism of the steps similar to that described in Appendix E may apply. After 3μ of growth, RHEED intensity oscillations, though weak, are readily observed. This implies that terraces with smooth (100) faces exist and the growth has transformed from three-dimensional to layer-by-layer. Figure 68 is for the Ga terminated stepped surface. Growth on the As terminated stepped surface does not show as great an improvement and is optically much rougher. This also occurs for GaAs growth on Ge when comparing the two domains. The reasons for this may be related to those speculated for the anisotropic growth of GaAs on the two misorientations discussed in Sec.5.1.

When comparing the results of growth of GaAs on Ge and Si, one should realize that a large density of dislocations can be formed in the latter system. The major differences we have observed with RHEED are that (1) the multi-layer to single-layer transition does not switch the domain orientation for GaAs on Ge, (2) the weak (111) facets are not observed for GaAs on Ge, and (3) the GaAs on Ge layers are generally smoother.

Each of these differences could be due to the strain at

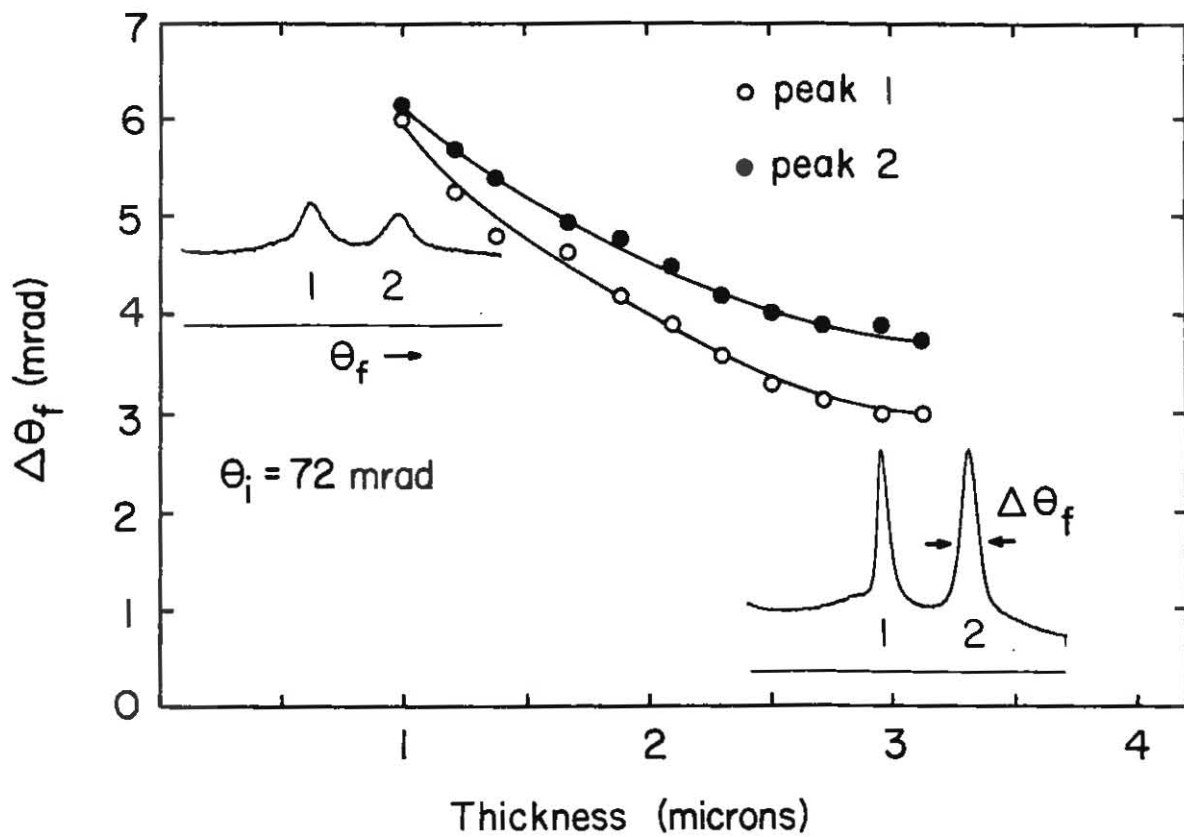


Fig. 68 GaAs surface ordering for "A" domain.

the heterointerface of GaAs and Si. In particular, the strain caused by the lattice mismatch is another energy that must be minimized when considering the domain orientation. Dislocations and subsequent twinning of layers may account for the (111) facets and for the rougher growth. Additionally, dislocations tend to be anisotropic [Bartels, 1977] which could play a role in the growth of "A" and "B" type domains. More work is needed in the area of dislocation characterization, as dislocations affect the optical and electrical properties of the layers.

Chapter 6

Summary and Conclusions

The main theme of this thesis is investigating the role of surface steps during the crystal growth and interface formation process. We have used RHEED to study the evolution of the atomic step structure in detail. In so doing we have developed a framework for modelling electron diffraction from steps. Furthermore, the RHEED calculations have been used in crystal growth simulations to understand the dynamics of the growth process. The underlying goal is to understand the interactions between adsorbed atoms and steps that leads to the growth of smooth epitaxial layers.

The main thrust of this investigation was to understand the interface formation in two important systems, namely that of GaAs on Ge(100) and GaAs on Si(100). These systems have promising technological applications, but the growth is only poorly understood. In particular, we have determined that surface steps are important in the heteroepitaxial interface formation process and that they play an important role in the subsequent growth.

Among the new results are that, for intentionally misoriented Ge(100) and Si(100) surfaces, the initial stage of MBE growth, As adsorption, leads to a multilayer step

transition. The step transition is not allowed at lower temperatures and monolayer steps are then observed. Growth of GaAs on the monolayer and multilayer stepped Si surfaces results in a single domain in each case, but the domains are found to give, respectively, Ga and As terminated step edges.

We find that the two types of GaAs step edges have different growth and structural properties — for both bulk and heteroepitaxial layers. In particular, heteroepitaxial GaAs growth proceeds more smoothly if there are Ga terminated step edges present. Furthermore, the diamond lattice allows a similar distinction in step types to be made for both Si and Ge. In this case, we find that the interaction of As with one of the two types of steps controls the GaAs domain formation on both Ge(100) and Si(100).

To understand the growth on stepped surfaces in more detail, we developed a non-linear partial differential equation to describe the time dependent behavior of homoepitaxial growth. The steps of the substrate are important in determining the boundary conditions for these equations. We find that the solutions of these equations show damped oscillations in quantities such as adatom concentration and step velocity. These oscillations are

sensitive functions of step separations and surface diffusion coefficients. The calculation of RHEED intensities from these surfaces also show damped oscillations. The damping is simply a consequence of a dissipative mechanism, that of convective growth, leading to a steady state step velocity. What is most remarkable is the close correspondence of these oscillations to the RHEED oscillations observed experimentally on intentionally stepped surfaces. We should point out that this is only a first treatment; further growth and diffraction models should include the clustering and coverage variation pointed out by Van Hove [1985].

We conclude that the initial stages of growth of GaAs on Si and Ge are more complicated than is currently believed. In particular, the results found in this investigation disagree with the interpretation that only double-layer steps can be allowed if antiphase domain free growth of GaAs is to be achieved. Instead, we determine that the type of steps initially present on the diamond lattice surface (monolayer or multilayer) appear to control the domain orientation of the GaAs, while the occurrence of both diamond sublattice surface domains does not a priori lead to the formation of antiphase domains in the epilayer.

Furthermore, we conclude that there are very strong anisotropies present on GaAs(100) surfaces that influence the quality of the epitaxy. For both Ge and GaAs surfaces, strong anisotropic growth effects are observed as the crystallographic direction of the misorientation is changed. This implies anisotropies in diffusion coefficient or in incorporation at step edges. As GaAs heteroepitaxy on Si and Ge is typically performed on misoriented substrates, these comparisons between the surface evolution during growth via heteroepitaxy and homoepitaxy are important for a further understanding of the growth process. Additionally, the comparisons between the experiments and the crystal growth simulations made in this investigation have given detailed information on the microscopic mechanisms of the epitaxy.

To summarize our efforts, we are further developing RHEED into an in situ surface sensitive tool that allows instant feedback on the MBE growth process. Information on the morphology of the surface and step structure can be obtained from the shape of the diffracted beams. By analyzing the shape of these RHEED streaks, the nature of the steps on the surface can be understood. In this thesis, steps have been shown to have strong implications on the growth process. Therefore by using RHEED, we have begun to understand the interactions between adatoms and steps that leads to the growth of a smooth epitaxial layer.

Appendix A

Surface Lattice Diffraction

To calculate the diffraction pattern from a two-dimensional array of surface atoms, one must first determine the periodicities of the surface lattice (including reconstruction) and then calculate the reciprocal lattice of this grid. We write the surface lattice as

$$\text{Lattice}(x, y) = \sum_n \sum_m \delta(x-na)\delta(y-ma)\delta(z) \quad (35)$$

The reciprocal space of this surface is the magnitude of the Fourier transform of the lattice.

$$I(s_x, s_y, s_z) = \sum_h \sum_k \delta(s_x - h2\pi/a)\delta(s_y - k2\pi/a) \quad (36)$$

Notice that there is no z dependence in this expression. For the RHEED geometry, we then use Eqs.(3,4,5) of the Ewald construction. Graphically, this is shown in Fig.69 for the beam directed along the x -axis, $\phi_i=0^\circ$. The glancing angle of the electrons causes the diffracted beams to follow circular contours with unequal spacings between the beams. In particular, the beams in the first zone are typically diffracted to angles off the phosphor screen.

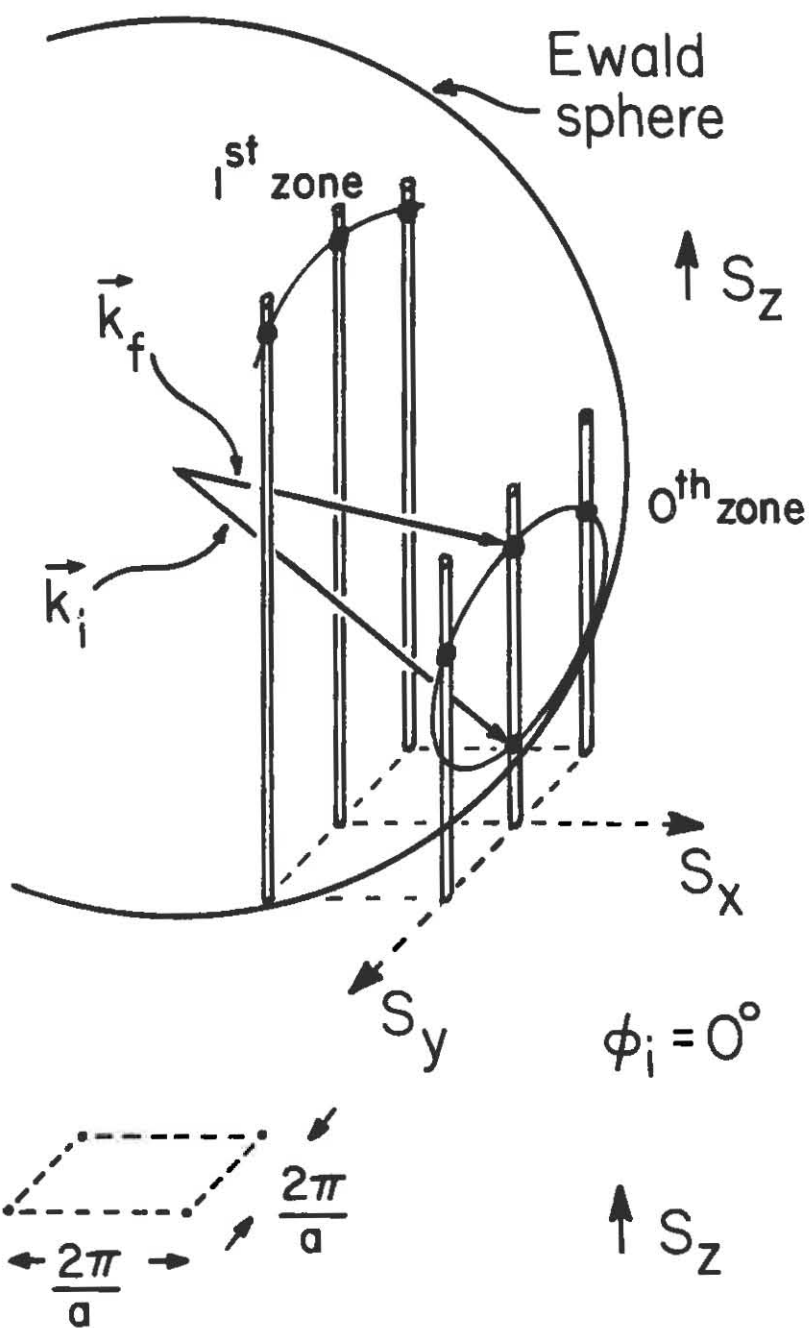


Fig. 69 Ewald construction for surface lattice.

Figure 70 shows the schematic diffraction patterns for GaAs and Ge in orthogonal beam azimuths ($\phi_i = 0^\circ$ and $\phi_i = 90^\circ$). The separation of the diffracted beams can be seen to be a function of geometry and surface reconstruction. Relating the observed reconstruction periodicities to the crystal orientation enables the domain orientation to be obtained.

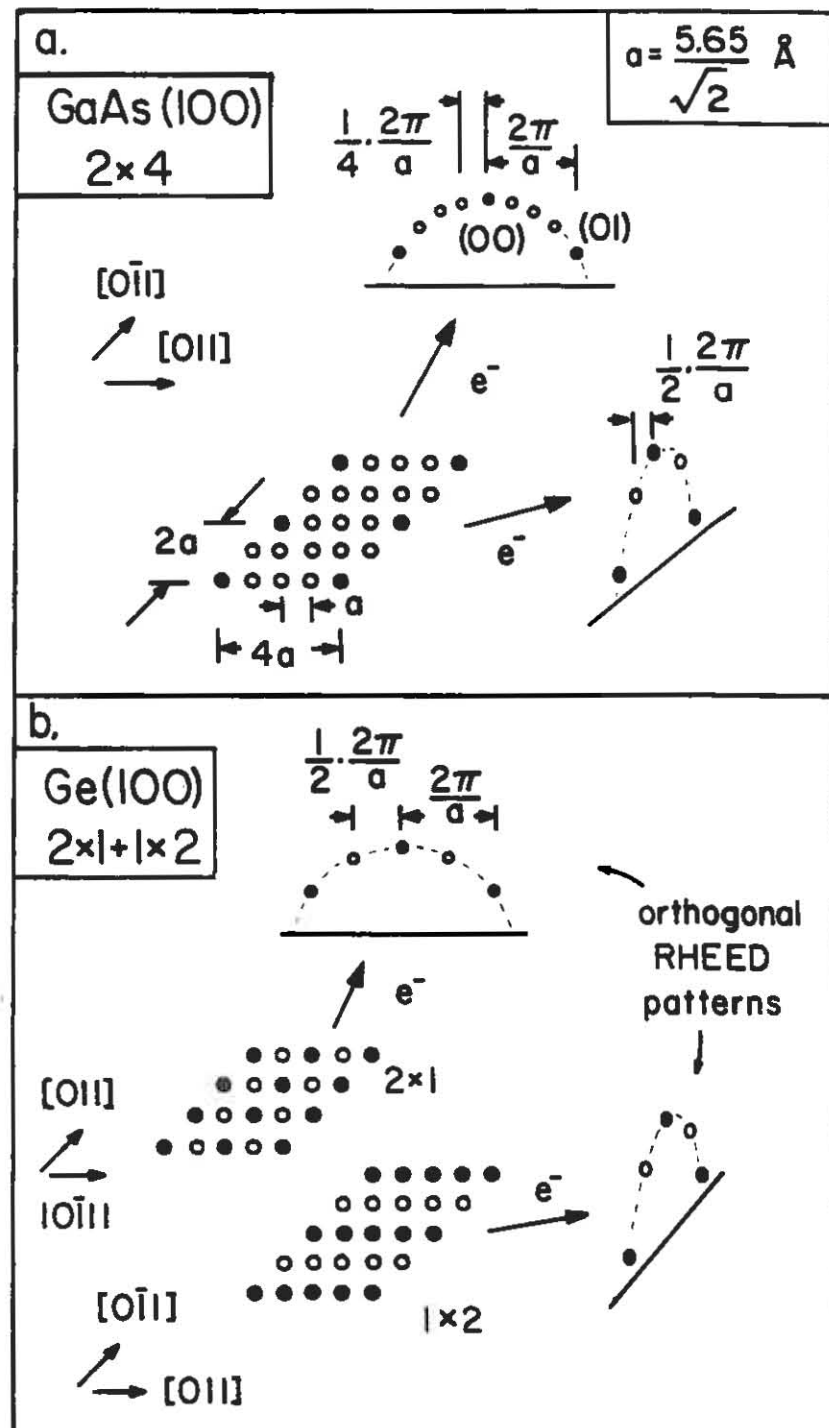


Fig. 70 RHEED patterns showing domain orientation.

Appendix B

Diffracted Intensity from Independent Rectangular Clusters

To calculate the diffracted intensity from a distribution of clusters assuming no interlayer correlations requires only the correlation function of a single cluster. Furthermore, if the shape is rectangular, the correlation function is separable, i.e. $C(x,y)=C_x(x)C_y(y)$. These correlation functions can then be given in terms of the probability distribution of side lengths L_x and L_y of a rectangle.

$$C_x(x) = \frac{1}{\langle L \rangle} \int_{u=x}^{\infty} (u-x) P_x(u) du \quad (37)$$

A similar expression holds for $C_y(y)$. Then the calculation of the two-dimensional Fourier transform of $C(x,y)$ gives the diffracted intensity. The result is,

$$I(s_x, s_y) = \left[\frac{2 - P_x(s_x) - P_x^*(s_x)}{\langle L_x \rangle s_x^2} \right] \cdot \left[\frac{2 - P_y(s_y) - P_y^*(s_y)}{\langle L_y \rangle s_y^2} \right] \quad (38)$$

where $P(S)$ is the Fourier transform of $P(L)$ and * denotes the complex conjugate. For a geometric distribution along x , $P_x(L_x) = \alpha \exp(-\alpha L_x)$, the Fourier transform is given by

$$P(s_x) = \frac{\alpha}{\alpha + i s_x} \quad (39)$$

A similar expression holds for the y -direction. Inserting Eq. 39 into Eq. 38 gives the diffracted intensity of Eq. 14.

Appendix C

Example of Disordered Staircase Diffraction

In this appendix, a terrace length probability distribution is assumed and the diffracted profile is calculated. As an example, we assume a "delayed exponential" probability density function where

$$P(L) = \alpha \exp[-\alpha(L-L_d)] \quad \text{for } L > L_d \quad (40)$$

The Fourier transform of this is given by,

$$P(S_x) = \frac{\alpha}{\alpha + iS_x} e^{-iS_x L_d} \quad (41)$$

and the diffracted intensity is calculated by substituting Eq.41 into Eq.15,

$$I(S_x, S_y, S_z) = \frac{2}{\langle L \rangle} \cdot \frac{(1 - \cos(S_z d)) \cdot \delta(S_y)}{[S_x^2 + \alpha \sin(S_z d + S_x d)]^2 + \alpha^2 [1 - \cos(S_z d + S_x d)]^2} \quad (42)$$

For this distribution, $\sigma = 1/\alpha$ and $\langle L \rangle = L_d + 1/\alpha$. One can see that if $1/\alpha \ll L_d$ (not much fluctuation in terrace lengths) then the intensity has peaks at $\pm \pi / \langle L \rangle$ for $S_z d = \pi$. The width of these peaks as a function of $\sigma = 1/\alpha$ is shown in Fig.41 for

a particular scattering geometry.

Appendix D

Time Dependent Solution to Linear Diffusion Equation

The method of obtaining a solution to the partial differential equation in Eq.20 is found in Crank, 1975, p.17. After separation of the variables, t and x, the adatom concentration can be written as

$$n(x,t) = \sum_m (A_m \sin \lambda_m x + B_m \cos \lambda_m x) \cdot \exp(-\lambda_m^2 Dt) \quad (43)$$

This is the natural response of the system, ignoring the form of the driving function. To calculate the forced, steady-state response, we set the time derivative in Eq.20 to zero. The solution to this equation is

$$n(x,\infty) = \frac{GL^2}{8Da} \cdot \left(1 - \frac{(2x-L)^2}{L^2}\right) \quad (44)$$

To calculate the coefficients A, B, and λ_m in Eq.43, observe that at $t=0$, the forced and natural response must sum to zero. One can see that Eq.43 is then simply the Fourier series expansion of Eq.44 over one period, L. The λ_m are then given as $m\pi/L$ and the A_m and B_m are the Fourier coefficients. The result of generating these coefficients for the steady state concentration profile of Eq.44 is

given in Eq. 21.

Appendix E

Stability of Propagating Steps

We have assumed that the staircases are highly ordered (all terraces of equal length) in calculating the adatom concentrations within the modified BCF theory. In fact the motion of adatoms toward the steps stabilizes this step train against fluctuations. In Fig.32, the staircase is considered stable against fluctuations if the number of adatoms collected at a step is greater from the lower terrace than from the upper terrace. This can be shown mathematically from a normal mode analysis [Gilmer,1973]. The latter can be understood with the help of Figs.20 and 35.

From Eqs. 23 and 24 and Fig.35, the current densities from above and below a step can be calculated, which results in more adatoms being collected from the terrace below a step (current densities are positive for adatoms moving left and negative for adatoms moving right). This means that during growth, the staircase is fed more by adatoms in front of its motion than its wake. As an example, assume a fluctuation occurred such that a consecutive short and long terrace appeared. According to Fig.61 the short terrace will increase in size because it gains its atoms from the terrace

in front of its motion. Then, since the terrace in front of it is larger, it has the capacity of collecting more atoms. This negative feedback process tends to equalize all terraces in the staircase.

Appendix F

Staircase Diffusion Pascal Computer Program

```

program BCF (input,output);
{1987 by GSP,GJW,PRP}

Type
  array1=array[1..500] of real;
  array2=array[1..20] of real;
Var
  L,                               {terrace length}
  i:integer;                        {x direction}
  totaltime,                         {simulation length}
  hop,                               {hopping rate}
  delta,                             {time increment}
  thickness,                          {layer thickness}
  velocity,                           {step velocity}
  growth,                            {rate of growth}
  time:real;                         {time}

  n,                               {adatom concentration}
  adatom:array1;                    {temporary adatom}

  m:array2;                          {temporary array}

begin {program}
  write(trm,'growth rate is 1/sec');
  writeln(trm);
  write(trm,'Input the terrace length >');
  read(L);
  writeln(trm);
  write(trm,'Input the diffusion coefficient >');
  read(hop);
  writeln(trm);
  write(trm,'Input the delta time >');
  read(delta);
  writeln(trm);
  write(trm,'Input the thickness >');
  read(thickness);
  writeln(trm);

  growth:=1;
  totaltime:=100;
  time:=0.0;
  for i:=1 to L+1 do

```

```
begin
    n[i]:=0;                      {initialize adatom}
end;

while time < totaltime do      {start growth}
begin
    if time>=thickness then growth:=0.0;  {stop}
    for i:=2 to L do
    begin                      {calculate temp adatom}
        m[1]:=growth;
        m[2]:=hop*(-2*n[i]+n[i+1]+n[i-1]);
        m[3]:=velocity*(n[i+1]-n[i]);
        adatom[i]:=delta*(m[1]+m[2]+m[3]);
    end;
    adatom[1]:=delta*(growth+hop*(n[2]+n[L])+veloc*n[2]);
    velocity:=adatom[1]/delta;  {calculate step velocity}
    for i:= 2 to L do          {calculate adatom conc.}
    begin
        n[i]:=n[i]+adatom[i];
    end;
    time:=time+delta;          {increment time}
    if keypressed then halt;  {stop}
end;
end.
```

Appendix G

Diffracted Intensity from an Adatom Concentration Profile

To calculate the diffracted intensity from a staircase with an additional spatially dependent concentration of adatoms on each terrace requires one simplifying approximation. That is, we assume the staircase is perfectly regular with each concentration profile identical. Then the correlation function $C(x,z)$ is periodic,

$$C(x-mL, z+md) = C(x, z) \quad (45)$$

where x and z are as shown in Fig.19 and m is an integer. The correlation function can then be restricted to one terrace. This can be calculated as

$$C_{11}(x) = \int_0^L n(u)n(u+x)du \quad (46)$$

where $n(u)$ is the adatom concentration and the double subscripts indicate adatom-adatom correlations. The Fourier transform of this is the diffracted intensity from these correlations.

$$C_{11}(s_x) = \int_{-\infty}^{\infty} \int_0^L n(u)n(u+x)du \cdot e^{-is_x x} dx \quad (47)$$

This double integral can be simplified by letting $w=u+x$.

Then,

$$C_{11}(s_x) = \int_0^L n(u)e^{is_x u} du \cdot \int_0^L n(w)e^{-is_x w} dw \quad (48)$$

or writing in a compact form $C_{11}(s_x) = n^*(s_x) n(s_x)$, where $n(s_x)$ is the Fourier transform of $n(x)$ and * denotes complex conjugate. The other correlation functions that need to be calculated are $C_{00}(x)$, $C_{10}(x)$, and $C_{01}(x)$. These are, respectively, substrate-substrate, adatom-substrate, and substrate-adatom correlations. Since the probability of an exposed substrate atom is simply $1-n(x)$, these correlation functions and their Fourier transforms can be similarly calculated.

$$C_{00}(s_x) = \int_0^L [1-n(u)]e^{is_x u} du \cdot \int_0^L [1-n(w)]e^{-is_x w} dw \quad (49)$$

$$c_{10}(s_x) = \int_0^L n(u) e^{is_x u} du + \int_0^L [1-n(w)] e^{-is_x w} dw \quad (50)$$

$$c_{01}(s_x) = \int_0^L [1-n(u)] e^{is_x u} du + \int_0^L n(w) e^{-is_x w} dw \quad (51)$$

At the out-of-phase condition, the intensity is given by

$$I(s_x) = c_{00}(s_x) + c_{11}(s_x) + e^{i\pi} c_{10}(s_x) + e^{-i\pi} c_{01}(s_x) \quad (52)$$

or by combining Eqs.(48,49,50,51,52),

$$I(s_x) = \left| \int_0^L [1-2n(x)] e^{-is_x x} dx \right|^2 \quad (53)$$

For the discrete lattice we are dealing with, this integral can be replaced by the following sum, evaluated at π/L .

$$I(s_x=\pi/L, s_z=\pi/d) = \left| \sum_{j=1}^N (1-2n_j(t)) e^{i\pi j/N} \right|^2 \quad (54)$$

Equation 54 was used to calculate the time dependent intensity oscillations shown in Fig.37.

References

[Aarts, 1986]

J.Aarts, W.M.Gerits, and P.K.Larsen, *Appl.Phys.Lett.* 48 (1986) 931.

[Akiyama, 1986]

M.Akiyama, Y.Kawarada, S.Nishi, T.Ueda, and K.Kaminishi, in *Proc.Mater.Res.Soc.* 67, ed. by J.C.C.Fan and J.M.Poate (Materials Research Society, Pittsburgh, PA, 1986), p.53.

[Arthur, 1968]

J.R.Arthur, Jr., *J.Phys.Chem.Solids* 39 (1968) 4032.

[Bartels, 1977]

W.J.Bartels and W.Nijman, *J.Crystal Growth* 37 (1977) 204.

[Biegelsen, 1987]

D.K.Biegelsen, F.A.Ponce, A.J.Smith and J.C.Tramontana, *J.Appl.Phys.* 61 (1987) 1856.

[Bringans, 1986]

R.D.Bringans, R.I.G.Uhrberg, M.A.Olmstead, and R.Z.Bachrach, *Phys.Rev.* B34 (1986) 7447.

[Burton, 1951]

W.K.Burton, N.Cabrera, and F.C.Frank, *Phil. Trans. Roy. Soc.* 243 (1951) 299.

[Cho, 1971]

A.Y.Cho, *J.Vac.Sci.Technol.* 8 (1971) S31.

[Cohen, 1986]

P.I.Cohen, P.R.Pukite, J.M.Van Hove, and C.S.Lent, *J.Vac.Sci.Technol.* A4 (1986) 1251.

[Cohen, 1987a]

P.I.Cohen, P.R.Pukite, and S.Batra, NATO proceedings on Thin Film Growth, ed. by B.Joyce and J.Venables (Plenum, NY, 1987)

[Cohen, 1987b]

P.I.Cohen and P.R.Pukite, *J.Vac.Sci.Technol.* A5 (1987) .

[Cowley, 1973]

J.M.Cowley and H.Shuman, *Surface Science* 38 (1973) 53.

[Cowley, 1981]

J.M.Cowley, *Diffraction Physics*, (North-Holland, Amsterdam,

1981).

[Crank, 1975]

J.Crank, The Mathematics of Diffusion, (Clarendon, Oxford, 1975).

[Dudley, 1987]

S.Dudley, J.Singh and K.K.Bajaj, J.Vac.Sci.Technol. B (1987)

[Fischer, 1986]

R.Fischer, H.Morkoc, D.A.Neumann, H.Zabel, C.Choi, N.Otsuka, M.Longerbone, and L.P.Erickson, J.Appl.Phys. 60 (1986) 1640.

[Foxon, 1975]

C.T.Foxon and B.A.Joyce, Surface Science 50 (1975) 434.

[Ghez, 1987]

R.Ghez, S.S.Iyer, and S.L.Delage, J.Vac.Sci.Technol. B5 (1987) 740.

[Giling, 1985]

L.J.Giling and W.J.P.Enckevort, Surface Science 161 (1985) 567.

[Gilmer, 1973]

G.Gilmer and P.Bennema, Crystal Growth, ed. by P.Hartman, (North-Holland, Amsterdam, 1973).

[Harrison, 1979]

W.Harrison, J.Vac.Sci.Technol. 16 (1979) 1492.

[Harris, 1981]

J.J.Harris and B.A.Joyce, Surface Science 103 (1981) L90.

[Heiblum, 1983]

M.Heiblum, E.E.Mendez, and L.Osterling, J.Appl.Phys. 54 (1983) 6982.

[Henzler, 1984]

M.Henzler, Appl.Phys. A34 (1984) 205.

[Hottier, 1977]

F.Hottier, J.B.Theeten, A.Masson, and J.L.Domange, Surface Science 65 (1977) 563.

[Ishizaka, 1986]

A.Ishizaka and Y.Shiraki, J.Electrochem.Soc. 133 (1986) 666.

[Kaplan, 1980]

R.Kaplan, Surface Science 93 (1980) 145.

[Kroemer, 1986]

H.Kroemer, in Proc.Mater.Res.Soc. 67, ed. by J.C.C.Fan and J.M.Poate (Materials Research Society, Pittsburgh, PA, 1986), p.3.

[Lagally,1985]

M.Lagally, in Methods of Experimental Physics: Surfaces, ed. by R.L.Park and M.G.Lagally, (Academic, Orlando, FL, 1985).

[Lent,1984]

C.S.Lent and P.I.Cohen, Surface Science 139 (1984) 121.

[Lent,1986]

C.S.Lent and P.I.Cohen, Phys.Rev. B33 (1986) 8329.

[Lewis,1986]

B.F.Lewis, R.Fernandez, A. Madhukar and F.J.Grunthaner, J.Vac.Sci.Technol. B4 (1986) 560.

[Madhukar,1983]

A.Madhukar, Surface Science 132 (1983) 344.

[Miyake,1938]

S.Miyake, Sci.Pap.Inst.Phys.Chem.Res.Tokyo, 34 (1938) 565.

[Moritz,1987]

W.Moritz, RHEED and Reflection Electron Imaging of Surfaces, ed. by P.K. Larsen, (Plenum Press, NY, in press).

[Neave,1983a]

J.H.Neave, B.A.Joyce, P.J.Dobson and N.Norton, Appl.Phys., A31 (1983) 1.

[Neave,1983b]

J.H.Neave, P.K.Larsen, B.A.Joyce, J.P.Gowers, and J.F. van der Veen, J.Vac.Sci.Technol. B1 (1983) 668.

[Neave,1985]

J.H.Neave, P.J.Dobson, B.A.Joyce, and J.Zhang, Appl. Phys. Lett. 47 (1985) 100.

[Olshanetsky,1977]

B.Z.Olshanetsky, S.M.Repinsky, and A.A.Shklyaev, Surf.Sci. 69 (1977) 205.

[Pashley,1987]

D.W.Pashley et al, preprint.

[Petroff,1979]

P.M.Petroff, A.C.Gossard, A.Savage, and W.Wiegmann, J.Crystal Growth 46 (1979) 172.

[Pimbley, 1985]

J.M.Pimbley, PhD Thesis, Rensselaer Polytechnic Institute (1985)

[Pukite, 1984a]

P.R. Pukite, J.M. Van Hove, and P.I. Cohen, Appl. Phys. Lett. 44 (1984) 456.

[Pukite, 1984b]

P.R.Pukite, J.M.Van Hove, and P.I.Cohen, J.Vac.Sci. Technol. B2 (1984) 243.

[Pukite, 1985]

P.R.Pukite, C.S.Lent, and P.I.Cohen, Surf.Sci. 161 (1985) 39.

[Pukite, 1987a]

P.R.Pukite and P.I.Cohen, J.Crystal Growth, 81 (1987) 214.

[Pukite, 1987b]

P.R.Pukite and P.I.Cohen, Appl.Phys.Lett. 50 (1987) 1739.

[Pukite, 1987c]

P.R.Pukite, S.Batra, and P.I.Cohen, Proceedings SPIE. 796 (1987) .

[Pukite, 1987d]

P.R.Pukite and P.I.Cohen, MRS Proceedings 91 (1987).

[Pukite, in press]

P.R.Pukite, S.Batra, and P.I.Cohen, RHEED and Reflection Electron Imaging of Surfaces, ed. by P.K. Larsen, (Plenum Press, NY, in press).

[Pukite, in press]

P.R.Pukite, G.S.Petrich, G.J.Whaley, and P.I.Cohen, Diffusion at Interfaces: Microscopic Concepts, ed. by M.Grunze and H.Kreuzer, (Springer Verlag, in press).

[Purcell, 1987]

S.T.Purcell, B.Heinrich, and A.S.Arrott, Phys.Rev. B35 (1987) 6458.

[Radulescu, 1987]

D.C.Radulescu, G.W.Wicks, W.J.Schaff, A.R.Calawa, and L.F.Eastman, J.Appl.Phys. (1987) 954.

[Rockett, 1987]

A.Rockett, Eighth MBE Workshop, 1987, Los Angeles, CA.

[Sakamoto, 1986]

T.Sakamoto and G.Hashiguchi, Jpn.J.Appl.Phys. 25 (1986) L78.

[Saloner, 1987]

D.Saloner, J.A.Martin, M.C.Tringides, D.E.Savage,
C.E.Aumann, and M.G.Lagally, J.Appl.Phys. 61 (1987) 2884.

[Saluja, 1987]

D.Saluja, P.R. Pukite, S.Batra and P.I.Cohen,
J.Vac.Sci.Technol. B5 (1987) 716.

[Somorjai, 1981]

G.A.Somorjai, Chemistry in Two Dimensions: Surfaces (Cornell University Press, Ithaca, 1981).

[Tromp, 1987]

R.M.Tromp, R.J.Hamers, J.E.Demuth, Phys.Rev. B23 (1986)
3657.

[Tsui, 1985]

R.K.Tsui, J.A.Curless, G.D.Kramer, M.S.Peffley and D.L.Rode,
J.Appl.Phys. 58 (1985) 2570.

[Van Hove, 1983a]

J.M.Van Hove, P.R. Pukite, P.I.Cohen and C.S.Lent,
J.Vac.Sci.Technol., A1 (1983) 609.

[Van Hove, 1983b]

J.M.Van Hove, C.S.Lent, P.R.Pukite and P.I.Cohen, J.Vac.Sci.
Technol., B1 (1983) 741.

[Van Hove, 1985a]

J.M.Van Hove, P.R.Pukite, and P.I.Cohen, J.Vac.Sci.Technol.
B3 (1985) 563.

[Van Hove, 1985b]

J.M.Van Hove, PhD Thesis, University of Minnesota, 1985.

[Venables, 1984]

J.Venables, G.D.T. Spiller, and M.Hanbucken, Rep.Prog.Phys.
47 (1984) 399.

[Voigtlaender, 1986]

K.Voigtlaender, H.Risken, and E.Kasper, Appl.Phys.A 39
(1986) 31.

[Walton, 1962]

D.Walton, J.Chem.Phys. 37 (1962) 2182.

[Wang, 1984]

W.I.Wang, Appl.Phys.Lett. 44 (1984) 1149.